AD 675 816

DISCLAIMER NOTICE

THIS DOCUMENT IS THE BEST QUALITY AVAILABLE.

COPY FURNISHED CONTAINED A SIGNIFICANT NUMBER OF PAGES WHICH DO NOT REPRODUCE LEGIBLY.

Office of Naval Research

Contract N00014-67-A-0298-0012

NR - 017 - 308

THE APPLICATION OF THE RATIO REFLECTOMETER TO ENERGY BAND STUDIES IN GERMANIUM AND GRAY TIN

By

Paul T. McElroy

May 1968

Technical Report No. HP-21

Technical Report No. ARPA-34

The research reported in this document was made possible through support extended the Division of Engineering and Applied Physics, Harvard University, by the Office of Naval Research, under Contract N00014-67-A-0298-0012 and by the Advanced Research Projects Agency under Contract ARPA SD-88.

Division of Engineering and Applied Physics

Harvard University Cambridge, Massachusetts

PREFACE

This technical report, entitled "The Application of the Ratio Reflectometer to Energy Band Studies in Germanium and Gray Tin", is the second of two related reports based on the author's work at Harvard. The first, HP-20 (also known as ARPA-33), is entitled "The Construction and Analysis of a Ratio Reflectometer". The report has been divided into these two parts both because of length and because individual readers will usually have greater interest in one than in the other. Cross references between the two parts have been minimized but not entirely eliminated.

TABLE OF CONTENTS

PREFACE. i

TABLE OF CONTENTS. iii

LIST OF FIGURES. v

LIST OF TABLES. vii

ABSTRACT. ix

Chapter IV. REFLECTIVITY MEASUREMENTS AND THEIR INTERPRETATION. 4-1

A. SOME COMMENTS ON THE THEORY OF REFLECTIVITY STRUCTURE. 4-1

B. GERMANIUM. 4-14

1. A Review of Prior Work. 4-14
2. The Reasons for Our Study of Germanium. 4-16
3. Samples. 4-17
4. Experimental Data and Their Interpretation. 4-18

C. GRAY TIN. 4-40

1. The Gray Tin Energy Bands. 4-40
2. A Review of Prior Work. 4-44
3. The Reasons for Our Study of Gray Tin. 4-47
4. Samples and Their Treatment. 4-47
5. Experimental Problems. 4-51
6. Experimental Data and Some Interpretation. 4-57
7. Interpretation of the Experimental Structure in Terms of Band Models. 4-66

D. H FIELD MEASUREMENTS, THIN FILM STUDIES, AND $\Delta R/R$ WORK IN GERMANIUM. 4-74

1. Magneto-Reflectivity Measurements in Germanium. 4-74
2. Thin Film Effects. 4-80
3. $\Delta R/R$ Measurements in Germanium. 4-85

Chapter V. COMPATIBILITY RELATIONSHIPS AND THE DEPENDENCE ON LIGHT POLARIZATION OF SELECTION RULES: THEIR APPLICATION TO UNDERSTANDING OF OPTICAL STRUCTURE AND IN COMPUTING ϵ_2. 5-1

A. SELECTION RULES AND COMPATIBILITY RELATIONSHIPS FOR OPTICAL TRANSITIONS IN THE DIAMOND STRUCTURE. 5-2

1. The Use of Group Theory in Determining Selection Rules. 5-3

2. Compatibility Relationships for Symmetries Modified by the Application of an Electric Field. 5-8

B. AN ESTIMATE OF ϵ_2 FOR THE FOUR $L_{3'} \rightarrow L_3$ TRANSITIONS. 5-13

1. The Polarization Dependence of the L Point Selection Rules. 5-13

2. A Calculation of ϵ_2 For Gray Tin. 5-16

3. An Estimate of the $\Delta R/R$ Signal Strength in Electroreflectivity. 5-22

4. A Comparison of the Computed Value of ϵ_2 and Experimental Results for Gray Tin. 5-28

5. Conclusions Concerning the ϵ_2 Calculation. 5-30

REFERENCES.

ACKNOWLEDGMENTS.

LIST OF FIGURES

FIGURE		PAGE
	CHAPTER IV	
4-1	First Brillouin Zone for the Diamond Lattice.	4-2
4-2	The Joint Density of States at M_0, M_1, M_2, and M_3 Critical Points.	4-9
4-3	The Change in the Dielectric Constant Induced by the Short Range Interaction.	4-9
4-4	Modifications of the Dielectric Function near Combinations of Critical Points due to the Short Range Interaction.	4-9
4-5	a. Change in ϵ_2 near Spherical Interband Edge due to Coulomb Electron-Hole Interaction. b. The Same near a Spherical M_3 Point.	4-9
4-6	Reflectivity Spectrum of Germanium. Temperature 300°K.	4-15
4-7	Reflectivity Spectrum of Germanium. Temperature 80°K.	4-19
4-8a	Energy Bands of Germanium along the Γ-L and Γ-X Lines in $\vec{k}$ Space, Including Spin-Orbit Splittings.	4-20
4-8b	Energy Bands of Germanium along the X-W, W-K, and K-Γ Lines. Does not Contain Spin-Orbit Splittings.	4-21
4-9	Experimental Data for Germanium near 3.2 eV.	4-27
4-10	Structure in the Reflectivity of Germanium Arising from the $\Gamma_{25'}(\Gamma_7^+) \rightarrow \Gamma_2'(\Gamma_7^-)$ Transitions.	4-39
4-11	Energy Bands of Gray Tin along the Γ-L, Γ-X, X-K, and K-Γ Lines in $\vec{k}$ Space. a. Single Group Bands. b. Double Group Bands.	4-41
4-12	Double Group Energy Bands of Gray Tin along the Γ-L and Γ-X Lines in $\vec{k}$ Space.	4-43
4-13	Electroreflectivity Spectrum of Gray Tin.	4-46
4-14	Reflectivity Spectrum of Gray Tin (Good Sample). Absolute Reflectivity Values Accurate to ±5%. Temperature 80°K.	4-48

FIGURE		PAGE
4-15	Reflectivity Spectrum of a Slightly Degraded Gray Tin Sample. Reflectivity Values are Relative. Temperature is Between 105°-80°K.	4-49
4-16	Reflectivity Spectrum of Gray Tin Showing Effect of CO_2 and H_2O Film.	4-52
4-17	Spectral Segments of Gray Tin Reflectivity from Fig. 4-15. This Plot Shows Need for Adjustment of the Segments and Need for Segment Overlap.	4-56
4-18	Reflectivity Spectrum of Gray Tin (Good Sample). Absolute Reflectivity Values Accurate to ±5%. Temperature 260°K.	4-58
4-19	Development of Structure in Cooled Gray Tin at Energies above the E_2 Peak.	4-65
4-20	The Effect of Thin Films of Various Thicknesses upon the Reflectivity of Germanium.	4-83
4-21a	Electroreflectivity Spectrum of the Germanium Λ Peaks. DC Voltage, 1.55 Volts. AC Voltage, 1.0 Volts rms.	4-86
4-21b	Electroreflectivity Spectrum of the Germanium Λ Peaks. DC Voltage, 1.04 Volts. AC Voltage, .15 Volts rms.	4-86
	CHAPTER V	
5-1	An Illustration for the Groups T_d and O_h.	5-17
5-2	An Illustration for the Groups C_2, C_{2v}, and C_{4v}.	5-17
5-3	An Illustration for the Groups C_{3v}, D_3, and D_{3d}.	5-17
5-4	Relationship of the Direction of Light Propagation and Applied Electric Field with the Various L Points in the Diamond Brillouin Zone.	5-17

LIST OF TABLES

TABLE		PAGE
	CHAPTER IV	
4-1	The Comparison of the Energies of Experimental Structure and the Energies of Certain Transitions Given by the k·p Model for Germanium.	4-30
4-2	The Comparison of the Energies of Experimental Structure and the Energies of Certain Transitions Given by the First Principles Band Model for Germanium.	4-30
4-3	Λ Peak Temperature Coefficients.	4-59
4-4	The E_2/E_1 Ratio and E_2 and E_1 Temperature Coefficients for a Number of Semiconductors.	4-63
4-5	The Comparison of the Energies of Experimental Structure and the Energies of Transitions Given by the k·p Band Model for Gray Tin.	4-68
4-6	The Comparison of the Energies of Experimental Structure and the Energies of Transitions Given by the First Principles Band Model for Gray Tin.	4-71
4-7	The Asymmetry Required in the Valence and Conduction Bands along Λ for Discrete Levels to Exist in the Presence of a Magnetic Field, Assuming Both Bands are Saddle Points.	4-79
	CHAPTER V	
5-1	Product Decomposition of the O_h Group Giving some Selection Rules at Γ in Diamond.	5-7
5-2	Zinc Blende Selection Rules at Γ.	5-8
5-3	Compatibility Relationships for O_h Symmetry and an Electric Field.	5-9
5-4	The Effect of an E(z) Field on Certain Γ Point Selection Rules.	5-10
5-5	The Effect of an E(v) Field on Certain Γ Point Selection Rules.	5-11
5-6	The Effect of an E(w) Field on Certain Γ Point Selection Rules.	5-12
5-7	Equivalence of Two L Point Notations.	5-14
5-8	The Dependence of the $L_3' \rightarrow L_3$ Selection Rules on Light Polarization.	5-15

TABLE		PAGE
5-9	A Table Showing the Computation of the Contribution of Each of the Eight L Points to the Factor $S_{jj'}$.	5-19
5-10	A Comparison of the Strength of the Four $L_{3'} \rightarrow L_3$ Transitions.	5-21
5-11	Compatibility Relationships for D_{3d} Symmetry and an Electric Field.	5-22
5-12	The Effect of an E(z) Field on Certain L Point Selection Rules.	5-23
5-13	The Effect of an E(y) Field on Certain L Point Selection Rules.	5-25
5-14	Energetic Order of Observed Structure and of the $L_{3'} \rightarrow L_3$ Transitions in Gray Tin, Arranged in Order of Decreasing Energy.	5-28

ABSTRACT

In our work we have conducted four related investigations: (1) the design and construction of a ratio reflectometer for optical measurements; (2) the description and analysis of a polarization dependent false structure in the reflectivity, which arises in the system monochromator; (3) the application of the ratio reflectometer to the accurate measurement of reflectivity structures in germanium and gray tin, which are then interpreted in terms of energy band models; and (4) the development of an improved method for theoretically computing ϵ_2 through the study of the dependence of the diamond double group selection rules on light polarization direction, and a suggested modification to the double group labels at L, with particular reference to gray tin.

In this technical report we discuss (3) and (4) while (1) and (2) are considered in Technical Report HP-20 (ARPA-33), entitled "The Construction and Analysis of a Ratio Reflectometer".

(3) Our studies of the reflectivity of gray tin and germanium served a number of purposes: to demonstrate the capability of our system to pick out fine details in reflectivity; to see if reflectivity studies could display structure which is either missing or confused in the differential techniques such as AC electroreflectivity, and thereby to provide a basis of comparison for these two

methods; to provide data for a Kramers-Kronig analysis giving n and k for Ge at low temperature and for gray tin.

Interpretation of the reflectivity structure in these two materials is not completely straightforward since the band models of different investigators such as Herman and Cardona differ significantly and since large regions of $\vec{k}$ space are now felt to contribute to individual peaks. In our analysis of structure, we have employed both the Cardona and Herman bands, hoping to find a basis for preference between them. The individual structural features we consider do not provide the basis for a clearcut choice.

We noted the following in germanium: The peak at 3.2 eV splits into a doublet at low temperature and is best interpreted as arising from a $\Delta_5 \rightarrow \Delta_1$ transition. A number of other studies in this region give highly conflicting results. The Σ-X peak at 4.46 eV shows a shoulder at the high energy side and we discuss the lack of a corresponding peak in electroreflectivity, as well as the narrowing of the reflectivity peak on cooling. We see some evidence in reflectivity of the $L_{3'} \rightarrow L_1$ transition, noted by Potter in polarization measurements, although our peaks are much weaker than his data would predict. We try to account for the difference in peak size in terms of scattering associated with sample surface distortion. We also see the direct gap transition from the split-off valence band; the size of our shoulder is comparable with that predicted by Potter's data.

We studied gray tin over the range .95-5.2 eV, with sufficient absolute amplitude accuracy to justify a Kramers-Kronig analysis. Studies were made at both 260° and 80°K. Problems due to sample degradation and film buildup in the cryostat were eliminated so that we feel all the structure reported is real.

The two Λ peaks (1.365 and 1.83 eV) at low temperature drop sharply at the high energy side of the peak, displaying their M_1 critical point character. Between the Λ and Σ-X (3.75 eV) peaks are three small features. Two, at 2.60 and 3.3 eV. are seen in electroreflectivity. The 3.3 reflectivity structure confirms the doubtful electroreflectivity feature. A third reflectivity feature, a shoulder at 2.85 eV, is not seen in electroreflectivity. We discuss varying possibilities for the identification of these three features plus an additional one at 2.28 eV seen only in electroreflectivity.

The $E_2(\Sigma\text{-}X)$ peak in gray tin is considerably smaller than its analog in other diamond and zinc blende semiconductors. We account for the small size by an appeal both to Kane's idea that E_2 is made up of transitions throughout a large part of the Brillouin zone and to the considerable band distortion created by the zero fundamental energy gap.

Above the E_2 peak, we have noted three structural features. Two of these coincide with two of the three electroreflectivity peaks in the same energy region. Combining these to give a total of four, we find the structure corresponds to the $L_{3'} \rightarrow L_3$

quadruplet in the Cardona k·p bands. They can also be related to transitions in the Herman bands.

In our studies of the electroreflectivity of germanium we note major changes in shape and large energy shifts when the AC electric field magnitude is changed. Of particular interest is the first reported effect of a magnetic field on the Λ transitions in germanium. In an E × H experiment we note significant decreases in the $\Delta R/R$ signal as H is increased. This is to be contrasted with our study of the reflectivity at the Λ peaks under H field where we noted no effect within .02% of the reflectivity.

We feel that thin oxide films can affect electroreflectivity studies employing the electrolytic technique and that films of CO_2 and water can affect low temperature reflectivity studies. Using a simple model and computer program, we display some of these effects for varying thicknesses of film.

(4) Optical selection rules and their modification under electric field were essential to our interpretation of the reflectivity and electroreflectivity structure. We outline the group theoretical procedure for determining the selection rules for the diamond double group and discuss their modification under electric field by applying compatibility relations.

These rules are applied in two cases. One is to the $\Gamma_{25'} \rightarrow \Gamma_{2'}$ transitions. The other, a study of the $L_{3'} \rightarrow L_3$ transitions, is of considerable interest. We consider an improved method for computing

ϵ_2 theoretically by noting the difference of the selection rules at the eight L points. Specifically, we note that the strength of the members of the $L_{3'} \rightarrow L_3$ quadruplet should be different from one another in reflectivity and electroreflectivity, and apply this discovery to comment on the missing structure in both of these experiments in gray tin. The comparison of theory and experiment suggests that the double group labels at $L_{3'}$ and those at L_3 should be reversed from their commonly published order.

BLANK PAGE

CHAPTER IV REFLECTIVITY MEASUREMENTS AND THEIR INTERPRETATION

A. SOME COMMENTS ON THE THEORY OF REFLECTIVITY STRUCTURE

In the Introduction we commented on how band calculations, which use a small amount of experimental data, can determine the band structure throughout the entire Brillouin zone. (The diamond zone is shown in Fig. 4-1.) This band structure, coupled with oscillator strength calculations based on the same wave functions used in the band calculation, can be used to calculate ϵ_2. This value in turn can be compared with experimental determinations of ϵ_2 over an extended energy range.

The comparison in ϵ_2, and by extension in R, can be made on the basis of three sets of quantities: the energies at which transitions occur, and the magnitude and line shape of the related optical structure. All three are relevant in the interpretation of germanium and gray tin structure discussed in this chapter. For instance the <u>energies</u> at which the $\Gamma_{25'} \rightarrow \Gamma_{15}$ transition in germanium gray tin and silicon occurs are in dispute (compare the assignments in Phillips [4-01] and in Herman et al. [4-02]; the <u>magnitude</u> of the Σ-X transition in the reflectivity of α-Sn is smaller in comparison with the Λ transition than in the other diamond and zinc blende semiconductors; and the <u>line shape</u> of the Σ-X transition in germanium is open to different interpretations.

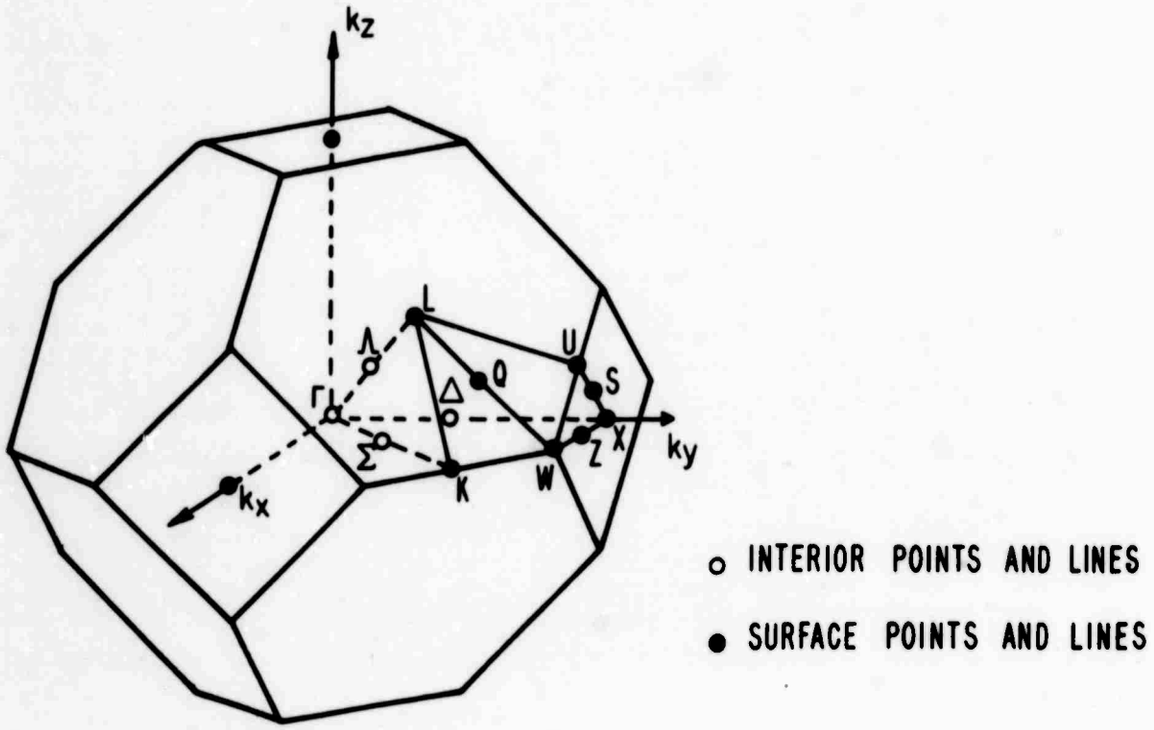

FIG. 4-1 FIRST BRILLOUIN ZONE FOR THE DIAMOND LATTICE
From ref. [5-08, Fig. 7]

CHAPTER IV REFLECTIVITY MEASUREMENTS AND THEIR INTERPRETATION

A. SOME COMMENTS ON THE THEORY OF REFLECTIVITY STRUCTURE

In the Introduction we commented on how band calculations, which use a small amount of experimental data, can determine the band structure throughout the entire Brillouin zone. (The diamond zone is shown in Fig. 4-1.) This band structure, coupled with oscillator strength calculations based on the same wave functions used in the band calculation, can be used to calculate ϵ_2. This value in turn can be compared with experimental determinations of ϵ_2 over an extended energy range.

The comparison in ϵ_2, and by extension in R, can be made on the basis of three sets of quantities: the energies at which transitions occur, and the magnitude and line shape of the related optical structure. All three are relevant in the interpretation of germanium and gray tin structure discussed in this chapter. For instance the <u>energies</u> at which the $\Gamma_{25'} \rightarrow \Gamma_{15}$ transition in germanium gray tin and silicon occurs are in dispute (compare the assignments in Phillips [4-01] and in Herman et al. [4-02]; the <u>magnitude</u> of the Σ-X transition in the reflectivity of α-Sn is smaller in comparison with the Λ transition than in the other diamond and zinc blende semiconductors; and the <u>line shape</u> of the Σ-X transition in germanium is open to different interpretations.

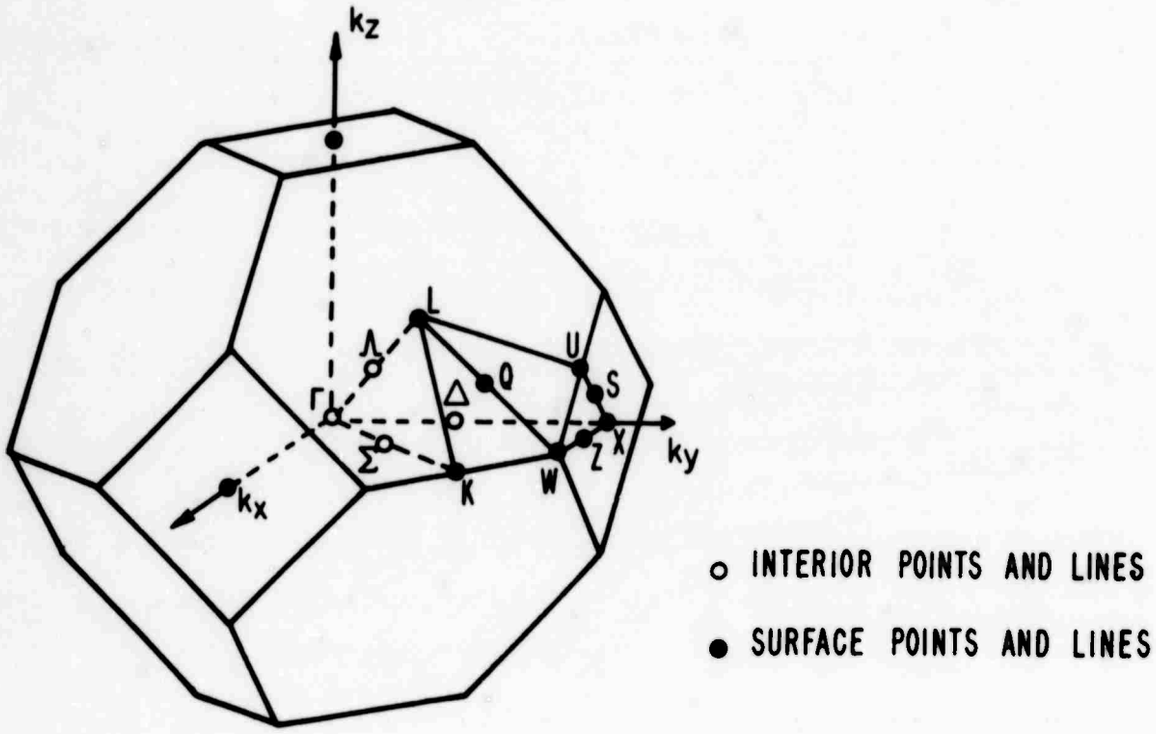

FIG. 4-1 FIRST BRILLOUIN ZONE FOR THE DIAMOND LATTICE
From ref. [5-08, Fig. 7]

The general theory of optical structure in solids is well described in the literature. In particular the review articles by Phillips [4-01], Knox [4-03], and Stern [4-04] cover many of the relevant points. Other useful reviews are those of Tauc [4-05, 4-06, 4-07], Zallen [4-08], and Grant [4-09]. New band structure calculations by Herman et al. [4-02], Kane [4-10], and Cardona-Pollak [4-11] are important supplementary data, necessary to a balanced view and interpretation. In the remainder of this section we summarize a number of the results from these references.

The reflectivity of a material can be expressed in terms of the macroscopic quantities, n and k, the components of the complex index of refraction.

$$R = \frac{(n-1)^2 + k^2}{(n+1)^2 + k^2} \tag{4.1}$$

In turn n and k can be related to $\tilde{\epsilon}$, the complex permittivity.

$$\epsilon_1 = \epsilon_0(n^2 - k^2) \ , \qquad \epsilon_2 = \epsilon_0\ 2nk \ , \tag{4.2a,b}$$

where ϵ_0 is the permittivity of free space. The imaginary component of $\tilde{\epsilon}$, ϵ_2, can be computed using a quantum mechanical model. The interband contribution to ϵ_2 is [4-01, Eqs. 2.7, 2.9, 2.10, 9.2]

$$\epsilon_2(\omega) = \frac{e^2h^2}{m} \Sigma_{j,j'} \Omega^{-1} \int_{B.Z.} \frac{f_{jj'}(\vec{k})}{E_{jj'}|\vec{\nabla}_k E_{jj'}|} dS_k \ , \tag{4.3}$$

where j' is the index for the bands with unfilled states, and j is that for filled states. The relation

$$E_{j'j} = E_{j'} - E_j = \hbar\omega \tag{4.4}$$

defines the surface S_k in $\vec{k}$ space. The oscillator strength of a given transition from band j to j' at wave vector $\vec{k}$ is

$$f_{jj'}(\vec{k}) = \frac{2}{3m} \frac{|\langle \vec{k}j|\vec{p}|\vec{k}j'\rangle|^2}{E_{j'j}(\vec{k})} \quad , \tag{4.5}$$

and it is evaluated using the one-electron Bloch wave functions. The joint density of states for transitions between bands j and j' is defined as

$$J_{jj'} = \frac{dN}{dE_{jj'}} = \Omega^{-1} \int \frac{dS_k}{|\vec{\nabla}_k E_{jj'}|} \quad . \tag{4.6}$$

It is a joint density since it depends on both bands.

We have modified Eq. 4.5 for the oscillator strength to include the effect of the polarization of the light radiation.†

---

†We were puzzled by the absence of a dependence on the light polarization in the expression for ϵ_2 in Brust [4-12] and Phillips [4-01]; a polarization dependence is to be expected since the Hamiltonian for the interaction of radiation and matter is of the form

$$H_{int} = e\vec{r}\cdot\vec{E} = e\vec{r}\cdot E\hat{n} \sim e\vec{p}\cdot\vec{A}/c \quad . \tag{4.7}$$

$\hat{n}$ is a unit vector in the direction of light polarization. The question was resolved by referring to a discussion in Seitz, Modern Theory of Solids, [4-13, Secs. 43 and 148], which has regularly been cited as a reference in the ϵ_2 formulations. The expression for P(t) (= the probability of a transition's occurring), which is used in the derivation of $\sigma = \omega\epsilon_2/4\pi$, has terms of the form (Eqs. 43.27 and 28)

$$|\langle j'|\hat{n}\cdot\vec{r}|j\rangle|^2 \quad . \tag{4.8}$$

When the $\cos^2\theta$ term is averaged over a solid angle, the matrix element becomes

$$\overline{|\langle j'|\hat{n}\cdot\vec{r}|j\rangle|^2} = \frac{|\langle j'|\vec{r}|j\rangle|^2}{3} \quad . \tag{4.9}$$

This averaging is a procedure which is valid in an isotropic medium only. In our Eq. 4.5 we have removed the factor 1/3 and reincorporated the polarization vector $\hat{n}$; the form of the equation is now essentially the same as that found in other references [4-06].

$$f_{jj'}(\vec{k}) = \frac{2}{m} \frac{|\langle \vec{k}_j | \hat{n} \cdot \vec{p} | \vec{k}_{j'} \rangle|^2}{E_{j'j}(\vec{k})} \tag{4.10}$$

This modified expression will be central to our analysis in Chapter V.

Equation 4.3 indicates that ϵ_2 at ω is determined by the sum over the allowed transitions from the filled to the unfilled bands separated by energy $\hbar\omega$. ϵ_2 is large in two sets of circumstances:

(1) When the joint density of states is singular and the oscillator strength is nonzero. Under these conditions the oscillator strength will help determine the importance of the transition to ϵ_2.

(2) When the oscillator strength is particularly large due to reinforcement by transitions at a Brillouin zone boundary (called umklapp enhancement), where there will often be a singularity in the joint density of states.

The singularities in the joint density of states resulting in large ϵ_2 occur under four similar situations, called van Hove singularities or critical points (Fig. 4-2), when the slopes of the initial and final state bands are equal. M_0 is the name given to the singularity when it arises from a three-dimensional minimum in the shape of the $E(\vec{k})$ curve of the final relative to the initial state. M_3 is a maximum, and M_1 and M_2 are saddle points.

At these critical points ϵ_2 (and hence R when we take ϵ_1 into account) will show structure similar to the van Hove singularities. Thus, the line shape of an experimentally measured R will help to identify transitions, especially since some critical points are expected to occur at points of high crystal symmetry in the Brillouin zone.

Line shape interpretations can become complicated by a number of factors:

(1) If a transition is umklapp enhanced, the line shape need not have a van Hove shape but will often be a peak [4-01, p. 72].

(2) Two or more van Hove singularities can cluster together in energy. Multiple critical points have been suggested as being responsible for the Σ-X peak in germanium [4-12] and the Λ peak in cadmium telluride [4-14].

(3) Structure in R and ϵ_2 need not arise solely from a van Hove singularity at points of high symmetry in the zone but can arise from transitions occurring over a large part of the zone. There will again be a singularity in the joint density of states, but it will not occur at one point in $\vec{k}$ space. Rather, the singularity will occur over a wide range of $\vec{k}$ values in which the final and initial state bands are parallel. The van Hove description is somewhat inappropriate here, although this large region of $\vec{k}$ space may contain a number of the van Hove singularities. The net result is that the line shape is not predictable from the simple van Hove models, but can be determined only by summing the contribution to ϵ_2 at a given energy from a band calculation encompassing all of $\vec{k}$ space.

This possibility was hinted at in the work of Brust [4-12, 4-15], when he noted that a cluster of critical points might contribute to the 3.4 eV peak in silicon and to that at 3.2 eV in germanium; but it was firmly established by the work of Kane [4-10] in calculating the band

structure of silicon using a form of pseudopotential theory. Carefully determining the resultant energy differences in the Brillouin zone to minimize sampling errors, he noted that the peak at 4.3 eV in silicon, known as the Σ-X peak, was not made up solely of contributions from these two symmetries. In fact the $X_4 \rightarrow X_1$ transition contributed less than 5% to ϵ_2. Large regions of $\vec{k}$ space created the rest of the peak. A similar effect was noted for the peak labeled $L_{3'} \rightarrow L_3$, while the contributions to the structure labeled $\Gamma_{25'} \rightarrow \Gamma_{15}$ were less conclusively identified.

Certain conclusions from this work seem inescapable. Some of the labeling of optical structure in the past in terms of transitions at high symmetry points are now merely nominal since many other directions and/or points may contribute as well. Experimental work (such as that of Gerhardt [4-18]) is necessary to establish the prime symmetry directions of much optical structure whose symmetry is established to date only by calculations.

A second conclusion is that we must place far less confidence in the van Hove singularity line shapes as a tool for experimental line shape evaluation and for transition identification, until such time as an extremely detailed sampling of the Brillouin zone is made following a band calculation in which one has complete faith. Then we will know if a particular bit of structure arises at one or more van Hove singularities or over a large volume of $\vec{k}$ space. Kane's work has pointed the way.

(4) The electron-hole interaction† is another factor complicating line shape interpretation. It is one of a number of correlation effects in solids which are ignored in the one-electron approximation but which become relevant when one considers the excited states of a crystal. The interaction is the Coulombic attraction of an electron in a conduction band and a hole in a valence band. Considered together as a single entity, they create a quasi-particle, often called an exciton. This exciton is like a hydrogen atom and can have both discrete and continuum energy states at an M_0 edge [4-17, 4-19]. These states significantly modify the one-electron absorption line shape (Fig. 4-5a).

An article by Velický and Sak [4-20] extends a number of these ideas to the three other types of van Hove singularity. They employ two separate approaches. The first presupposes a short range interaction of the electron and hole, giving something like a Frenkel exciton. The solution is exact, and fails to display any discrete levels. The result

$$\epsilon_2(\omega) = |1 + gF(\omega)|^{-2}\, \epsilon_2^{(0)}(\omega) \qquad (4.11)$$

shows that $\epsilon_2(\omega)$, the dielectric constant in the presence of the electron-hole interaction, is just the one-electron dielectric constant, $\epsilon_2^{(0)}(\omega)$, which is found in our Eq. 4.3, multiplied by an amplification factor. This factor contains g, the coupling constant

---

†The electron-hole interaction is treated in the literature under several titles which we cite here: exciton [4-17]; Frenkel and Wannier excitons [4-03]; parabolic, hyperbolic (or saddle point), and hybrid excitons [4-01]; resonance and antiresonance [4-01]; a form of collective excitation [4-18].

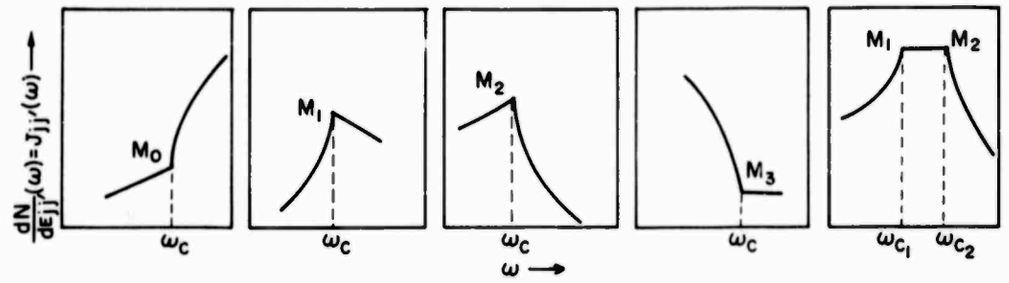

FIG. 4-2 THE JOINT DENSITY OF STATES AT M_0, M_1, M_2, AND M_3 CRITICAL POINTS. THE FINAL FIGURE SHOWS THE RESULTANT JOINT DENSITY OF STATES WHEN M_1 AND M_2 CRITICAL POINTS OCCUR CLOSE TOGETHER IN ENERGY. From ref. [4-01, Fig. 3].

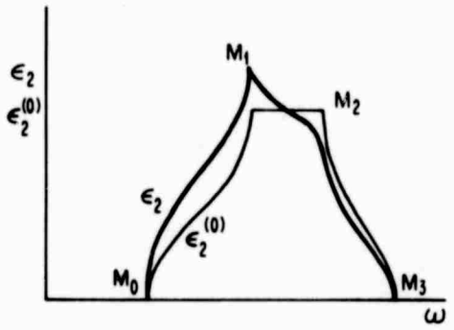

FIG. 4-3 THE CHANGE IN THE DIELECTRIC CONSTANT INDUCED BY THE SHORT RANGE INTERACTION. After ref. [4-20, Fig. 1].

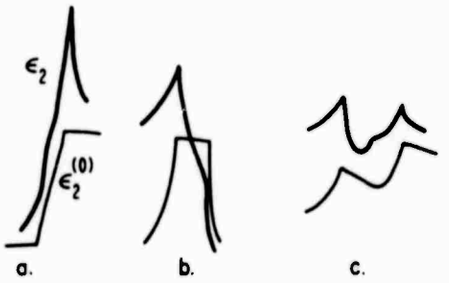

FIG. 4-4 MODIFICATIONS OF THE DIELECTRIC FUNCTION NEAR COMBINATIONS OF CRITICAL POINTS DUE TO THE SHORT RANGE INTERACTION (a) M_0-M_1; (b) M_1-M_2; (c) M_1-M_1. After ref. [4-20, Fig. 2].

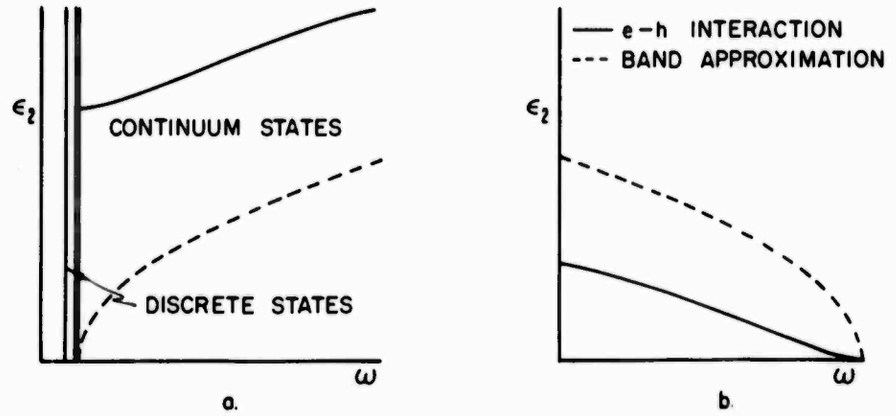

FIG. 4-5 a. CHANGE IN ϵ_2 NEAR SPHERICAL INTERBAND EDGE DUE TO COULOMB ELECTRON-HOLE INTERACTION. b. THE SAME NEAR A SPHERICAL M_3 POINT. After ref. [4-20, Fig. 3].

of the interaction, and $F(\omega)$, a Kramers-Kronig transform of the joint density of states. As displayed in Figs. 4-3 and 4-4, the factor results in an enhancement of M_0 and M_1 edges and a weakening of M_2 and M_3 edges.

When Elliott [4-17] employed a Coulombic interaction of the electron and hole within the effective mass approximation at an M_0 edge, he noted discrete levels (Fig. 4-5a). Velický and Sak use this method in their second approach. While discrete levels cannot exist at the M_1, M_2, and M_3 edges, the Coulombic interaction does distort the shape of the edges just as the short range interaction did. Figure 4-5b shows the effect of the interaction at an M_3 edge. In parallel work Duke and Segall [4-21] conclude that excitons cannot exist as metastable particles at M_1 and M_2 edges. Velický and Sak extend their analysis with Coulombic interaction one step further, by noting the distortion of the M_0 discrete excitonic levels by other bands.

The electron-hole interaction can cause even more extensive changes: Toyozawa et al. [4-22] noted that the shapes of ϵ_2 for the four types of critical points shown in Fig. 4-2 could be interchanged by varying the parameter g in Eq. 4.11.

Spatial dispersion is yet another mechanism resulting in the modification of excitonic line shape. This dispersion of the electromagnetic radiation arises when there are other means of energy transport within a crystal besides the electromagnetic field [4-23].

The effect of the discrete excitonic lines at an M_0 edge is dramatically demonstrated as temperature is reduced; the absorption edge peaks sharply [4-19]. By analogy the sharpening with decreasing temperature of the reflectivity peaks, corresponding to transitions at the other types of critical points, has been attributed to excitons [4-01]. We now see that such sharpening could not be due to discrete levels.

It is not always immediately obvious which mechanism is appropriate to account for line shape. For example the structure in the 3.5 eV peak in CdTe, as seen at low temperature, was initially attributed to a cluster of critical points by Marple and Ehrenreich [4-14]. Since the peak seemed to exhibit resonant and antiresonant features (i.e., it looked like constructive and destructive interference), Phillips attributed the effect to discrete levels in an M_1 exciton [4-01]. Velický and Sak show similar resonant and antiresonant structure at an M_1 edge arising from the electron-hole interaction (see our Fig. 4-4c) and not from discrete levels. What is clear from this is that one can no longer appeal quite so freely to the concept of the exciton, composed of discrete and continuous levels, to account for peculiarities in line shape.

We now face the general question of band calculations and what faith one is to place in them. Works include those of Cohen-Bergstresser [4-24], Brust [4-12], Phillips [4-01], Cardona-Pollak [4-11], Herman et al. [4-02], Dresselhaus-Dresselhaus [4-25], and Kane [4-10]. The authors

make differing claims as to the accuracy of their own particular approach. The fact is that while most calculations show the same general shape for the bands, they often differ in energy differences between bands by amounts greater than the usually stated errors in the methods -- .1 eV. For example Kane's value for the $\Gamma_{25'} \rightarrow \Gamma_{2'}$ transition in silicon is 3.3 eV, while both Brust and Cohen-Bergstresser find 3.8 eV. All three use a pseudopotential technique. Further, in the calculations of Herman et al. the $\Gamma_{25'} \rightarrow \Gamma_{15}$ transition is .5 to .8 eV lower than in Cohen-Bergstresser's pseudopotential calculations in germanium, silicon, and gray tin (where the supposed $\Gamma_{25'} \rightarrow \Gamma_{15}$ energy is one of those fitted by adjustment of the pseudopotential parameters). This difference results in a major change in the identification of certain structure.

Which one of these calculations is one to choose? Philosophically, that of Herman et al. is the most satisfying since it is a "first principles" approach involving a self consistent potential and charge distribution later modified slightly by experiment. The semi-empirical pseudopotential method [4-12, 4-01, 4-24, 4-10] using a small number of parameters has given considerable insight into band structure. But the free electron bands from which it starts undergo large distortion in response to the pseudopotential parameters. In contrast the modified first principles approach of Herman et al. requires little distortion. The Fourier expansion approach of Dresselhaus and Dresselhaus employs a tight binding approximation and fits

13 parameters. The semi-empirical k·p method [4-11] should be excellent for new structure since it fits 15 parameters. The success of these two methods presupposes the accuracy of identification of experimental structure and energy differences used to determine the parameters, which is just the point put in question by Herman's work.† Hence, Fourier expansion and k·p bands should ultimately rest on a first principles calculation, establishing the accuracy of structure identification. The "right" calculation probably is still to be made, and may well be the result of a melding of techniques.

In interpreting our own data, we will lean on more than one calculation and will try to see if the data dictate a preference. We shall call on $\Delta R/R$ and photoemission data which will bear on or support our own comments.

---

†We adduce two examples of how the k·p bands change radically as one changes these parameters.

(1) Cardona [4-26, p. 26] notes that the k·p gray tin bands shift from a form similar to the Cohen-Bergstresser values to Herman's values [4-27] as he varies the value of the E_0' parameter.

(2) The gray tin bands as originally published had a spin-orbit splitting at L_3, of .42 eV and at L_3 of .23 eV [4-28]. By changing the identification of $\Delta R/R$ structure found in ref. [4-28], Higginbotham, Pollak, and Cardona in a later article [4-29] changed the latter splitting markedly to ~.9 eV. This change was made without any explanation of why the former value of .23 was in error. This is particularly puzzling since the ΔL_3 value is derivable from some formulae given in a third paper [4-30] and is far less than .9 eV. At any rate, the changed identification and splitting involve a change in certain k·p parameters and a consequent sizable change in the band structure. We comment on this latter approach, which we feel to be in error, in Chapter V.

B. GERMANIUM

1. A Review of Prior Work

As a group IV semiconductor of central importance, germanium has received an extraordinary amount of experimental and theoretical attention. Even when narrowing our interest to reflectivity, we find that a number of different studies have been made. We shall give a brief review of those earlier papers directly relevant to the present study. In 1959 Philipp and Taft [4-31] measured the reflectivity over a sufficient energy range (1-10 eV) to permit Kramers-Kronig analysis of the data. They noted the 4.46, 3.2, 2.2 eV peaks seen in our Fig. 4-6 as well as a peak at 6.0 eV. Philipp and Ehrenreich [4-32] extended the measurement and analysis further into the vacuum ultraviolet. Prior to their work Archer [4-33] had studied the polarization parameters of reflected light in a limited energy range (1.75-3.5 eV). Tauc and Antončík [4-34] noted that the 2.15 eV peak was actually split into two peaks at 2.10 and 2.30 eV, and Tauc, working with Abrahám [4-35], examined the behavior of this peak in germanium-silicon alloys in an attempt to better understand the relative band structures of the two materials. Cardona and Sommers [4-36] examined the behavior both with temperature down to 80°K and, with doping, of the peaks at 4.46 and 2.10-2.30 eV. Donovan, Ashley, and Bennett [4-37] measured samples which had been electropolished rather than mechanically polished and etched, and were thereby able to sharpen the structural splitting at 2.1-2.3 eV and to note a new shoulder at 2.47 eV. Their work also minimized

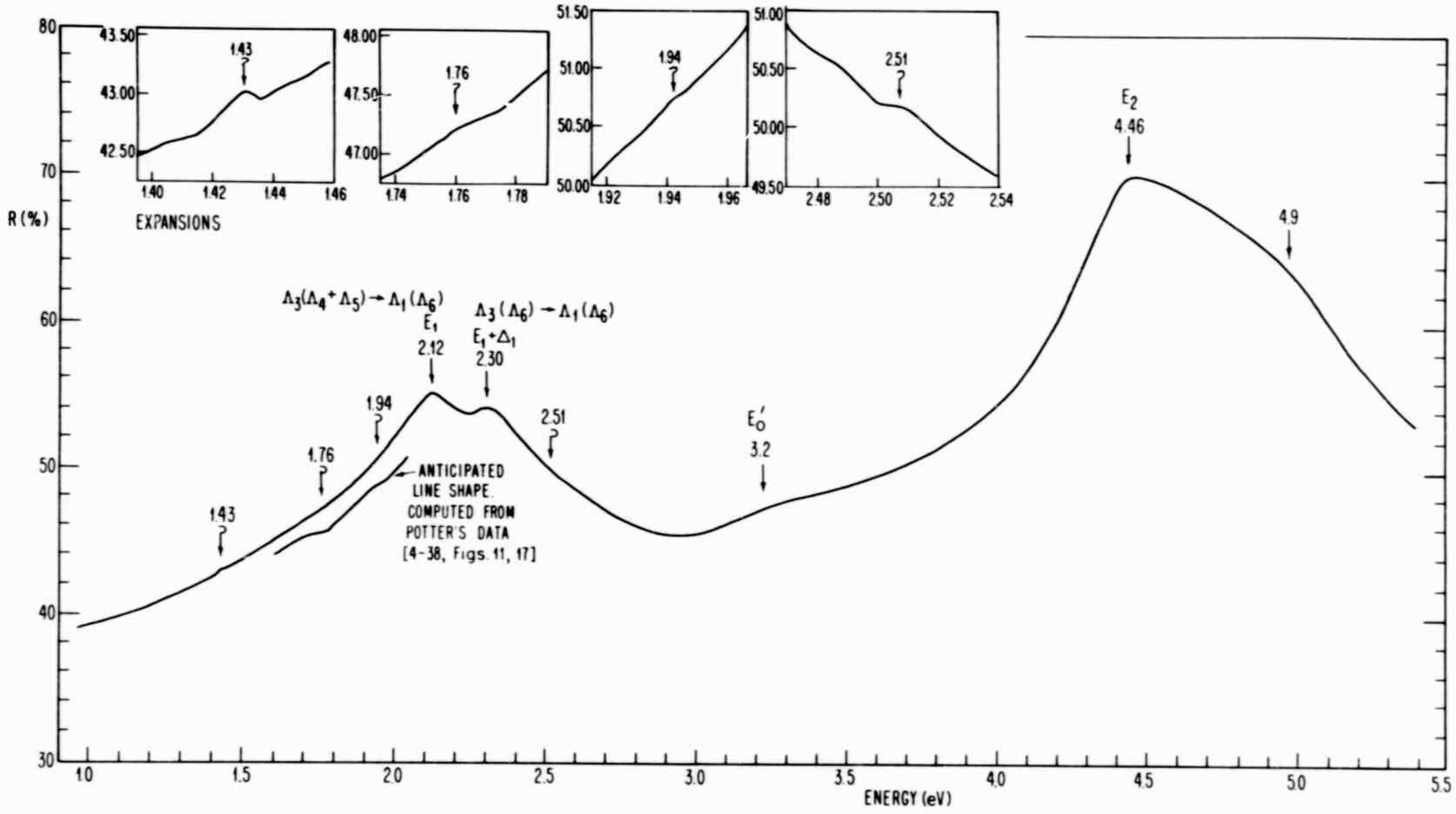

FIG. 4-6 REFLECTIVITY SPECTRUM OF GERMANIUM. TEMPERATURE 300°K. This drawing is a composite.

the effects of oxide films on the samples. Potter [4-38] using a type of reflection polarization technique, noted new structure in n and k at 1.74-1.94 eV and evidence of the Γ transitions corresponding to the minimum direct energy gap.

Other techniques have been applied to the same region originally examined by reflectivity. Workers have studied absorption in thin epitaxial films [4-39, 4-09] or in thinly ground samples [4-40]. Seraphin [4-41] pioneered electroreflectivity studies, which revealed new structure near 3.4 eV, and Cohen and Phillips [4-42] have analyzed the photoemission studies of Gobeli and Allen, relating the data to the pseudopotential band structure.

The results of these and other studies have been incorporated in the calculations of band structure already discussed. The major present difference among the band structures is in the energy of the $\Gamma_{25'} \rightarrow \Gamma_{15}$ transition and consequently in the identification of the optical structure observed near 3.2 eV. Pseudopotential and k·p models regard this energy as that of the transition, while the studies of Herman et al. suggest that this transition is closer to 2.7 eV.

2. The Reasons for Our Study of Germanium

We decided to study yet again the reflectivity of germanium for the following reasons:

(1) To determine R at low temperature over a range adequate to permit later a Kramers-Kronig analysis of the data. Most of the previous studies mentioned tended to examine the temperature dependence

of selected peaks only, and Potter's study gives n and k over a limited range. Our work at 80°K, well below θ_D = 350°K, reduces the broadening effects of phonon interactions on the reflectivity structure.

(2) To look for fine structure throughout the full energy range both at room and liquid nitrogen temperature.

(3) To look for the effects of magnetic field on the larger structural features in reflectivity.

3. Samples

The samples studied were all cut from a high quality n-type single crystal ingot.† The etch pit density was low, and the impurity density of $2 \times 10^{14}/cm^3$. was well below that found to cause peak energy shifts [4-36]. Samples of various orientations, necessary for the H field measurements, were cut from the ingot, ground, polished with .1 μ compound (Linde B) and then etched.‡ Samples intended for low temperature measurements were placed in the cryostat within minutes of the completion of the etch so as to minimize oxide film formation. They were mounted in a simple sample holder with a spot of glue at one end only, so as to minimize strain. Details of cryostat operation and problems are discussed in the section on gray tin. The effect of film formation is discussed in Sec. IV-D-2.

---

†The sample had a resistivity of 8 ohm-cm. and was received from Bell Laboratories.

‡CP-4 etch was used in most studies: 3 parts 50% HF, 5 parts 70% HNO_3, 3 parts $HC_2H_3O_2$ (glacial acetic), 8-10 drops of Bromine/50 cc. An iodine etch recommended by S. Groves [4-43] was tried since it was purported to give sharp structure: 100 cc. HNO_3, 50 cc. HF, 98 cc. Acetic (CH_3COOH), 12 cc. I_2 solution where the solution is 25 gm. I_2 in 1 liter Acetic acid. The removal rate is 1.5 mil/min.

4. Experimental Data and Their Interpretation

Figure 4-6 is a plot of the reflectivity of germanium at room temperature while Fig. 4-7 is that at liquid nitrogen temperature. (Note: the absolute values of R will not be as accurate as is claimed in the work of Donovan, Ashley and Bennett -- $\pm$.1%. We are subject to errors of $\pm$ 5% as described in Sec. IV-C-5-c.) Each point of interest is labeled in three ways. First, there is the energy of the transition as given by our data, placed above an arrow pointing to the peak. If the arrow shaft is a question mark, the structure was not seen under all conditions and may be suspect to the degree discussed in the text for that peak. The second label is the peak notation developed by Cardona and now in general use (e.g., E_2, E_0') [4-44]. This is a label for the reflectivity structure without reference to the region or regions of the Brillouin zone accounting for the structure. This notation is quite relevant since all diamond and zinc blende semiconductors show much the same reflectivity structure. Finally, there is the label describing the region of the Brillouin zone where this transition is felt to take place. Remembering the work of Kane, cited earlier, we note that these labels are often nominal, particularly in the case of large amplitude peaks. The transition labels will usually be quite accurate at the fundamental indirect and direct gaps, and perhaps for some of the smaller peaks.

The interpretation will be made in terms of the band structure of Cardona and Pollak [4-11], found in ref. [4-30] with spin-orbit splittings explicitly included. It is reproduced in our Figs. 4-8a and b.

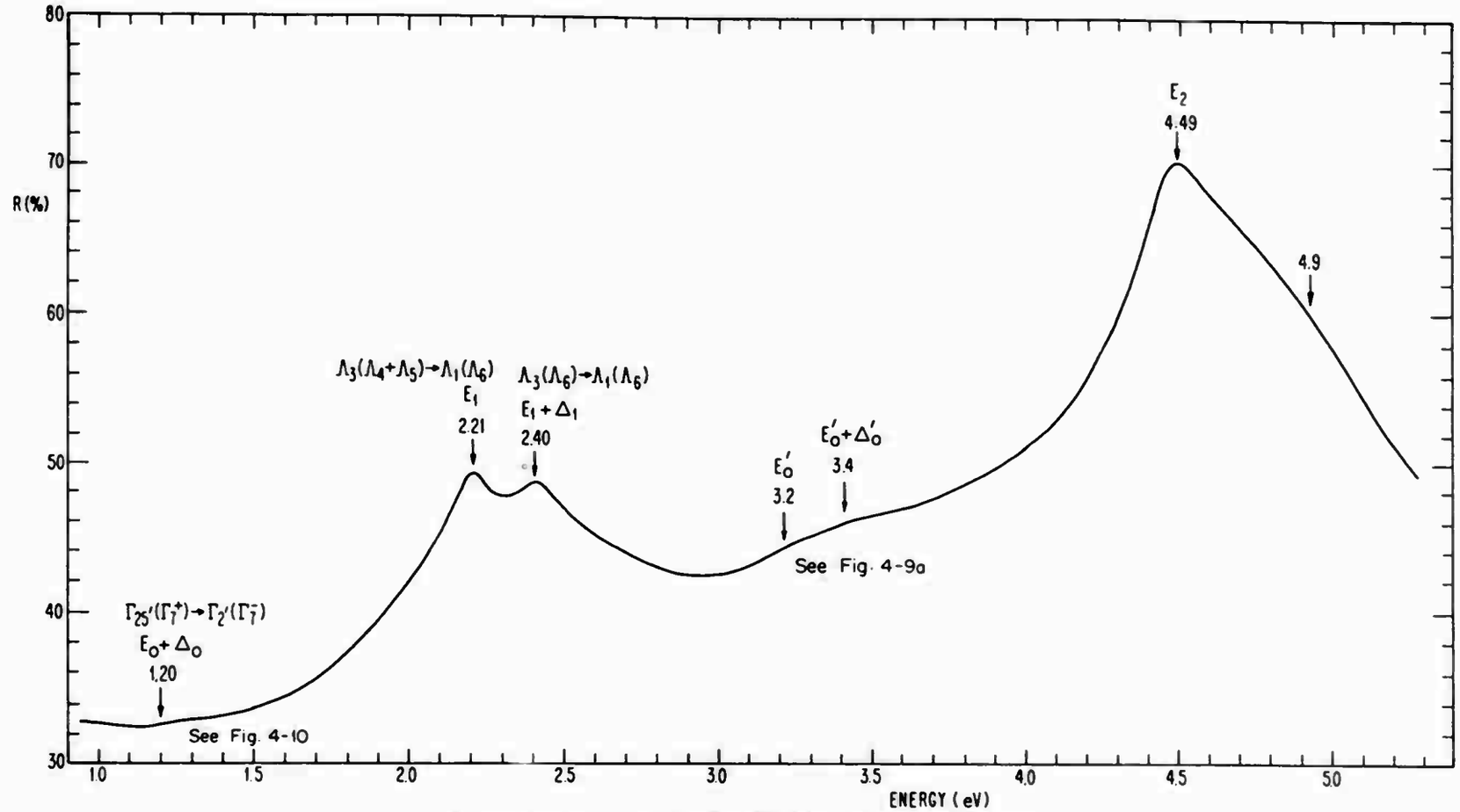

FIG. 4-7 REFLECTIVITY SPECTRUM OF GERMANIUM. TEMPERATURE 80°K

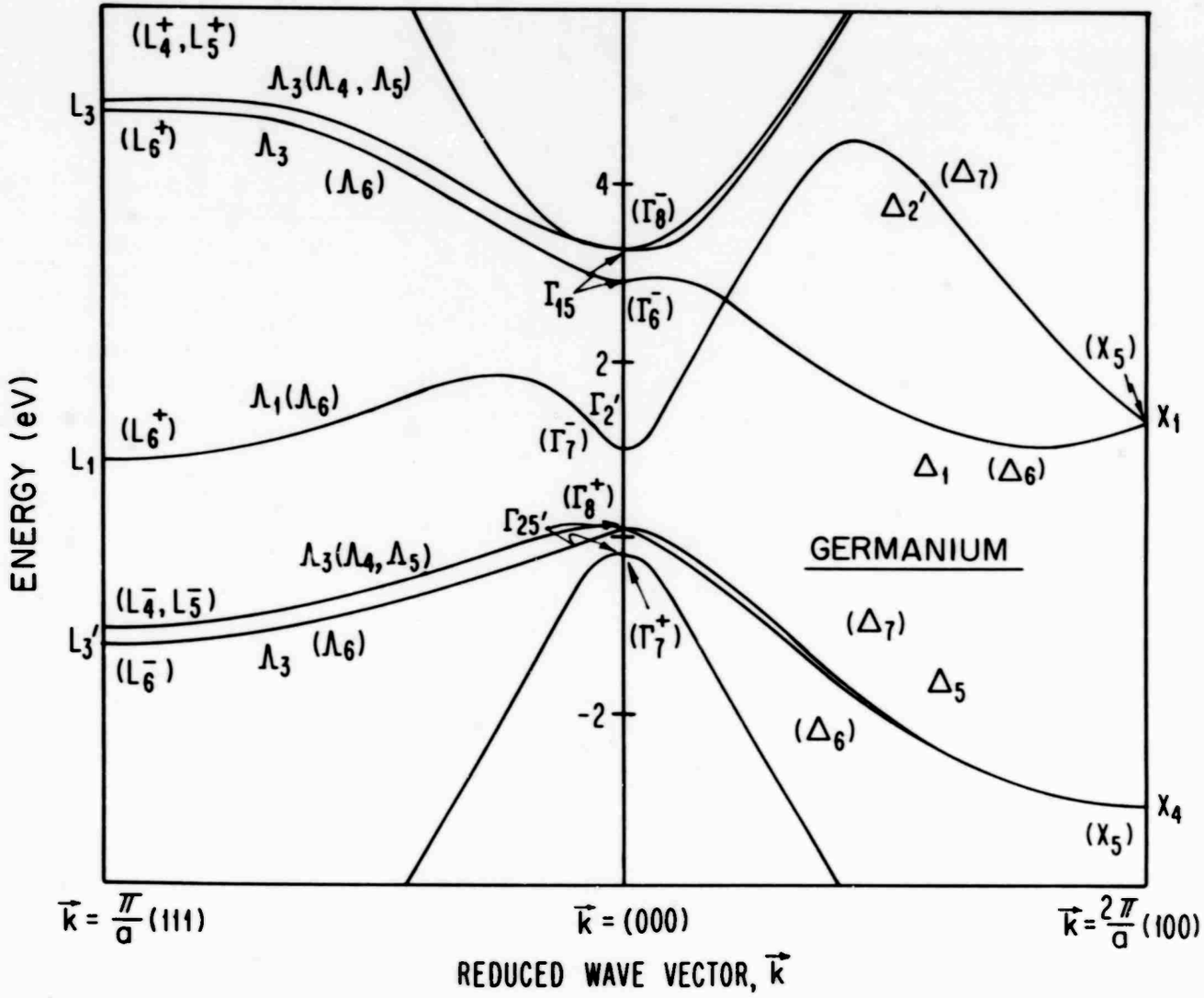

FIG. 4-8a ENERGY BANDS OF GERMANIUM ALONG THE Γ-L AND Γ-X LINES IN $\vec{k}$ SPACE, INCLUDING SPIN-ORBIT SPLITTINGS. From ref. [4-30, Fig. 2]

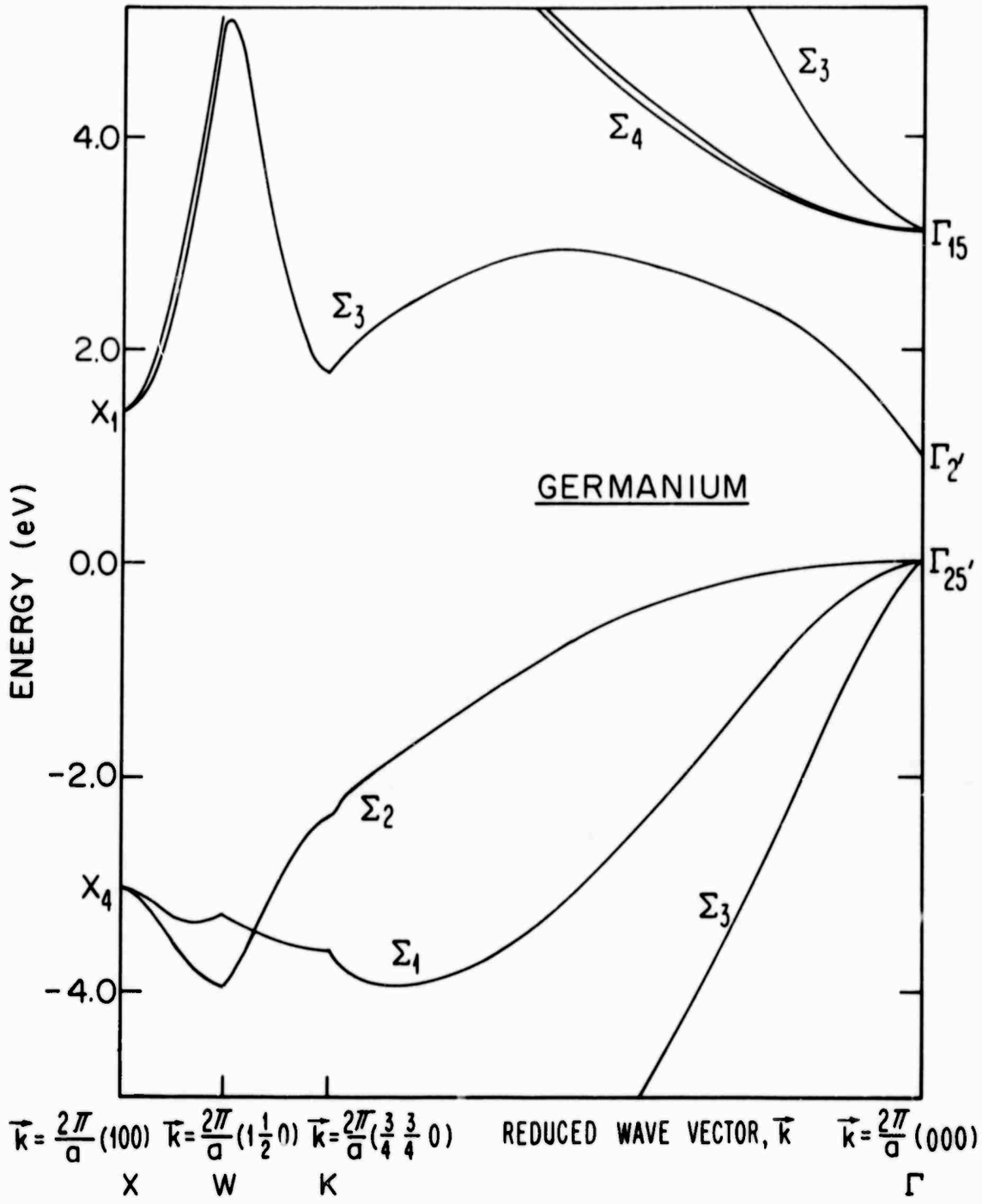

FIG. 4-8b ENERGY BANDS OF GERMANIUM ALONG THE X-W, W-K, AND K-Γ LINES. DOES NOT CONTAIN SPIN-ORBIT SPLITTINGS. From ref. [4-11, Fig. 4]. Σ notation corrected from ref. [4-02].

Reference will be made to the calculation of Herman et al. at appropriate points.

Before proceeding to a detailed discussion of the structure, we summarize our own discoveries: a shoulder in the E_2 peak, splitting of the 3.2 eV peak, and observation of structure in reflectivity at 1.76, 1.94, and 1.2 eV, the last due to a $\Gamma_{25'} \rightarrow \Gamma_{2'}$ transition.

a. Structure at 4.46 eV and at 4.9 eV(E_2). The 4.46 eV peak, which shifts to 4.49 eV at liquid nitrogen temperature (Figs. 4-6 and 4-7), is what is generally called the Σ-X peak [4-12] and is now felt, on the basis of Kane's work, to be made up of transitions from a number of regions of $\vec{k}$ space. The shoulder at 4.9 eV has not been reported before for germanium. When a similar shape was noted in indium antimonide for the E_2 peak, the peak was labeled X and the shoulder Σ by Phillips [4-01, p. 148] since transitions at these points were then thought to be the primary contributors. We will not apply these labels for three reasons. First, Kane's observations have made such identification suspect. Second, Dresselhaus and Dresselhaus [4-25, p. 668] state that there will generally be no critical points at X. Specifically, they find no critical points corresponding to the $X_4 \rightarrow X_1$ transition in germanium.† Third, electroreflectivity, with its narrow line width, often picks out critical points more strikingly than does straight reflectivity work; yet, neither the

†Like Kane, Dresselhaus and Dresselhaus find that the E_2 peak is made up of contributions from large regions of $\vec{k}$ space. The $\Sigma_2 \rightarrow \Sigma_3$ transitions and transitions along the L-U line (Fig. 4-1) are important.

$\Delta R/R$ work in germanium nor that in indium antimonide shows the twin peaks (one for each critical point) that we would expect on the basis of the reflectivity. On the other hand silicon, which shows a shoulder in its reflectivity at E_2 [4-45], shows a corresponding splitting in its electroreflectivity [4-30].

If the germanium 4.46 eV peak and its 4.9 eV shoulder were made up solely of the contributions from two critical points, such as the transitions $\Sigma_2 \rightarrow \Sigma_3$ and $X_4 \rightarrow X_1$, then we could expect both to exhibit $\Delta R/R$ structure. Their $\sim$.4 eV separation is wide enough that both should be resolved. Kane's work provides a clue as to why we might see structure in R that is not present in $\Delta R/R$ (as in the case of germanium), or alternatively, see structure in $\Delta R/R$ which is matched in R (as in silicon at E_2). The R peak and shoulder are the summed effect of transitions over large regions of the zone. The various transitions add a positive contribution to ϵ_2 regardless of whether the effective masses of the joint density of states are positive (M_0) or negative (M_3) or both, as in a saddle point (M_1, M_2). This is not so in electroreflectivity, where both the sign of the joint effective mass components selected by the applied electric field and the type of critical point determine the sign of $\Delta\epsilon_1$ and $\Delta\epsilon_2$ [4-46]. Masses of different sign from different regions of the Brillouin zone could result in the cancellation of the net $\Delta R/R$ signal at some energy (as in germanium at 4.9 eV), whereas, masses of like sign could result in an enhancement (as in silicon). This cancellation may be only partial, and a signal might be visible if special care were taken to minimize

the increasing noise level afflicting optical measurements above about 4.5 eV.†

Thus, on the basis of the combined electroreflectivity and reflectivity data, and also of Kane' studies in silicon, it is inadvisable at this point to identify the shoulder and peak in the E_2 structure in terms of specific Brillouin zone transitions.

Comparing Fig. 4-6 and Fig. 4-7, we see a sharpening of the 4.46 eV structure as the temperature is lowered. In making this comparison, we superpose the curves for the 80°K and 300°K runs in the region between the E_1 and E_2 peaks. There is a narrowing of less than .05 eV on the low energy side and of .1 eV or more on the higher.

There are at least two possible explanations for the narrowing which should be considered: (1) band spacing change, and (2) phonon broadening of the transition.

(1) The peak is made up of contributions from many parts of the zone which could have different temperature coefficients. Then the peak narrowing might result from a relative change of the band spacing so that those bands contributing to the peak become more

---

†Ghosh [4-47] claims to have seen evidence of both an M_1 and M_2 singularity in his $\Delta R/R$ data in the 4.2-4.5 eV range. We feel his identification is unwarranted for three reasons: (1) The $\Delta R/R$ data have not been reduced to $\Delta\epsilon_1$ and $\Delta\epsilon_2$. This is generally essential for accurate identification of the type of critical point. (2) He appears to assume that the only directions in $\vec{K}$ space which contribute to $\Delta R/R$ are those along which the E field of the light has a component. This seems incorrect to us. (3) The structural feature at 4.5 eV which he associates with an M_2 transition, decreases with increasing applied electric field, exactly counter to the predictions of the one-electron Franz-Keldysh theory [4-46, 4-48].

closely grouped in energy. An analogous difference in pressure coefficients has been noted by Herman et al. [4-02] in germanium where the $\Sigma_2 \rightarrow \Sigma_3$ and $X_4 \rightarrow X_1$ coefficients differ by a factor of 1.75. Unfortunately, when we consider actual temperature coefficients, this mechanism will not account for the peak behavior, for it suggests that the high energy side of the peak should move to higher energies rather than to lower as we observe.†

(2) The effect of phonons on broadening a given transition depends on the phonon population, determined by temperature, and on the over-all electron and phonon band structures. The latter determine the symmetry of those phonons which contribute and whether absorbed phonons will be as significant as emitted ones [4-49]. The broadening effect of phonons is particularly striking when one considers experiments displaying the electron-hole interaction; a sharp peak in absorption due to discrete excitonic levels in the direct gap of germanium is wiped out as the temperature is increased to room temperature [4-19]. In analogy the dramatic sharpening of some reflectivity peaks on cooling has been accounted for by appealing to quasi-stable discrete excitonic levels at M_1 and M_2 singularities [4-01]. Although these levels probably do not exist [4-21, 4-20], the electron-hole interaction can accentuate a peak in comparison

---

†The top of the E_2 peak has the coefficient -1.8×10^{-4} eV/°C, a value less than the coefficient $\sim -4.0 \times 10^{-4}$ eV/°C which is usually found (positive coefficients occur only rarely). If the bands contributing to the higher side of the E_2 peak have this more common order of coefficient, they would move to higher energies faster than the peak as temperature is lowered, leading to broadening.

with its shape predicted by the one-electron theory (Figs. 4-3 and 4-4). Perhaps the true explanation of the sharpening of our peak and of others lies in a proper consideration of the combined effects of phonons and the electron-hole interaction.

b. Structure at 3.2 eV (E_0'); 3.4 eV ($E_0'+\Delta_0'$). The 3.2 eV peak in Fig. 4-6 is seen to split into a doublet at 3.2 and 3.4 eV in the low temperature scan shown in Fig. 4-7. Figure 4-9 contains an expanded view of this structure as well as other experimental evidence from this energy range. The photoemission work of Gobeli and Allen [4-42] shows a strong shoulder at 3.25 $\pm$ .05 eV and a weak shoulder at 3.55 $\pm$ .05 eV, while more recent electroreflectivity work of Cardona et al. [4-30] shows bumps whose average position is 3.33 and 3.15 eV (Figs. 4-9b and c). Allowing for experimental error, these three experiments agree in suggesting a doublet with a splitting of about .2 eV, but there are a number of discrepancies in the three remaining electroreflectivity experiments. Seraphin [4-41], Ghosh [4-50], and Shaklee, Cardona, and Pollak in their original work [4-51] show very different results (Figs. 4-9d, e, and f).

It is just this energy region around 3.3 eV where the dispute between the band model of Herman et al. and the semi-empirical k·p and pseudopotential models is most marked. For the moment let us consider the structure from these six experiments in terms of the k·p bands, turning later to the first principles bands.

Originally Ehrenreich, Philipp, and Phillips [4-52] identified the reflectivity structure at 3.2 eV in germanium and at 3.5 eV in

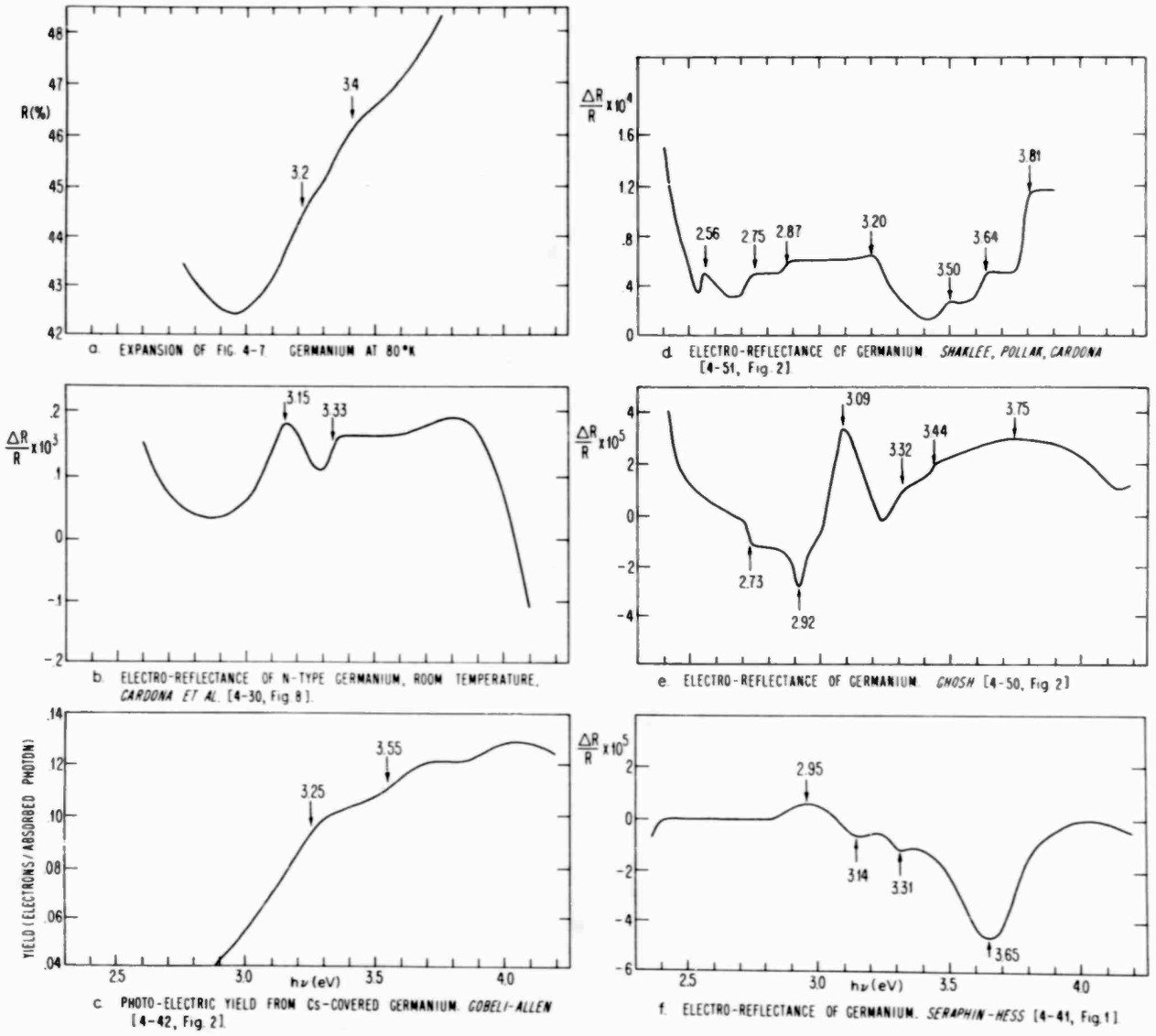

FIG. 4-9 EXPERIMENTAL DATA FOR GERMANIUM NEAR 3.2 eV

silicon as due to the $\Gamma_{25'} \rightarrow \Gamma_{15}$ transition. The idea that the silicon structure might arise from transitions along Δ and not at Γ was developed independently by Gerhardt [4-16] on the basis of uniaxial stress measurements and by Brust [4-15] on the basis of a detailed pseudopotential calculation. Later Cardona et al. [4-30] suggested that the $\Delta_5(\Delta_7) \rightarrow \Delta_1(\Delta_6)$ and $\Delta_5(\Delta_6) \rightarrow \Delta_1(\Delta_6)$ transitions, which have a splitting of .17 eV in the k·p model, might account for the electroreflectivity structure in germanium. This value fits the experimental doublet splitting of .18 eV found in the later experiments [4-30]. Gerhardt's work in silicon and some comments of Cardona et al. in ref. [4-30] can be combined to give additional support to the idea of a Δ transition in germanium. In studying germanium-silicon alloys, Cardona et al. have noted the equivalence of the 3.4 eV peak in silicon and the 3.2 eV peak in germanium, suggesting that both have the Δ symmetry found in silicon.

The left half of Table 4-1 is a listing of the k·p energies associated with the $\Gamma_{25'} \rightarrow \Gamma_{15}$ and $\Delta_5 \rightarrow \Delta_1$ transitions, the spin-orbit splittings, and the optical selection rules (Sec. V-A-1-a, and 2-a) with and without electric field. The right half lists the energies of the structural features in a number of experiments. The inferred values of spin-orbit splittings are in parentheses.

Six of the seven experiments support the concept of a spin-orbit split $\Delta_5 \rightarrow \Delta_1$ transition.

Only the first studies of Shaklee, Pollak, and Cardona are consistent with the calculated $\Gamma_{25'} \rightarrow \Gamma_{15}$ transition energies. The calculated spin-orbit splittings are close to experimental splittings, and the missing peak, $\Gamma_7^+ \rightarrow \Gamma_6^-$, is forbidden in reflectivity and hence might be weak in electroreflectivity. The Ghosh[†] and Seraphin data cannot be identified in terms of the computed $\Gamma_{25'} \rightarrow \Gamma_{15}$ energies, as can be seen in the table; there are no consistent spin-orbit splittings.

There is a fair amount of structure which is not accounted for in this model. It is listed in the table.

We see then that there are conflicting data arising in the $\Delta R/R$ studies. Some are consistent with Γ transitions, some with Δ, and some fit in with no band features.

Associated with an electroreflectivity peak corresponding to a transition at a critical point, there are subsidiary ripples [4-46], known as satellites, which are a natural consequence of the Franz-Keldysh effect, the name given to the effect of an electric field on optical transitions. Varying experimental conditions, such as AC and DC field strength,[‡] doping, and the method of field application, can modify the structure. For instance by just varying the AC level, this

---

[†]In later work [4-47] Ghosh reports new data in the 2.5-3.6 eV range which differs somewhat from his original report. By qualitatively fitting these new data with the peak and first satellite of one M_1 and four M_0 edges, he sees evidence of one $\Delta_5 \rightarrow \Delta_1$ and four $\Gamma_{25'} \rightarrow \Gamma_{15}$ transitions. However, the experimental spin-orbit splitting of .13 eV for Γ_{15} is much less than the computed value of .36 eV.

[‡]The reason for the broadening in the $\Delta R/R$ signal with increasing field has been discussed recently by Aspnes et al. [4-53]. The dielectric constant, ϵ_2, with field is shown to be a convolution integral over $\vec{K}$ space of ϵ_2 without field and an Airy integral: increasing the electric field results in more and more of $\vec{K}$ space contributing to the integral.

TABLE 4-1 THE COMPARISON OF THE ENERGIES OF EXPERIMENTAL STRUCTURE AND THE ENERGIES OF CERTAIN TRANSITIONS GIVEN BY THE K·P MODEL FOR GERMANIUM

k·p Model Energies					Experimental Energies (inferred splittings in parentheses)						
Transition	Allowed in R?	Allowed with E Field?	Energy in eV	Spin-orbit Splitting	R		Photo-emission	ΔR/R			
					This work	Donovan et al. [4-37]	Gobeli-Allen [4-42]	Cardona et al. [4-30]	Seraphin et al. [4-41]	Ghosh [4-50]	Shaklee et al. [4-51]
$\Gamma_{25'} \rightarrow \Gamma_{15}$											
$\Gamma_7^+ \rightarrow \Gamma_8^-$	Yes		3.48	0.29							3.50 (0.30)
$\Gamma_8^+ \rightarrow \Gamma_8^-$	Yes		3.19	0.36							3.20 (0.32)
$\Gamma_7^+ \rightarrow \Gamma_6^-$	No	Yes	3.12								Probably weak
$\Gamma_8^+ \rightarrow \Gamma_6^-$	Yes		2.83								2.88
$\Delta_5 \rightarrow \Delta_1$											
$\Delta_6 \rightarrow \Delta_6$	Yes		3.31	0.17	3.4 (0.2)		3.55 ±.05 (.3 ± .1)	3.33 (0.18)	3.31 (0.17)	3.32 (0.23)	
$\Delta_7 \rightarrow \Delta_6$	Yes		3.14		3.2	3.2	3.25 ±.05	3.15	3.14	3.09	
Unaccounted for					2.51	2.47			3.65	3.75	3.81
									2.95	3.44	3.64
										2.95	2.75
										2.73	2.56

TABLE 4-2 THE COMPARISON OF THE ENERGIES OF EXPERIMENTAL STRUCTURE AND THE ENERGIES OF CERTAIN TRANSITIONS GIVEN BY THE FIRST PRINCIPLES BAND MODEL FOR GERMANIUM. SPIN-ORBIT SPLITTINGS ARE TAKEN FROM REF. [4-30]

First Principles Model Energies					Experimental Energies (inferred splittings in parentheses)						
Transition	Allowed in R?	Allowed with E Field?	Energy in eV	Spin-orbit Splitting	R		Photo-emission	ΔR/R			
					This work	Donovan et al. [4-37]	Gobeli-Allen [4-42]	Cardona et al. [4-30]	Seraphin et al. [4-41]	Ghosh [4-50]	Shaklee et al. [4-51]
$\Gamma_{25'} \rightarrow \Gamma_{15}$											
$\Gamma_7^+ \rightarrow \Gamma_8^-$	Yes		3.01	0.29							
$\Gamma_8^+ \rightarrow \Gamma_8^-$	Yes		2.72	0.36						2.73	2.75
$\Gamma_7^+ \rightarrow \Gamma_6^-$	No	Yes	2.65								2.56
$\Gamma_8^+ \rightarrow \Gamma_6^-$	Yes		2.36		2.51	2.47					
$\Delta_5 \rightarrow \Delta_1$											
$\Delta_6 \rightarrow \Delta_6$	Yes		~3.1		3.2	3.2		3.15	3.14	3.09	
$\Delta_7 \rightarrow \Delta_6$	Yes		~2.9						2.95 (0.19)	2.92 (0.17)	2.88
Unaccounted for					3.4		3.55	3.33	3.65	3.75	3.81
							3.25		3.32	3.44	3.64
										3.32	3.50
											3.20

author has changed the shape of the $\Delta R/R$ structure associated with each of the Λ peaks in germanium from a single positive to a negative and positive peak containing additional structure (Fig. 4-21).

Reflectivity measurements are not complicated by satellite structure. Our reflectivity data show only a doublet and no evidence of other features such as the strong peak around 3.65 eV observed in Seraphin's data. This is evidence, in addition to the study by Gobeli-Allen[†] and the later work of Cardona et al., that the structure seen corresponds to transitions along Δ (provided we interpret the structure in terms of the k·p bands). Some of the remaining structure is very possibly extraneous in the senses discussed in the paragraph above.

In conclusion, our structure at 3.2 and 3.4 eV is consistent with the k·p model, but a considerable body of data from other experiments is not.

c. Structure at 2.51 eV? Herman et al. feel quite strongly that the $\Gamma_{25'} \rightarrow \Gamma_{15}$ transitions should be centered at 2.7 eV. Is there any experimental evidence to support this? Donovan, Ashley, and Bennett have seen a very weak shoulder at 2.47 eV in reflectivity, although Potter, using samples prepared by Donovan, does not report any structure here in his very careful and sensitive polarization studies.

Our work showed no evidence with the following exception: in one sample, in one run only, we saw the small bump at 2.51 eV shown

[†]Cohen and Phillips originally interpreted the structure measured by Gobeli and Allen as due to $\Gamma_{25'} \rightarrow \Gamma_{15}$ transitions.

in Fig. 4-6. This would have been rejected as illusory except for the fact that this was the same run where we saw the L point structure (Sec. IV-B-4-f) predicted by Potter's polarization studies; the L point structure was also hard to reproduce. This structure at 2.47-2.51 eV may arise from the $\Gamma_8^+ \rightarrow \Gamma_6^-$ transition in the first principles bands as indicated in Table 4-2.

Ludeke and Paul [4-54] have studied the effects of an AC uniaxial stress on the transmission of thin germanium films. Their data show a bump at 2.7 eV in the $\Delta I/I_0$ curves for light polarized perpendicular to the strain axis. The character of this bump is uncertain, however, since it does not appear in the more significant curves showing Δn, Δk, $\Delta\epsilon_1$, and $\Delta\epsilon_2$.

d. Conclusions on the Different Band Models. In Table 4-2 we list the same structural features found in Table 4-1, this time in relation to the energies found in the bands calculated by Herman et al. They have not published spin-orbit splittings so we have adjusted the energies using the splittings derived by Cardona et al. [4-30]. As in our comparison with the k·p bands, some of the structure fits in with Δ transitions, some with Γ, and much is unidentified.

The k·p model does not account for the weak structure in the 2.5-2.9 eV range, while the model of Herman et al. fails to account for the comparatively stronger structure in the 3.2-3.7 eV range. In either case the troublesome structure might arise at general points in the zone not shown in the usual $E(\vec{k})$ plots along symmetry directions in $\vec{k}$ space. Over-all the k·p model is a somewhat better fit in the

entire 2.5-3.6 eV range, but this could well be a result of the assumptions used to determine the parameters employed in the calculation.

These discrepancies will be resolved only after further experimental work giving consistent results. Examination of the reflectivity at helium temperature in the range 2.5-3.6 eV might help in sharpening the 3.2, 3.4, and 2.5 eV structure and in determining if there is any other. While it is desirable to make measurements which will give data on the symmetries in $\vec{k}$ space of the various transitions, it is not clear what techniques will be best. AC uniaxial stress measurements in transmission [4-54] and reflection [1-15] have generally poor resolution and fail to display the 3.2 eV splitting. Probably further refinement of electroreflectivity techniques, coupled with further work on $\Delta R/R$ line shapes, will point the way. What is desirable in such a measurement is minimum line width. Ludeke and Paul [4-55] have noted that a technique for field application using a sandwich comprised of the sample, vapor-deposited quartz, and vapor-deposited tin chloride gives line widths at room temperature comparable to those given by the electrolytic technique. The sandwich can be cooled to the temperature of liquid helium while the electrolytic package freezes at around -100°C. Consequently, upon cooling, the sandwich technique gives significantly improved line widths. As an example consider the ratio of the $\Delta R/R$ line widths in CdTe at 3.5 eV--line width occurring in the electrolytic technique at 300°K: sandwich line width at 300°K: sandwich line width at 6°K = 4:3:1.

e. Structure at 2.12 eV (E_1); 2.30 eV ($E_1 + \Delta_1$). We have noted nothing new in the peaks. We have used the size of the dip between the two peaks (distance from the valley to the top of $E_1 + \Delta_1$) as a measure of the quality of surface preparation. The dip of .25% compares well with the Donovan, Ashley, and Bennett value of .3%. Potter's samples showed a similar dip, so that our sample appears to be comparable in the quality of its surface and should therefore display the other fine structures in reflectivity seen by Potter.

f. Structure at 1.76 eV; 1.94 eV. Potter [4-38] in making polarization measurements on reflected light at the pseudo-Brewster angle, noted structure at 1.74 and 1.94 eV at room temperature and at 1.84 and 2.04 eV at 120°K. He has attributed these to the $L_{3'} \rightarrow L_1$ transitions, partly on the basis of shape and partly on the basis of the equality of their temperature coefficients with those of the Λ peaks. Using his experimental parameters (his Fig. 11), we have plotted in Fig. 4-6 the expected shape and size of the two shoulders in reflectivity. The lower energy shoulder deviates from a smooth line by .5%; the upper, by .3%. Both changes should be large enough to be seen easily.

Nevertheless, they proved very difficult to find and were seen conclusively in only one sample (albeit on different occasions). As seen in Fig. 4-6, they are much smaller than predicted. Using the temperature coefficients implied by Potter's measurements made at 120°K and 300°K, we see that the shoulders should occur at 1.86 and 2.06 eV at 80°K. No evidence was found of them at this temperature.

We thought that, since the quality of our surface seemed comparable to Potter's, the L point peaks should be of comparable size as well. Although this was not borne out in practice, smaller structure found very near the same energies and inferred to correspond to Potter's structure gives confirmation to his results.

It is possible to suggest a reason for the difference in magnitude between the L peaks in our and Potter's data and the agreement at Λ. Let us assume that the electropolishing used by Potter results in less surface damage than is caused in our technique of sample preparation. This is certainly possible since the Donovan, Ashley, and Bennett electropolished samples gave some of the sharpest structure observed for germanium. Surface damage results in a distortion of the lattice constant, a, and in turn the energy bands will be shifted, as we know from the measurements of pressure coefficients and deformation potentials (the latter is dE_g/da). The shift will vary from one point to another on the sample surface as the distortion varies.

In particular, point $L_1(L_6^+)$ will assume a range of values. Then the lifetime of an electron in that state, formerly long, since the state was the minimum of the conduction band, will decrease since there will be lower energy states (L_6^+ states at other spatial points) into which the electron can scatter. The decreased lifetime will result in broadening of the transition shoulder which will become harder to discern. Other transitions, such as that at Λ, will be affected less since the excited conduction band state already has many states into which to scatter.

If this analysis is correct, it reinforces the claim of Donovan, Ashley, and Bennett to having found a superior method of sample surface preparation in the electropolishing technique.

A different determination of the L point energies is found in the work of Ghosh [4-50]. His reasoning, based on line shape, is given in great detail in a later work [4-47]. He concludes that shoulders seen in certain instances in the electroreflectivity spectrum at 2.05 and 2.24 eV are due to M_0 singularities, presumably the $L_{3'} \rightarrow L_1$ transitions. His argument is certainly plausible, but we feel that two other line shape phenomena, possibly operating together, should be considered as alternatives.

(1) Experimentally [4-30, Figs. 32, 33, 35-37], the peaks in $\Delta\epsilon_1$ and $\Delta\epsilon_2$ are displaced energetically by up to .05 eV, although theoretically they coincide. In careful work a splitting could be noted from this effect. The shoulder might be such a splitting merged into the main peak by broadening.

(2) Satellites are predicted theoretically, and can be studied in detail [4-56, 4-46]. At an M_1 critical point satellites can exist either above or below the energy gap depending on the direction of the electric field and the joint effective mass values. When we sum the effect of the eight Λ critical points, we can get satellites on both sides of the gap. It is of interest here that Ghosh did not see the shoulders in all crystal orientation [4-47, p. 11]. (A major difficulty with using this mechanism to explain the shoulder is that the

low energy satellites are probably weaker than those on the high energy side, due to the probable sizes of the transverse and longitudinal masses at Λ.)

g. Structure at 1.43 eV. The bump at 1.43 eV (Fig. 4-6) was found in one sample on a number of occasions during room temperature measurements, although not in low temperature runs. One such occurrence was the run in which the data corroborating Potter's L point discoveries were found.

Thinking only in terms of energy differences, the transition $L_3'(L_6^-) \rightarrow \Gamma_{25}'(\Gamma_8^+)$ = 1.54 eV or $L_3'(L_4^-,L_5^-) \rightarrow \Gamma_{25}'(\Gamma_8^+)$ = 1.35 eV. The objections to this identification are manifold, however. First, no similar transition, separated by the spin-orbit splitting of .19 eV, was found. Next, the only way in which this transition could occur is if empty states at Γ_8^+ were created by thermal excitation. Very few would be created in this way since our sample is intrinsic and the few impurities are n-type. Finally, the transition is indirect. The matrix elements of such transitions are usually an order of magnitude weaker than those in direct transitions. Thus, we expect this transition to be very weak in our sample since there are few states available and the oscillator strength is low.

However, since there seems to be no other source for the transition in terms of the band model, it would be interesting to look at the reflectivity of a highly doped p-type sample in this region. The dopant should be chosen to minimize the ionization energy, and the operating temperature set low enough so that scattering can be

reduced consistent with complete ionization of the impurity. Under these circumstances we could increase the density of empty final states at Γ_8^+.

h. Structure at 1.2 eV ($E_0 + \Delta_0$). Potter, in addition to seeing the L point transitions in his polarization measurements, was able to see the transitions at the minimum direct gap $\Gamma_{25'}(\Gamma_8^+) \rightarrow \Gamma_{2'}(\Gamma_7^-)$ and at the associated spin-orbit split gap $\Gamma_{25'}(\Gamma_7^+) \rightarrow \Gamma_{2'}(\Gamma_7^-)$. These transitions were seen at both 300°K and 120°K. The $\Gamma_{25'}(\Gamma_7^+) \rightarrow \Gamma_{2'}(\Gamma_7^-)$ transition at liquid nitrogen temperature is within the spectral range of our system. The shoulder should occur at about 1.175 eV = 1.055 μ. In addition to being seen in these polarization measurements, this gap has been observed in absorption [4-57] and electroreflectivity [4-58, 4-59].

It was indeed seen as indicated in Fig. 4-7. Figure 4-10 contains a number of curves in the region of the transition. The first is a plot of the expected structure based on Potter's data at 120°K. The second and third are room temperature and liquid nitrogen temperature runs in one sample prepared with the CP4 etch, while the fourth and fifth are similar runs in another sample prepared with the iodine etch. In both samples we see the smooth descent at room temperature transformed to a shoulder at liquid nitrogen temperature, although the size of the shoulder is larger (.2%) in the second than in the first (.1%) sample. The second sample's structure approximates that predicted by Potter's data.

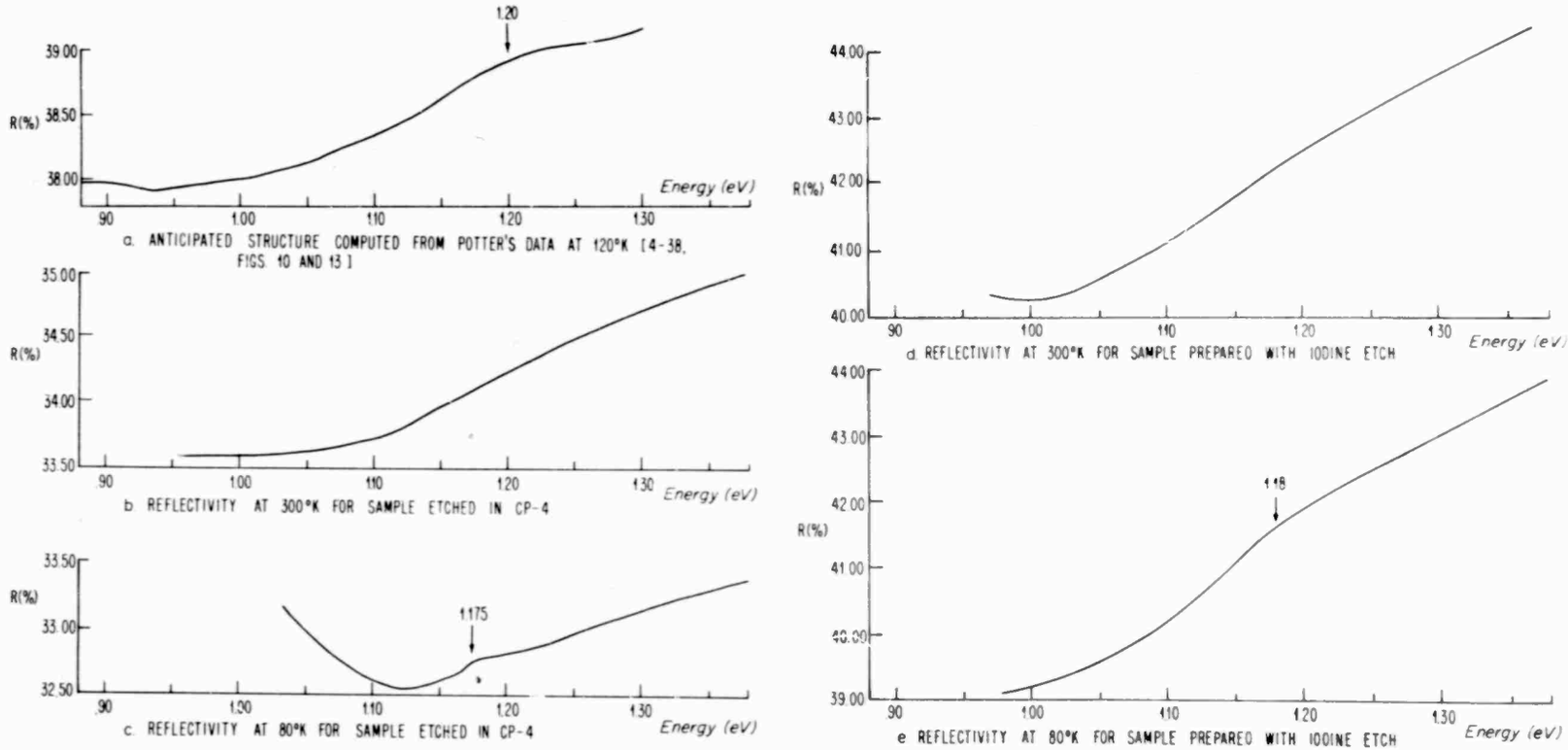

a. ANTICIPATED STRUCTURE COMPUTED FROM POTTER'S DATA AT 120°K [4-38, FIGS. 10 AND 13]

b. REFLECTIVITY AT 300°K FOR SAMPLE ETCHED IN CP-4

c. REFLECTIVITY AT 80°K FOR SAMPLE ETCHED IN CP-4

d. REFLECTIVITY AT 300°K FOR SAMPLE PREPARED WITH IODINE ETCH

e REFLECTIVITY AT 80°K FOR SAMPLE PREPARED WITH IODINE ETCH

FIG. 4-10 STRUCTURE IN THE REFLECTIVITY OF GERMANIUM ARISING FROM THE $\Gamma_{25}'(\Gamma_7^+) \rightarrow \Gamma_2'(\Gamma_7^-)$ TRANSITION

Thus, despite many claims in the past to the contrary, it is possible to see the effect of the fundamental gap in simple reflection measurements, provided a high amplitude resolution system is employed.

C. GRAY TIN

1. The Gray Tin Energy Bands

Gray tin (α-Sn)[†] occupies a unique position in the family of semiconductors. Although it lies in the group IV column of the periodic table with diamond (carbon), silicon, and germanium, its peculiar band structure makes it a semi-metal. This remarkable discovery was made by Groves and Paul [4-60] while attempting to account for the pressure dependence of the conductivity and of the Hall coefficient in gray tin. If one looks at the band structure of germanium in Fig. 4-8a and of gray tin in Fig. 4-11b, he can follow the changes in the normal band configuration of germanium which were postulated by Groves and Paul in their α-Sn model. Imagine for the moment that the energy band states at Γ ($\vec{k} = 0$) in germanium are disconnected from the $\vec{k} \neq 0$ values. Then Γ_7^- (Γ_2, in the single group notation) is moved downward between the two $\Gamma_{25'}$ states--Γ_8^+ (a double state) and Γ_7^+. The two states at Γ_8^+ remain tied together. On the basis of k·p perturbation theory the upper of the two states at Γ_8^+ (the one connecting to L_4^-, L_5^- in germanium) is unaffected by the Γ_7^-

[†]Gray tin is known as α-Sn and is distinguished from β-Sn, the normal metallic phase for tin. α-Sn is stable only below 13°C.

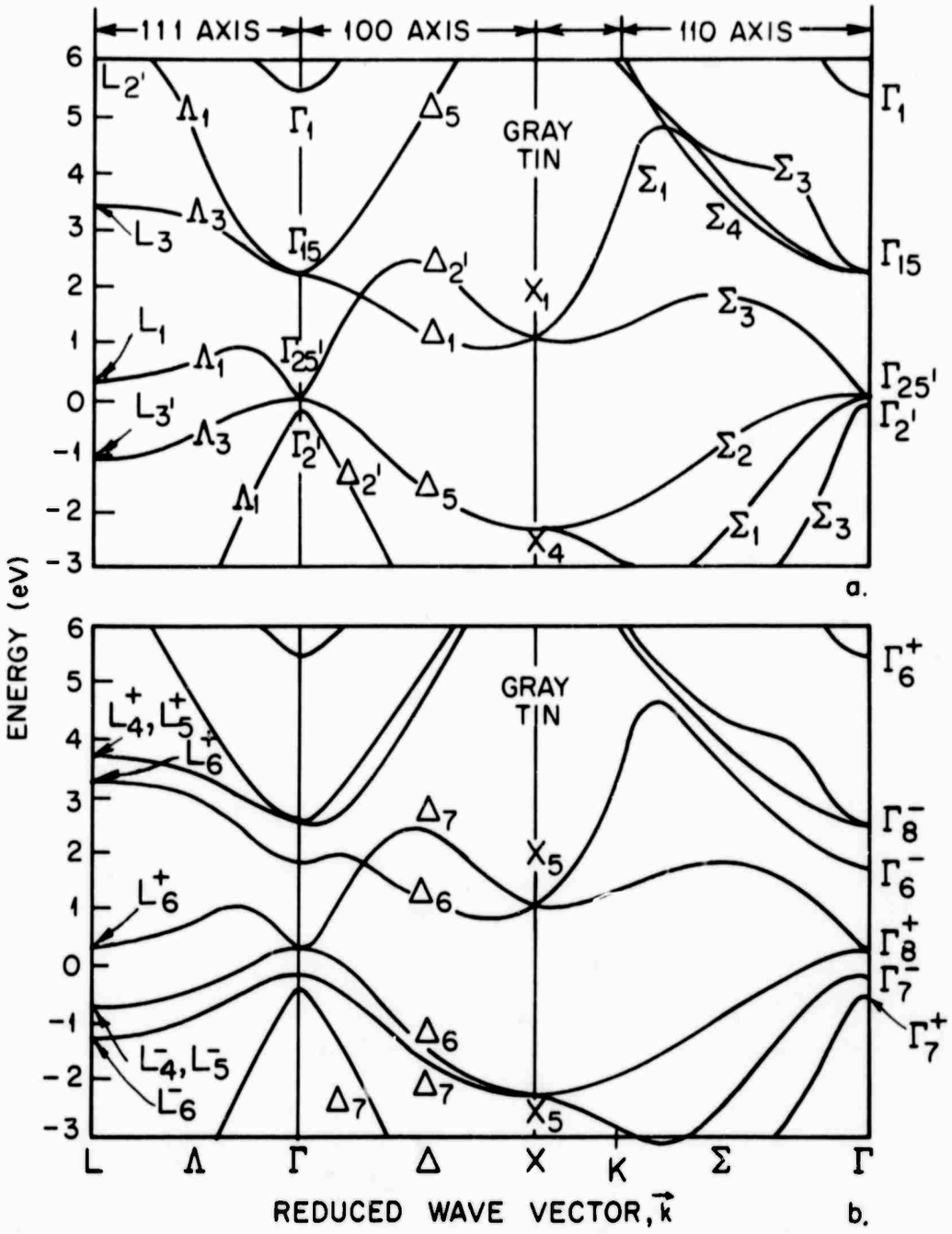

FIG. 4-11 ENERGY BANDS OF GRAY TIN ALONG THE Γ-L, Γ-X, X-K, AND K-Γ LINES IN $\vec{k}$ SPACE. a. SINGLE GROUP BANDS. b. DOUBLE GROUP BANDS. From ref. [4-27, Fig. 2]. (The position of the missing K point has been determined and added to original drawing after consulting [4-24]. Λ labels have been added.)

change, while the lower one is now curved upward. Meanwhile, the relative positions of the states at the edge of the zone (e.g., at the L and X points) have not been rearranged. By considering the group theoretical compatibility (or connectivity) relations, Groves and Paul [4-61] showed that Γ_7^+, Γ_7^- and Γ_8^+ states joined with the L and X states via energy bands of the general shape and with the symmetry shown in Fig. 4-11. These compatibility relations establish the consistency of the symmetry relations of those various parts of the Brillouin zone connected by the bands.

The interesting consequence is that the topmost valence band is the $L_4^-, L_5^- - \Gamma_8^+ - X_5$ band ($L_3' - \Gamma_{25}' - X_4$ band in single group notation) while the lowest conduction band is the $L_6^+ - \Gamma_8^+ - X_5$ band ($L_1 - \Gamma_{25}' - X_1$ in the single group). Their separation at Γ is zero regardless of changes in temperature or hydrostatic pressure and the resultant material is a perfect semi-metal.

The Groves-Paul work established the zero energy gap at Γ_8^+ and the position of L_6^+ at .08 eV above Γ_8^+. Estimating the Γ_7^- position from effective mass data and Γ_7^+ from atomic spin-orbit splittings, the bands were then sketched in.

The bands shown in Figs. 4-11 and 4-12 are more extensive than those of the Groves-Paul original model. Figure 4-12 has been made on the basis of k·p perturbation theory [4-28] using additional data from reflectivity and electroreflectivity measurements. Figure 4-11 shows the bands from the first principles calculation of Herman et al.

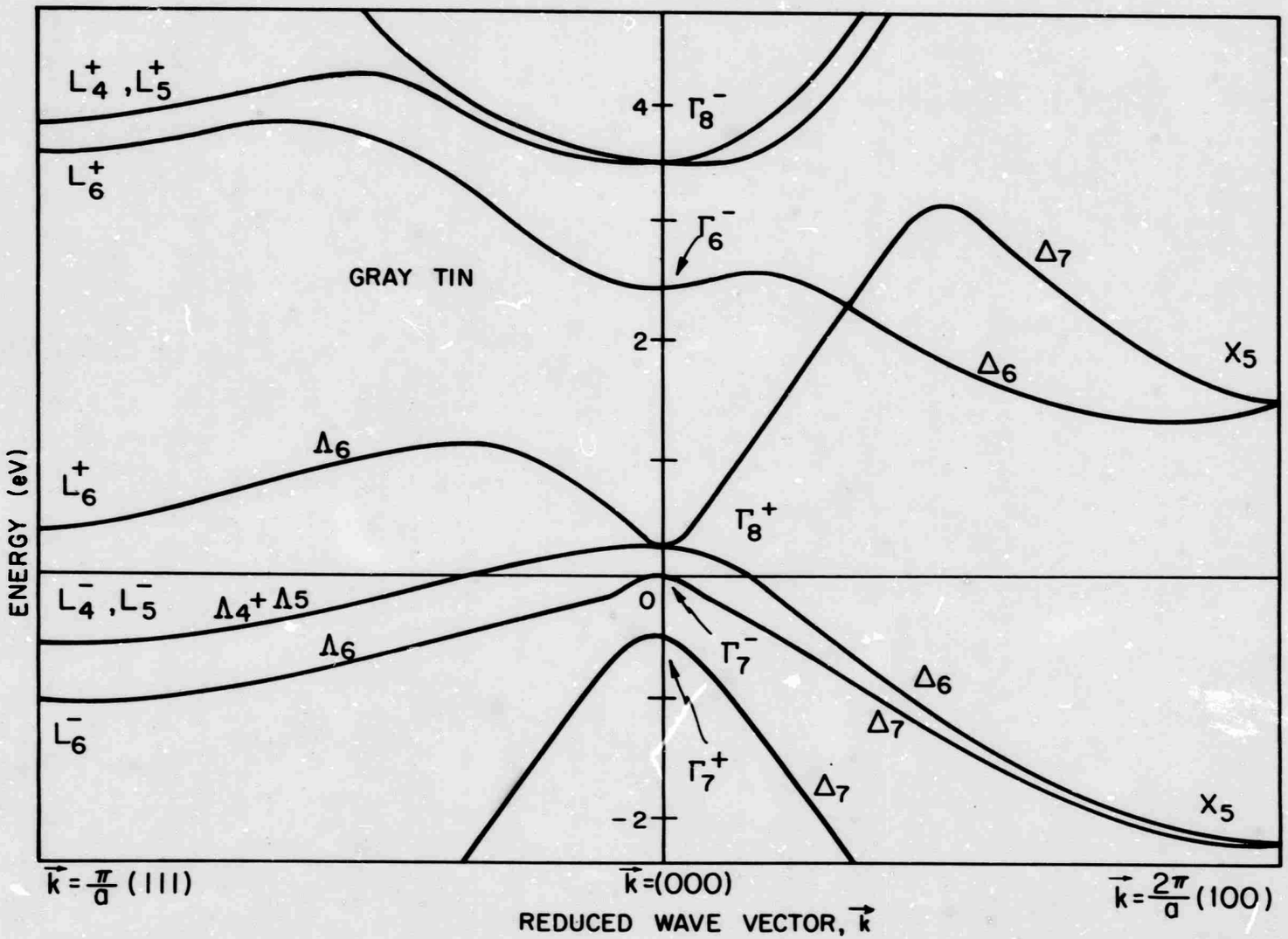

FIG. 4-12 DOUBLE GROUP ENERGY BANDS OF GRAY TIN ALONG THE $\Gamma-L$ AND $\Gamma-X$ LINES IN $\vec{k}$ SPACE. From ref [4-28, Fig. 2]. (Δ and Λ labels have been added.)

[4-27 and 4-02] in which they purport to use only those energy differences firmly supported by direct experiment. Within that framework this should include only the zero and .08 eV band gaps of Groves-Paul cited in the paragraph above and two effective masses. But Herman et al. use the Groves-Paul estimated positions of Γ_7^- and Γ_7^+ in addition to the .08 gap. This is not serious in practice for the resultant errors in energy estimates will probably be less than .1 eV.†

In considering the structure we observed in our α-Sn measurements, we shall make reference to both band models. We can expect differences since the $\Gamma_{25'} \rightarrow \Gamma_{15}$ separation is quite different in the two models.

2. A Review of Prior Work

Busch and Kern [4-62] review the data on gray tin through 1960. Groves and Paul [4-60, 4-61] discuss relevant work after that date. Their own work marked the turning point in our understanding of gray tin with its identification as a semi-metal rather than a semiconductor.

A few optical studies have been made. Becker [4-63] was unable to observe any transmitted light in the wavelength range 2 to 35 μ.

---

†For instance, using effective mass data, Groves and Paul estimate the $\Gamma_8^+ \rightarrow \Gamma_7^-$ gap to be somewhere in the range .3 to .4 eV [4-60, 4-61], whereas Herman et al. use the .4 eV value. The Groves-Paul value of .67 eV for the $\Gamma_7^+ \rightarrow \Gamma_8^+$ gap is estimated from the atomic spin-orbit splitting of α-Sn and the analogous atomic and crystalline splittings in germanium [4-61, p. 3-15]. The k·p theory [4-30] gives a value of .77 eV for this separation, while Herman et al. use a value of .72 eV.

This is not surprising now, in view of the zero band gap. The infrared reflectivity studies of Lindquist and Ewald [4-64], made over the range 1 to 25 μ, give a value for the $\Gamma_{25'}(\Gamma_8^+)$ valence band effective mass ranging from .38 to .49 m_o. Cardona and Greenaway [4-65] measured the reflectivity in the range .8 to 4.8 eV. In analogy with many semiconductors, E_1, $E_1+\Delta_1$ and E_2 structure was noted at 1.28, 1.755, and 3.65 eV, and identified with the two spin-orbit split L point transitions† and X point transition, respectively. In a note added in proof, the authors suggested that very weak structure, possibly occurring around 2.8 eV, was due to $\Gamma_{25'} \rightarrow \Gamma_{15}$ transitions. In addition they cited some structure at 4.4 eV which might be due to the $L_{3'} \rightarrow L_3$ transitions. This structure did not appear in their published reflectivity spectra.

An electroreflectivity study [4-28] revealed a large amount of additional structure which was identified with the aid of the Cardona-Pollak gray tin bands. The spectrum is shown in Fig. 4-13 and identification of the various peaks is found in Table 4-5. There is structure which is felt to arise from $L_{3'} \rightarrow L_3$, $\Gamma_{25'} \rightarrow \Gamma_{15}$, and $\Delta_5 \rightarrow \Delta_1$ transitions.

Energy band calculations include those of Herman et al. [4-02, 4-27], of Cardona and Pollak in [4-28], and of Cohen and Bergstresser [4-24].

---

†This was prior to Brust's work [4-12] which established such transitions as occurring at Λ within the zone.

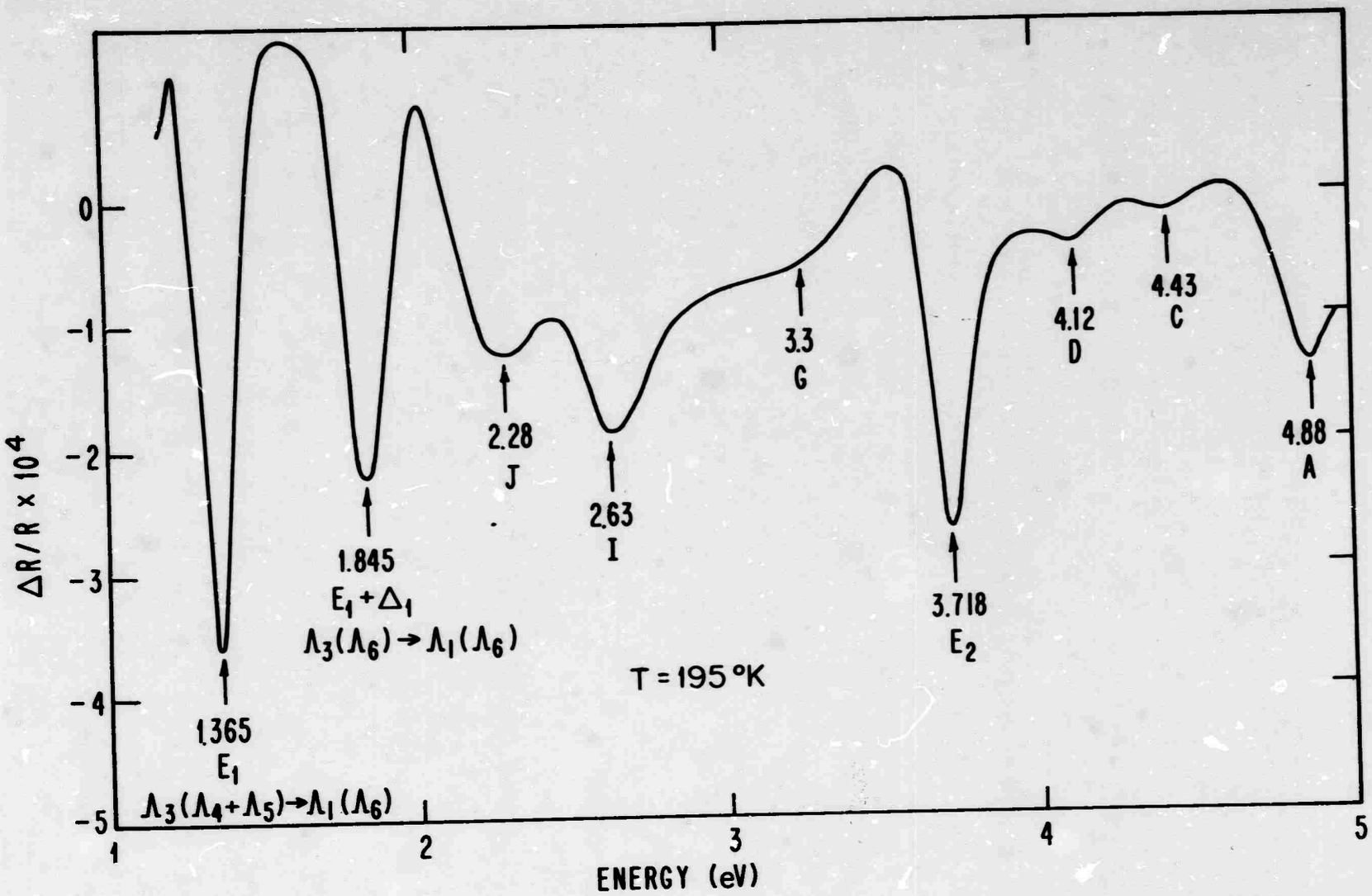

FIG. 4-13 ELECTRO-REFLECTIVITY SPECTRUM OF GRAY TIN. From ref. [4-28, Fig. 1]

3. The Reasons for Our Study of Gray Tin

Our motivation for repeating the study of the reflectivity done by Cardona and Greenaway stemmed from a consideration of the results of the electroreflectivity experiments in which we participated and which will be discussed in Sec. IV-C-6. It seemed that:

(1) a careful comparison of the spectra of R and $\Delta R/R$ could be used to show the relative efficacy of the two experiments in determining the energies of critical points.

(2) some ill-established reflectivity structure near 2.8 eV and cited in ref. [4-65] should be reinvestigated with a more sensitive system.

(3) a study over a wide spectral range which measured absolute rather than relative reflectivity could be used to determine n and k. The optical constants are needed, in particular, for the reduction of the electroreflectivity data.

Thus, the goal was to measure the reflectivity of gray tin in the range 2300Å-1.3 μ[†] at temperatures in the range 80°-290°K.

4. Samples and Their Treatment

The samples used were grown in this laboratory by S. Groves using the Ewald-Tufte method [4-66]. The surfaces were often large (e.g., 5 × 15 mm.) and very smooth and highly reflecting. Since the samples are grown from mercury solution, there is the possibility of residual mercury in the bulk and on the surface. Any seen on the surface was removed by cotton swabs immersed in cooled methyl alcohol.

[†]Ref. [4-64] provides R values at higher wavelengths.

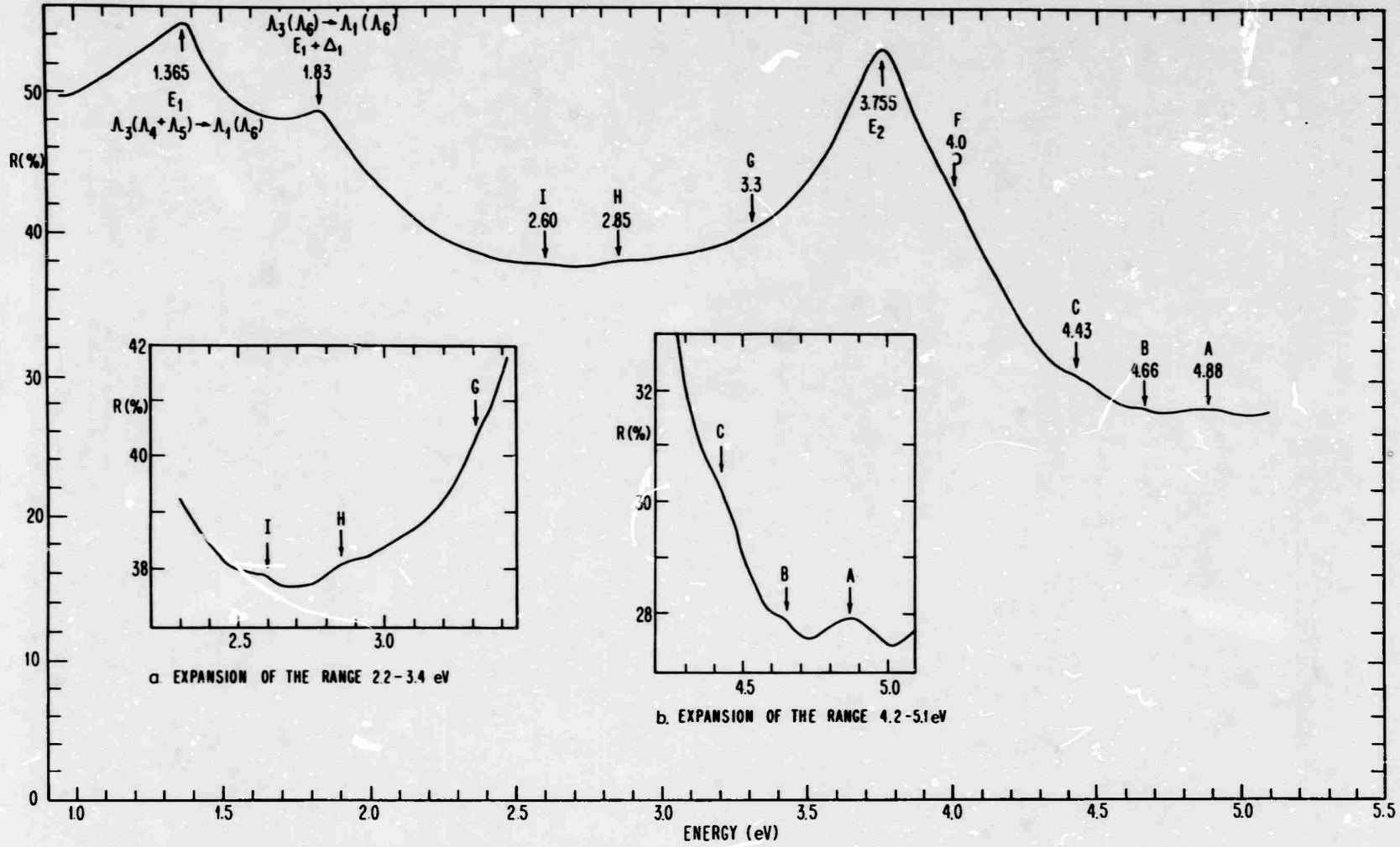

FIG. 4-14 REFLECTIVITY SPECTRUM OF GRAY TIN (GOOD SAMPLE). ABSOLUTE REFLECTIVITY VALUES ACCURATE TO ±5%. TEMPERATURE 80°K.

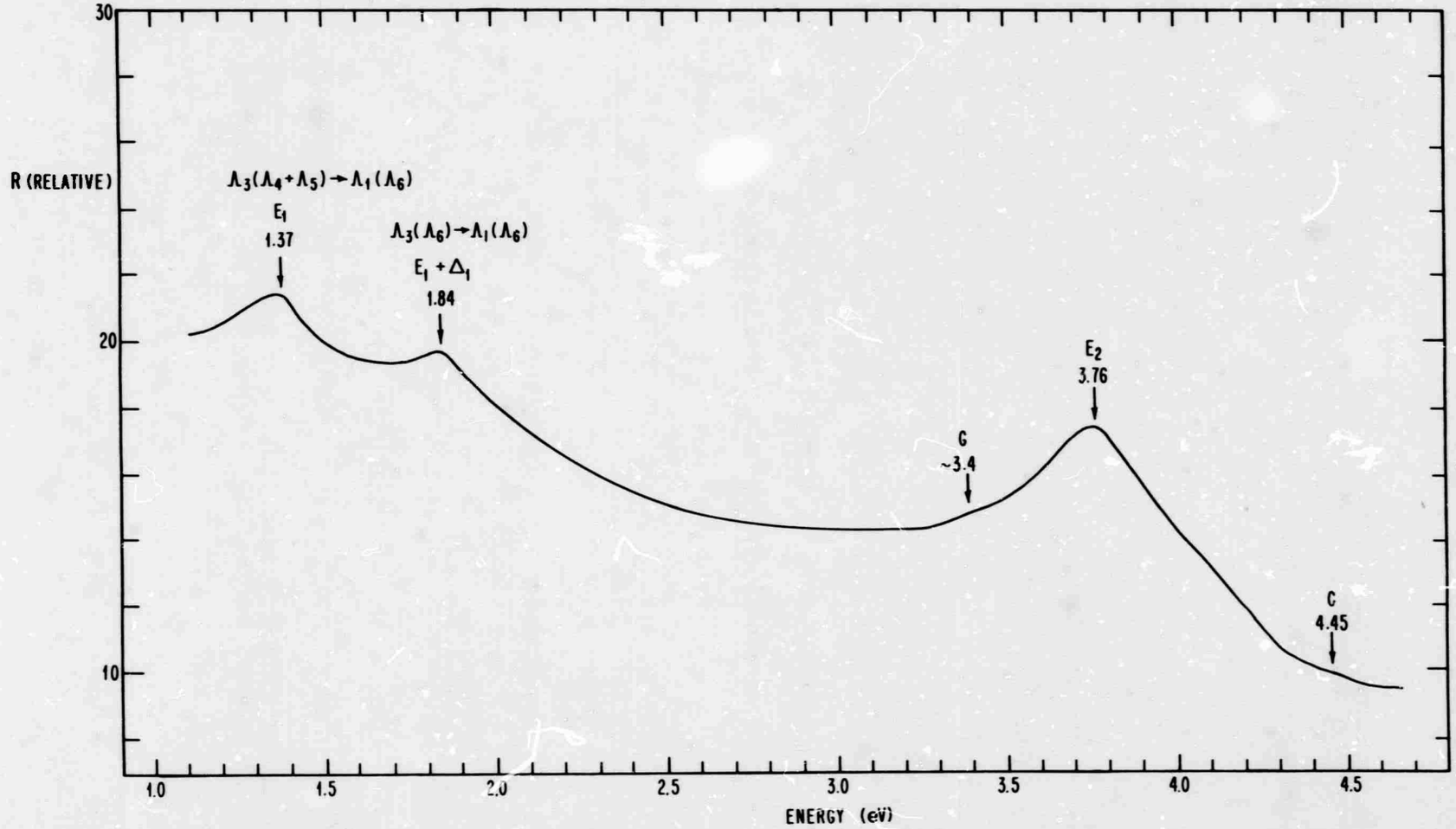

FIG. 4-15 REFLECTIVITY SPECTRUM OF A SLIGHTLY DEGRADED GRAY TIN SAMPLE. REFLECTIVITY VALUES ARE RELATIVE. TEMPERATURE IS BETWEEN 105° – 80°K.

In any case residual mercury on an undamaged surface will not give any structure in reflectivity in our spectral range, since, between 2 and 5 eV, mercury's reflectivity decreases smoothly from 76 to 68% [4-67]. Inclusions of mercury in the bulk migrate freely above ~ 0°C. If they break through the surface they destroy it. Before the actual breakthrough very fine cracks will develop in the sample surface, accompanied by a degradation in the reflectivity. Figure 4-14 shows a "good" surface and Fig. 4-15 a degraded one. We note the less pronounced structure at the Λ peaks and a decrease in the relative size of the X peak. Much of the fine structure has disappeared.

In consequence great care must be taken at all stages to ensure that the samples are kept below, say, -5°C. For example, a cooled iodine etch, applied in an attempt to improve the absolute reflectivity, destroyed the surface, presumably because the exothermic reaction on the surface varied the sample temperature. Fortunately, the reflectivity of the crystals as grown is usually good enough that etches are not needed.

The sample holder is a block of oxygen-free copper with a well cut into it. The sample is placed inside the cooled well and glued to the bottom with a dot of GE cement.† Sample and holder are then placed in a freezer at -20°C for 48 hours to permit drying.

A knowledge of the temperature of the sample is very desirable both when making temperature-dependent studies and to prevent sample

---

†No. 7031 Adhesive and Insulating Varnish and No. 9424 Thinner. General Electric Co., Chemical Division, Pittsfield, Massachusetts

loss through too high a temperature. Thermocouple leads could not be attached directly to the sample but were secured to the sample holder. Cerrolow 117 solder†, melting at 117°F, was deposited on the sample holder before the sample was attached. The twin thero-couple leads were joined with a much higher melting point solder. Later (when the block was added to the cryostat), the thermocouple could be attached to the cooled sample block with just a touch of a cool iron.

5. Experimental Problems

a. Water and CO_2 films. The cooled sample, mounted on a cold finger inside the cryostat, serves as a cold trap for any gases which freeze above the temperature of liquid nitrogen. These trapped gases naturally form a thin film. The effect of thin films in creating false structure and magnitude changes is discussed in detail in Section IV-D-2. One dramatic demonstration of this effect occurred during the gray tin studies. Figure 4-16 shows many small ripples imposed on the Σ-X and L point structure. While this is an extreme case, there were other instances where the L point structure became confused as a film built up and slowly distorted the highest energy (4.9 eV) peaks.‡

When the film thickness becomes comparable with the wavelength of light, it can be identified from a shimmer of color similar to oil

---

†Cerro de Pasco Copper Corp., 40 Wall St., New York, New York

‡The ratio system is particularly adept at displaying quickly such time dependent phenomena.

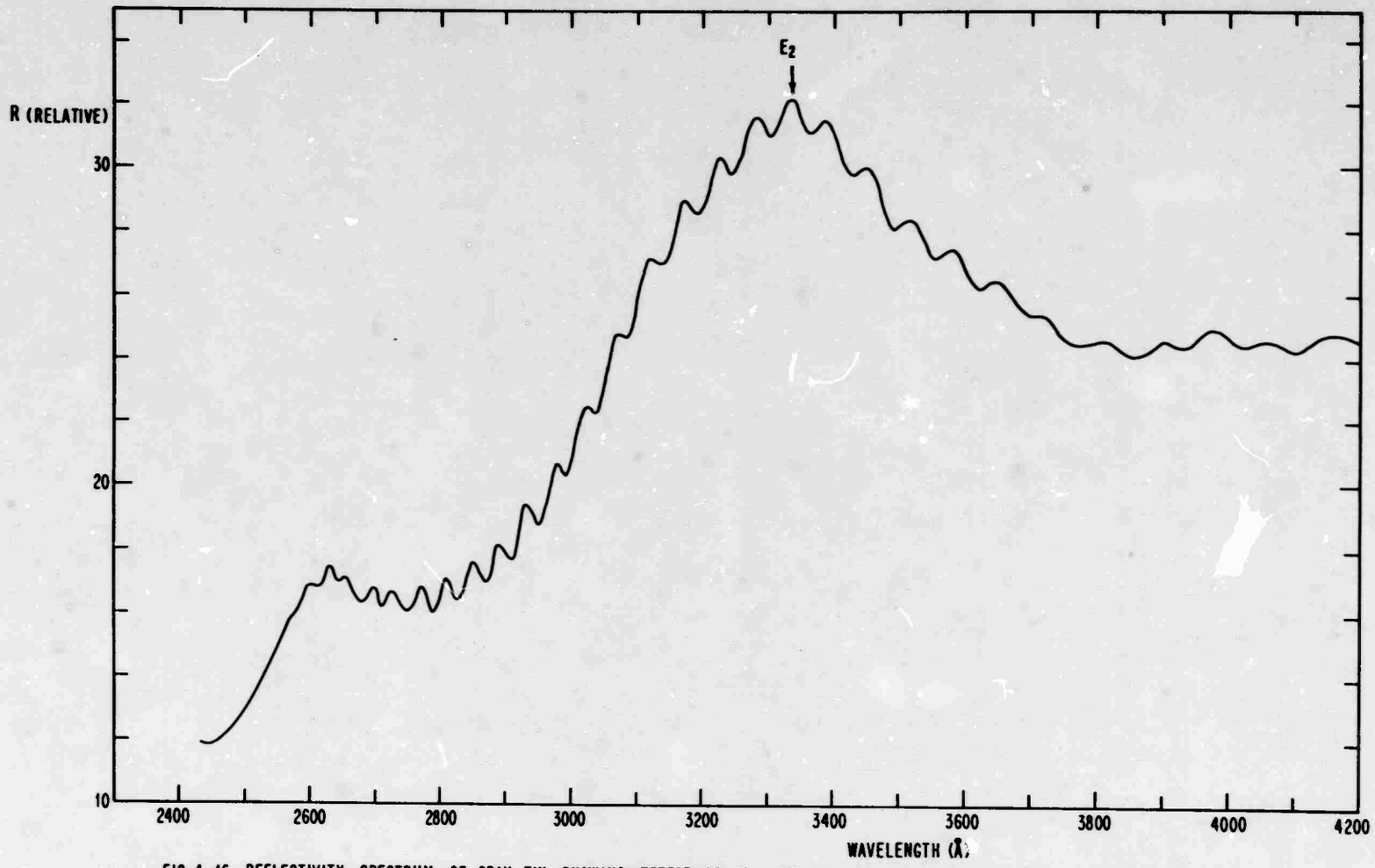

FIG. 4-16 REFLECTIVITY SPECTRUM OF GRAY TIN SHOWING EFFECT OF CO_2 AND H_2O FILM. REFLECTIVITY VALUES ARE RELATIVE.

slick on water. By noting the change of the appearance of this film as the temperature is raised, the film components can be identified. At the sublimation temperature of dry ice the film suddenly becomes milky; it disappears near -20°C, the temperature at which water vapor can be pumped from a sampl surface. Thus, we deduce CO_2 and H_2O as the main components of the films we observed.

The elimination of the film required attention to the cryostat and vacuum system to remove all sources of gas leaks. Two cold traps were used, one very close to the cryostat. No rubber hose was employed; all connections were made with soldered metal tubing. The cryostat was pumped continuously for more than 48 hours prior to use. To eliminate outgassing, all joints were heated. The cryostat section on which the sample holder was to be mounted was removed from the cryostat, cooled quickly, the sample mounted, and the unit returned to the cryostat within 15 minutes. Sample plus cryostat at -10°C were then pumped for one hour until all frozen water vapor was lifted. Only then was the sample cooled to lower temperatures.

One of the first effects of film buildup (Sec. IV-D-2 and Fig. 4-20) is a decrease in the magnitude of the reflectivity. Since the high energy peaks are most affected, we monitored the height of the E_2 peak during the course of any low temperature measurement. If it remained constant, we judged that no film buildup had occurred.

As an alternative to our procedure, the use of cryostats at the temperature of liquid helium is a way to eliminate film buildup. Gases freeze out on the liquid nitrogen shield before reaching the

sample. One must still contend with any films frozen out on the sample as it is cooled down.

b. The Question of the Reality of the Structure Observed above 3.7 eV. A number of samples exhibited structure above the E_2 peak (3.65 eV), but not always in a consistent way. Since the structure is small, experimental conditions had to be optimized and the structure displayed in a convincing way. First, since the transmission of the polarizer falls off sharply below 2900Å, it was not used in that range. This avoided false structure which could arise from the combination of high scattered light and the known structure in the polarizer transmission in this region (described generically in Sec. II-A-5-a-(2)).†

Secondly, the false structure created by the xenon spike at 2530Å was eliminated by smoothing the data. This is also an example of the structure effect described in Sec. II-A-5-a-(2).

Excellent samples were used and every effort was made to keep them good. Thin films were eliminated. The changes in structure with temperature could not have been due to films for two reasons:

(1) The E_2 peak magnitude generally did not change in time at a given temperature.

(2) The highest energy bump at 4.88 eV is visible at both 290°K and 80°K. As temperature decreases, this bump shifts to shorter

†The reader may be concerned about the elimination of the polarizer. It is generally employed to eliminate false structure in the reflectivity arising from light polarized perpendicular to the monochromator slit (Chapter III). However, we did not experimentally observe any false structure from this source below 2900Å so that the polarizer is not needed in this range.

wavelength. If it were only a bump due to the film, it would shift to longer wavelength as we increase the rate of film buildup on lowering temperature (provided we assume that the refractive index of the film does not change significantly with temperature). The effect of increased film thickness can be seen by comparing the curves for 100Å and 200Å films in Fig. 4-20.

The final proof of the reality of the structure was that it was found in more than one sample.

c. Considerations Affecting the Absolute Accuracy of R Measurements. Figure 4-17 reproduces the ratio reflectometer display of reflectivity data for an α-Sn sample over an extended wavelength range. The various segments correspond to changes in one or more system components such as source, grating, or detector. The segments do not match perfectly because with each component change we get a related change in sample or detector illumination.

To get a smooth curve, one segment is scaled relative to another in their overlap region. Extensive overlap of any two segments is important. Then, whey they are joined, only structure common to both is included and one rejects any bump artificially created at the point of junction.

A general examination of the differences in overlap regions in a number of samples has shown that absolute magnitudes will be reproduced within only ± 5% of full scale accuracy.

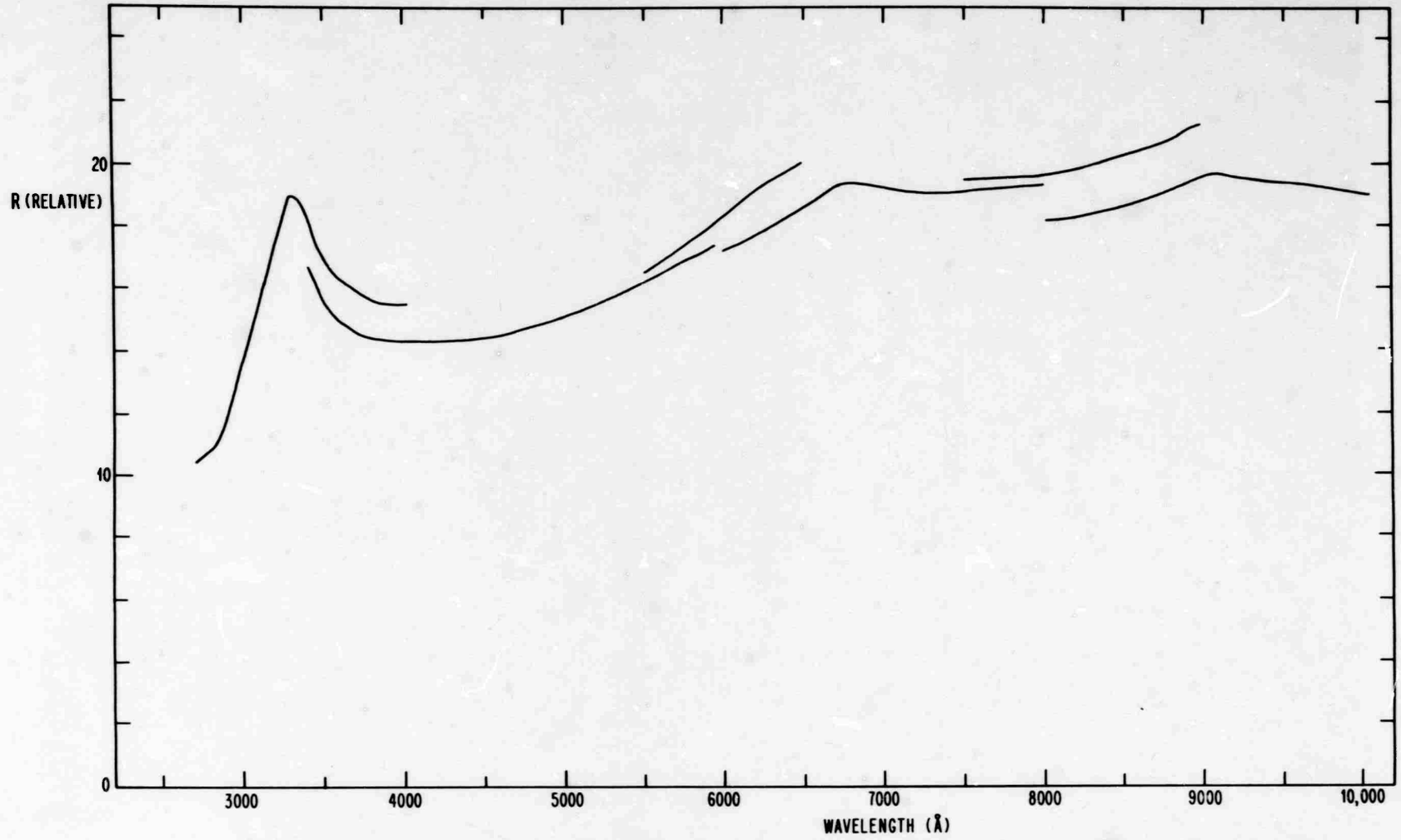

FIG. 4-17 SPECTRAL SEGMENTS OF GRAY TIN REFLECTIVITY FROM FIG. 4-15 THIS PLOT SHOWS NEED FOR ADJUSTMENT OF THE SEGMENTS AND NEED FOR SEGMENT OVERLAP.

6. Experimental Data and Some Interpretation

The discussion of the experimental data will be divided into two parts:†

(1) The experimental reflectivity structure and its relationship to the electroreflectivity structure. This will include some discussion on line shapes and magnitudes.

(2) Identification of the combined reflectivity and electroreflectivity structure within the framework of two separate band models: the k·p bands of Cardona and Pollak and the first principles bands computed by Herman et al.

The figures of α-Sn reflectivity represent the best, or combinations of the best, scans which we made. Figure 4-18 shows the results at 260°K while Fig. 4-14 shows those at 80°K. Figure 4-19 shows the changing structure at the high energy end of the spectrum as the temperature is lowered.

The structure has been labeled in a fashion similar to that employed for germanium:

(1) The energy of the structure peak.

(2) Letter labels for the peaks. The standard notation found in the literature is used where appropriate (the "E" letters), while other letters are used for that structure less surely correlated with like structure in other diamond and zinc blende materials.

---

†Discussion of high energy structure which is expected on the basis of the k·p energy bands and which is missing in reflectivity and electroreflectivity is to be found in Chapter V.

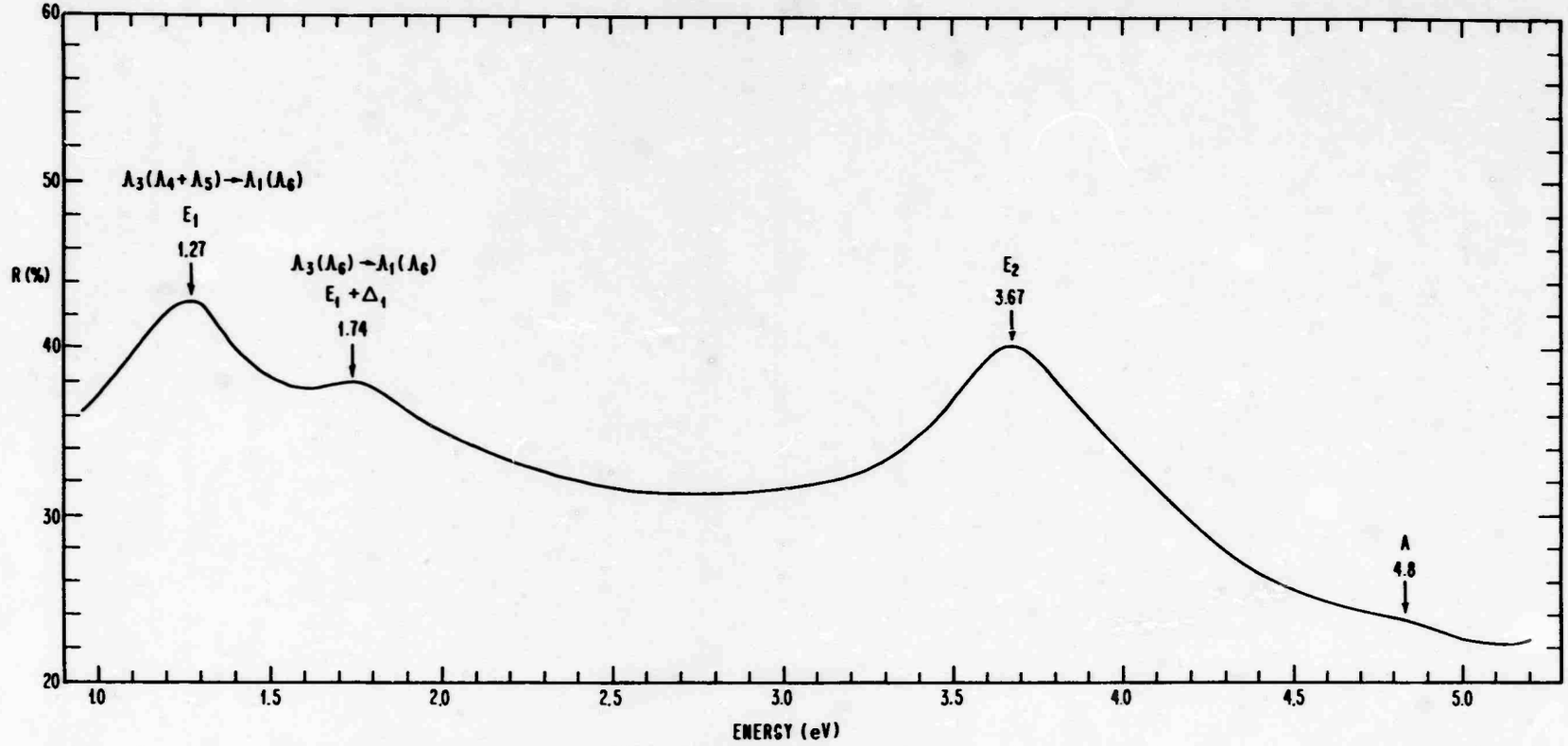

FIG. 4-18 REFLECTIVITY SPECTRUM OF GRAY TIN (GOOD SAMPLE). ABSOLUTE REFLECTIVITY VALUES ACCURATE TO ± 5%. TEMPERATURE 260 °K.

(3) Transitions are labeled in terms of Brillouin zone symmetries where band models give the same interpretation.

Figure 4-13 is taken from "Electroreflectivity and Band Structures of Gray Tin" of which we were one of the co-authors.

The right-hand half of Tables 4-5 and 4-6 give both sets of structure (R and $\Delta R/R$).

a. Structure at:

1.365 $\pm$ .01 eV in R at 80°K and at 1.365 eV in $\Delta R/R$ at 195°K (E_1)

1.83 $\pm$ .01 eV in R at 80°K and at 1.845 eV in $\Delta R/R$ at 195°K ($E_1 + \Delta_1$)

These structural features correspond to the $\Lambda_3 \rightarrow \Lambda_1$ transitions.† They give a spin-orbit splitting of .48 eV in electroreflectivity and .465 eV in reflectivity. The peak temperature coefficients, determined by the two methods, are shown in Table 4-3.

TABLE 4-3. Λ PEAK TEMPERATURE COEFFICIENTS

(in units of 10^{-4} eV/°C)

Experimental Method	E_1	$E_1 + \Delta_1$
R	-4 (-1.45+0)	-6.5(-1.0+1.8)
$\Delta R/R$	-5.4($\pm$ 0.6)	-4.2($\pm$ 0.6)

Although the central values of the temperature coefficients from reflectivity suggest that the two peaks close as the temperature is

†Recent $\Delta R/R$ measurements by Hamakawa et al. [4-68] suggest that the $E_1 + \Delta_1$ peak in germanium may arise from an M_3 critical point, and hence is not due solely to the $\Lambda_6 \rightarrow \Lambda_6$ transition.

increased and those from electroreflectivity suggest that they separate, within their errors both experimental results are consistent with separation. Moreover, electroreflectivity gives the more sensitive measure of the temperature coefficient. The reflectivity peaks are not so sharp and their broadening with increasing temperature creates the greater errors.

One point worth noting is the very striking line shape at low temperature, looking very much like an M_2 edge. Both germanium and α-Sn show the same asymmetry about the peak maximum, although it is more pronounced in α-Sn. This similarity to an M_2 edge is <u>not</u> inconsistent with Brust's assertion that this structure arises at an M_1 edge. The line shapes shown in Fig. 4-2 for the various types of edges are those predicted for ϵ_2, while R is a function of both ϵ_1 and ϵ_2. The Kramers-Kronig analysis of R for germanium, performed by Philipp and Taft, shows that ϵ_1 is the major contributor to the line shape for energies up to and including the Λ peaks. We can expect a similar effect in α-Sn. Thus, the question becomes one of determining how the M_1 edge in ϵ_2 affects the shape of ϵ_1 and hence of R.

Velický [4-69] has examined the Kramers-Kronig relationships (which relate ϵ_2 and ϵ_1) to see the effect, over short energy ranges, of the sudden change in one of these parameters on the other. Potter [4-38], in extending this work, specifically noted that if ϵ_2 undergoes a steep rise at energies less than the transition at some ω_c (as in M_1 in Fig. 4-2), then ϵ_1 will fall steeply for ω greater than

ω_c. A steep descent at energies above the peak is what we indeed see in the reflectivity spectra. The sharpness of the descent has probably been enhanced by the electron-hole interaction in a fashion similar to that shown in Fig. 4-4a.

b. Structure at:

2.28 eV in $\Delta R/R$, (J)

2.60 eV in R at 80°K, 2.63 eV in $\Delta R/R$ at 195°K, (I)

2.85 eV in R at 80°K, (H)

3.3 eV in R at 80°K, 3.3 eV in $\Delta R/R$ at 195°K, (G)

These four weak structural features lie between the strong structure associated with the E_1 and E_2 peaks. The structural features in R and $\Delta R/R$ occurring at the same energy (features G and I) are given the same labels since we feel they arise from the same transition. This view is supported by the observation that the Λ structure in R at 80°K is at the same energy as that in $\Delta R/R$ at 195°K. Similar coincidences will be noted at the high energy end of the spectrum.

Point G in the $\Delta R/R$ spectrum is very weak and it may be due to satellite effects. The occurrence of structure at the same energy in the reflectivity spectrum, however, establishes the reality of the transition.

The absence of the 2.28 eV peak in reflectivity is not surprising since the transition would create structure on the rising slope of the Λ peaks, where it would be more difficult to see, than, say, the H and I structure, which is found in the flat reflectivity valley.

However, the absence of the H structure in electroreflectivity is puzzling. As we see in the next section, neither band model suggests why it should be missing.

c. Structure at:

3.75 ± .01 eV in R at 80°K and at 3.718 eV in $\Delta R/R$ at 195°K, (E_2) The sharpening of this peak with temperature is similar to the effect found in germanium, and may also be due to an electron-hole interaction. It does not show the pronounced shoulder seen in the room temperature germanium runs. In analogy with the other diamond zinc blendes this peak has been nominally designated the Σ-X peak.

The most striking feature of this reflectivity spectrum in relation to that of the other diamond and zinc blende semiconductors is that the height of this peak is comparable with that of the Λ peaks, whereas in the others it is much higher [4-32, Figs. 1 and 3]. This is not due to either poor samples or thin films.

We postulate that the diminished size of E_2 is due to the combined effect of the marked distortion of the bands by the zero energy gap at Γ, and the fact that the E_2 peak is made up of transitions from much of $\vec{k}$ space. In Kane's work on silicon two of the five major contributions to the E_2 peak come from regions of $\vec{k}$ space lying along the 110 direction, and all five lie in 110 planes. The bands of α-Sn along the 110 direction (K-Σ-Γ) seen in Fig. 4-11 are quite different from those in germanium (Fig. 4-8b) due to the zero energy gap at Γ_8^+ in α-Sn. The Σ_2 and Σ_3 bands do not appear to be parallel over any of their range. Thus, we might expect that a number

of the transitions contributing to ϵ_2 at E_2 and hence to R in most semiconductors (exemplified here by germanium and silicon) will not occur in α-Sn, and R will be weaker.

The reasonableness of this hypothesis is supported by an examination of the reflectivity structure of HgTe [4-70] and HgSe [4-71, 4-72], both felt to be zero band gap semiconductors [4-73]. In HgTe and HgSe, as in α-Sn, the E_2 peak is comparable in magnitude to the E_1 peaks.

TABLE 4-4 THE E_2/E_1 RATIO AND E_2 AND E_1 TEMPERATURE COEFFICIENTS FOR A NUMBER OF SEMICONDUCTORS

Material	Direct or Indirect Gap	Value of Direct Gap in eV	E_2/E_1	$(dE_1/dT) \times 10^4$ eV/°C	$(dE_2/dT) \times 10^4$ eV/°C
Ge	Indirect	.805 (293°K) [4-74, p.5]	1.25 [4-32]	-4.2 ± .4 [4-65]	-1.8 ± .5 [4-36]
α-Sn	Direct	0.0 [4-60]	.93 This work	-5.4 ± .6 [4-28] -4 (-1.5+0) This work	-3.5 ± .6 [4-28] -4.5 ± 1.3 This work
HgTe	Direct	0.0 [4-73]	1.04 (293°K) 0.98 (77°K) [4-70]	5.5 [4-70]	-5 [4-70]
HgSe	Direct	0.0 [4-73]	0.97 [4-72, 4-71]	-4.3 ± .6 [4-65]	-6.0 ± 1 [4-72]
GaSb	Direct	.70 [4-44]	1.19 [4-71]	-4.2 ± .6 [4-65]	-6.2 ± .5 [4-75]
InSb	Direct	.18 [4-44]	1.29 [4-76]	-5.3 ± .3 [4-75]	-5.4 ± .5 [4-75]

The temperature coefficients of the interband energy differences in many semiconductors of the diamond and zinc blende families are nearly the same, a fact which is poorly understood at present. An exception is the transition(s) giving the E_2 peak in germanium. From Table 4-4 we see that the smallness of this coefficient is not continued in α-Sn or the compound semiconductors. It is hard to see a correlation between the temperature coefficients and the other properties of the band structure noted in the table. By contrast there does seem to be a correlation between the occurrence of a zero band gap and the E_2/E_1 height ratio.

d. Structure at 4.0 eV in R? (F). This structure is highly questionable. It was seen only occasionally and was then very weak and the energy value was poorly defined. Although we doubt its reality, we mention it for two reasons: so that investigators using lower temperatures or other techniques could look in this region, and so that the relevance of such structure to the two band models could be determined. It does fit into both band models.

e. Structure at:

4.12 eV in $\Delta R/R$ at 195°K, (D)

4.43 eV in R at 80°K and at 4.43 eV in $\Delta R/R$ at 195°K, (C)

4.66 eV in R at 80°K, (B)

4.88 eV in R at 80°K and at 4.88 eV in $\Delta R/R$ at 195°K, (A)

The reflectivity structure is seen in both Figs. 4-18 and 4-14. The development as temperature is lowered is shown in Fig. 4-19. The coincidence of R and $\Delta R/R$ values at both A and C is like that seen at

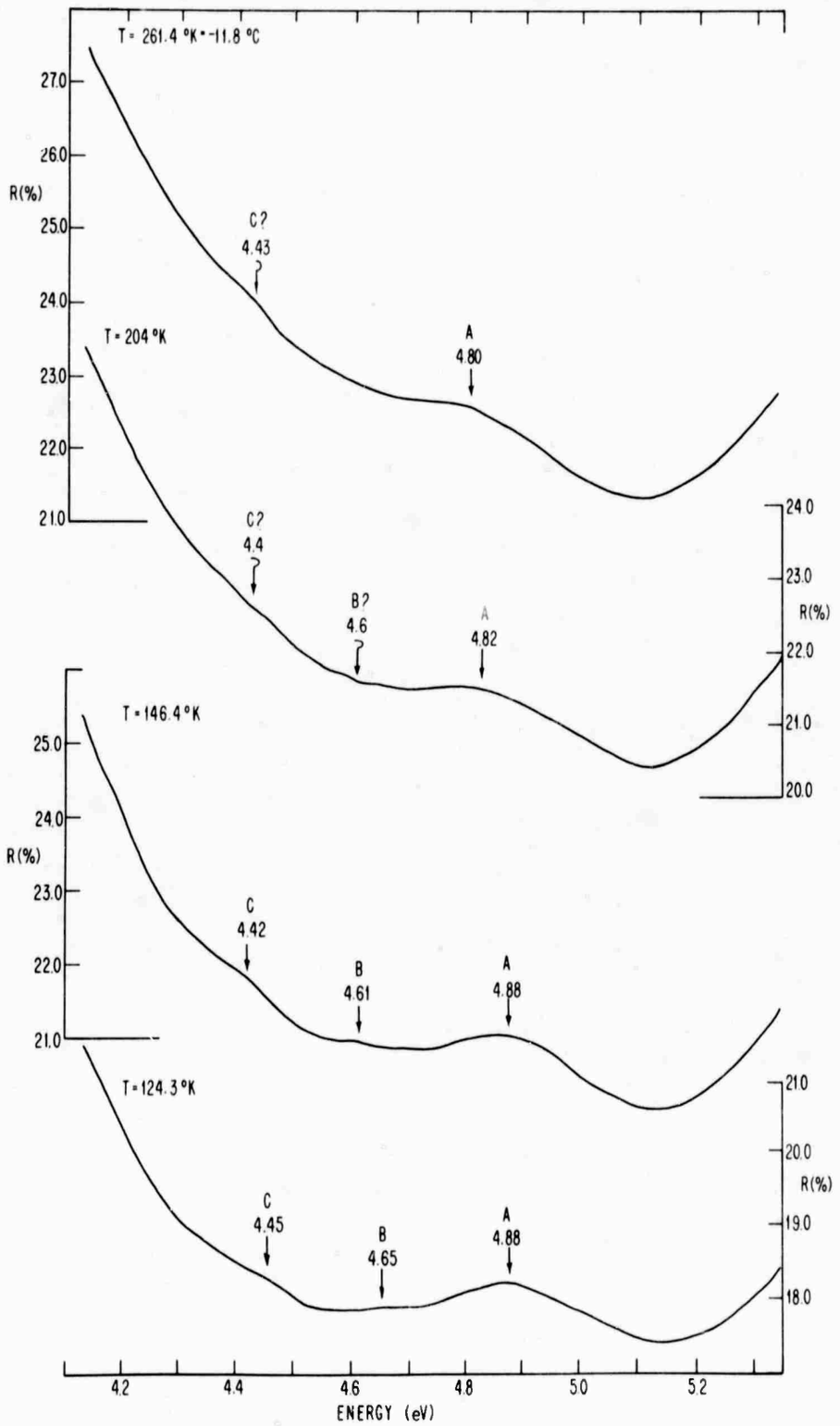

FIG. 4-19 DEVELOPMENT OF STRUCTURE IN COOLED GRAY TIN AT ENERGIES ABOVE THE E_2 PEAK.

E_2, G, I, E_1, and $E_1 + \Delta_1$ before. Hence, we have assumed that the coincident R and $\Delta R/R$ values correspond to the same transition. The errors in each type of measurement are about $\pm$ .02 to .03 eV.

These four structure points are listed in both Table 4-5 and Table 4-6 where they find differing identification in the two band models.

7. Interpretation of the Experimental Structure in Terms of Band Models

Tables 4-5 and 4-6 contain information for the comparison of the energies at which structure in R and $\Delta R/R$ occurs and the supposed corresponding energies from the calculated band structure.

The left half of each table contains data extracted preferably from the relevant written discussions and, failing that, from the drawings of the bands. There are entries for each transition in terms of its Brillouin zone symmetry, its selection rules in reflectivity and electroreflectivity, its energy and its spin-orbit splittings. The procedure for developing these selection rules is found in Chapter V.

In the work of Cardona, Shaklee, and Pollak, the careful reader will find various inconsistent spin-orbit splittings for α-Sn, all supposedly derived from the same k·p model. For instance, ref. [4-30] implicitly contains three different sets. One is found in Table VI. Repeating the authors' calculation of the tabular entries by employing a formula in the text, we found a second set. We computed a third from some printed energy values for the L point transitions. A fourth set of L point spin-orbit splittings is contained in ref. [4-28].† The

†A final set of values, which is not intended to be consistent with these others, is given in a recent paper [4-29]. We discuss this in Chapter V. See also our note in Sec. IV-A.

differences are as high as 20%; the extreme case results in a variation of .22 eV for the value of the Γ_{15} splitting. The independent investigator has no basis for deciding which set of splittings is correct. Having no test, we simply chose those splittings apparently used to compute the band picture found in ref. [4-28] and reproduced in our Fig. 4-12.

The entries on the right of Tables 4-5 and 4-6 give the energies determined from the structure in R and $\Delta R/R$, matched as well as possible with the calculated values.

a. The k·p Bands. Let us make the comparison with the k·p calculations first. We assume that the group of three peaks in R and that in $\Delta R/R$ correspond to four transitions between two sets of two levels each, one transition being unobservable in each type of experiment. A self-consistent assignment of energies of the transitions is given in the last ("combined") column, where the energies are adjusted within the experimental error. The absolute energies differ somewhat from the k·p calculation, but the calculated splittings of .23 eV for the L_3 band and of .42 eV for the $L_{3'}$ band [4-28] compare reasonably well with the experimental values of .27 eV and .49 eV.

The $\Delta_5 \rightarrow \Delta_{2'}$ transitions are in the same energy range as the $L_{3'} \rightarrow L_3$ transitions so that structure from the two sets could be superposed.

Peaks F (questionable) and G may arise from two of the three allowed transitions at $\Gamma_{25'} \rightarrow \Gamma_{15}$. One is disallowed in reflectivity.

TABLE 4-5 THE COMPARISON OF THE ENERGIES OF EXPERIMENTAL STRUCTURE AND THE ENERGIES OF TRANSITIONS GIVEN BY THE K·P BAND MODEL FOR GRAY TIN

k·p Model Energies					Experimental Energies					
Transition	Allowed in R?	Allowed with E Field?	Energy in eV	Spin-orbit Splitting	R Peak at 80°K		ΔR/R Peak at 195°K		Combined	
					Label	Energy in eV	Label	Energy in eV	Energy in eV	Inferred Splittings
$L_{3'} \rightarrow L_3$										
$L_6^- \rightarrow L_4^+, L_5^+$	Yes[1]	[2]	4.78	0.23	A	4.88 ±.02	A	4.89 ±.02	4.90	0.27
$L_6^- \rightarrow L_6^+$	Yes[1]	[2]	4.55	0.42	B	4.66 ±.03			4.63	0.49
$L_4^-, L_5^- \rightarrow L_4^+, L_5^+$	Restricted[1]	[2]	4.36		C	4.43 ±.02	C	4.43 ±.02	4.41	
$L_4^-, L_5^- \rightarrow L_6^+$	Yes[1]	[2]	4.13				D	4.12 ±.02	4.14	
$\Delta_5 \rightarrow \Delta_{2'}$										
$\Delta_7 \rightarrow \Delta_7$	Yes		~4.50							
$\Delta_6 \rightarrow \Delta_7$	Yes		~4.35							
$\Gamma_{25'} \rightarrow \Gamma_{15}$										
$\Gamma_7^+ \rightarrow \Gamma_8^-$	Yes		4.00	0.77	F	4.0?				0.7
$\Gamma_8^+ \rightarrow \Gamma_8^-$	Yes		3.23	1.06	G	3.3	G	3.3		1.0
$\Gamma_7^+ \rightarrow \Gamma_6^-$	No	Yes[3]	2.94							
$\Gamma_8^+ \rightarrow \Gamma_6^-$	Yes		2.17				E_0', J	2.28		
$X_4 \rightarrow X_1$	Yes		3.75		E_2	3.75	E_2	3.718		
$\Gamma_{2'} \rightarrow \Gamma_{15}$										
$\Gamma_7^- \rightarrow \Gamma_8^-$	No	Yes[3]	3.48	1.06						
$\Gamma_7^- \rightarrow \Gamma_6^-$	No	Yes[3]	2.42							
$\Delta_5 \rightarrow \Delta_1$ (doublet)	Yes		~3.0	0.38 max						
					H	2.85				
					I	2.60	$E_0' + \Delta_0'$, I	2.63		
$\Lambda_3 \rightarrow \Lambda_1$										
$\Lambda_6 \rightarrow \Lambda_6$	Yes		1.69	0.49	$E_1 + \Delta_1$	1.832	$E_1 + \Delta_1$	1.845	1.845	0.48
$\Lambda_4, \Lambda_5 \rightarrow \Lambda_6$	Yes		1.20		E_1	1.365	E_1	1.365	1.365	

[1] See the discussion in Sec. V-B-1 and Table 5-8.

[2] See the discussion in Sec. V-B-3 and Tables 5-11, 5-12, and 5-13.

[3] See the discussion in Sec. V-A-2-a, especially the last two paragraphs. See also Table 5-6.

If we assign the J peak in $\Delta R/R$ to this transition as well, then we can compute both spin-orbit splittings of .7 and 1.0 eV. The theoretical values are .77 and 1.06.

The electroreflectivity peaks at J and I were tentatively assigned in ref. [4-28] to either of two transitions. The first choice was the $\Delta_5 \rightarrow \Delta_1$ doublet which is seen in other materials (see our discussion of germanium as an example). The splitting of .35 eV agrees with the calculated maximum splitting for those transitions (.38 eV). In objection it was noted [4-28] that there are no critical points along Δ in the k·p bands near the regions where the experimental and theoretical splittings are matched. Consequently, this cannot be considered an identification. In later work Pollak, Higginbotham, and Cardona [4-26, p.26] claim a better fit by using the J energy (E_0' in their terminology) as one of the k·p parameters. In effect they adjust the k·p parameters to fit a preconceived notion of the identification. Therefore, this cannot be construed as proof that J and I are due to Δ transitions.

The second choice was the pair of transitions from Γ_7^- and $\Gamma_8^+ \rightarrow \Gamma_6^-$, at 2.42 and 2.17 eV respectively. This could occur only if the $\Gamma_7^- \rightarrow \Gamma_6^-$ transition, disallowed in reflection, became allowed in electroreflection. We have examined this transition using the group theoretical approach to selection rules and have found it is indeed allowed (Sec. V-A-2-a).

Nevertheless, our reflectivity measurements prevent our ascribing these two peaks to the Γ transitions. Since the I peak in R

occurs at the same energy as a peak in $\Delta R/R$, we feel they are due to the same transition. Thus, they cannot correspond to the $\Gamma_7^- \rightarrow \Gamma_6^-$ transition, forbidden in reflection.

Neither transition assignment is then acceptable for the I structure. It is not identified in the k·p bands. In constrast J can be ascribed to the $\Gamma_8^+ \rightarrow \Gamma_6^-$ transition, and we have done so.

Our reflectivity peak H is also not identifiable. At 2.85 eV it corresponds closely with the $\Gamma_7^+ \rightarrow \Gamma_6^-$ transition at 2.94 eV, but this is not allowed (see Sec. V-A-1-a) in reflection.

The $X_4 \rightarrow X_1$ transition is used as one of the parameters in the k·p calculation so its coincidence with the E_2 peak is predetermined. However, the center of gravity of the Λ peaks was not used as a parameter in the germanium-silicon calculations [4-11] and we assume they were not here. The computed and experimental values differ by less than .01 eV. The Λ peak spin-orbit splitting, .48 eV, is the basic experimental splitting used to calculate all other splittings [4-30, p.718].

In conclusion the k·p bands fit much of the data, but fail to account for two items of structure, the reflectivity peaks H and I (and I in $\Delta R/R$). These bands in their present published form are less complete than some others. Transitions along the X - K and K - Γ directions might account for the unidentified structure.

b. Bands Computed Using First Principles. As with the k·p bands, we suggest possible identifications of observed α-Sn structure in terms of the bands computed by Herman et al. [4-27]. While the

TABLE 4-6 THE COMPARISON OF THE ENERGIES OF EXPERIMENTAL STRUCTURE AND THE ENERGIES OF TRANSITIONS GIVEN BY THE FIRST PRINCIPLES BAND MODEL FOR GRAY TIN

First Principles Model Energies					Experimental Energies					
Transition	Allowed in R?	Allowed with E Field?	Energy in eV	Spin-orbit Splitting	R Peak at 80°K		ΔR/R Peak at 195°K		Combined	
					Label	Energy in eV	Label	Energy in eV	Energy in eV	Inferred Splittings
$L_3, \rightarrow L_3$										
$L_6^- \rightarrow L_4^+, L_5^+$	Yes[1]	[2]	4.91	0.45-0.46	A	4.88	A	4.89	4.88	0.45
$L_6^- \rightarrow L_6^+$	Yes[1]	[2]	4.45	0.49-0.50	C	4.43	C	4.43	4.43	0.45
$L_4^-, L_5^- \rightarrow L_4^+, L_5^+$	Restricted[1]	[2]	4.41							
$L_4^-, L_5^- \rightarrow L_6^+$	Yes[1]	[2]	3.96		F	4.0			4.0	
$\Sigma_1 \rightarrow \Sigma_3$	Yes		4.75		B	4.66				
							D	4.12		
$\Delta_5 \rightarrow \Delta_2,$										
$\Delta_7 \rightarrow \Delta_7$	Yes		4.02	0.18						
$\Delta_6 \rightarrow \Delta_7$	Yes		3.84		E_2	3.75	E_2	3.718	3.72	
					G	3.3	G	3.3		
$\Sigma_2 \rightarrow \Sigma_3$	Yes		~2.90							
$\Delta_5 \rightarrow \Delta_1$										
$\Delta_7 \rightarrow \Delta_6$	Yes		2.88	0.40	H	2.85			2.85	0.23
$\Delta_6 \rightarrow \Delta_6$	Yes		2.48		I	2.62	$E_0' + \Delta_0'$, I	2.63	2.62	
$\Gamma_{25}, \rightarrow \Gamma_{15}$										
$\Gamma_7^+ \rightarrow \Gamma_8^-$	Yes		2.89	0.67	H	2.85			2.85	0.57
$\Gamma_8^+ \rightarrow \Gamma_8^-$	Yes		2.22	0.70			E_0', J	2.28	2.28	
$\Gamma_7^+ \rightarrow \Gamma_6^-$	No	Yes[3]	2.19							
$\Gamma_8^+ \rightarrow \Gamma_6^-$	Yes		1.52							
$\Gamma_2, \rightarrow \Gamma_{15}$										
$\Gamma_7^- \rightarrow \Gamma_8^-$	No	Yes[3]	2.70							
$\Gamma_7^- \rightarrow \Gamma_6^-$	No	Yes[3]	1.97							
$\Lambda_3 \rightarrow \Lambda_1$										
$\Lambda_6 \rightarrow \Lambda_6$	Yes		1.7	0.5	$E_1 + \Delta_1$	1.832	$E_1 + \Delta_1$	1.845	1.845	0.48
$\Lambda_4, \Lambda_5 \rightarrow \Lambda_6$	Yes		1.2		E_1	1.365	E_1	1.365	1.365	

[1] See the discussion in Sec. V-B-1 and in Table 5-8.

[2] See the discussion in Sec. V-B-3 and in Tables 5-11, 5-12, and 5-13.

[3] See the discussion in Sec. V-A-2 a, especially the last two paragraphs. See also Table 5-6.

single group bands have been computed from the first principles approach, the spin-orbit splittings have not [4-27]. The procedure which was employed [4-02] was a form of k·p technique adapted to the first principles bands. However, the values differ significantly from the k·p spin-orbit calculations of Cardona et al.

Possible identifications are found in Table 4-6. The $L_{3'} \rightarrow L_3$ transition is now a triplet rather than a quadruplet, since the predicted spin-orbit splittings of $L_{3'}$ and L_3 are nearly identical. All members of the triplet are seen in our data only if we include the suspect point at 4.0 eV.

Our point B at 4.66 eV corresponds to a $\Sigma_1 \rightarrow \Sigma_3$ transition.

The $\Delta_6 \rightarrow \Delta_7$ transition at 3.84 eV might be part of the large E_2 peak at 3.75. Interestingly enough the bands do not appear to be parallel at X so that the $X_4 \rightarrow X_1$ transition of 3.37 eV probably does not contribute; this is in accord with the observation of Dresselhaus and Dresselhaus [4-25] that critical points generally do not occur at X. $\Delta_7 \rightarrow \Delta_7$ at 4.02 eV may be related to bump D at 4.12 eV.

The $\Delta_7 \rightarrow \Delta_6$ and $\Delta_6 \rightarrow \Delta_6$ transitions occur near Γ and could well be correlated with peaks H and I at 2.85 and 2.62 eV. The computed separation of .40 differs from the experimental value of .23 eV. This is not as serious as it seems for two reasons. The separation may be smaller as the k·p calculations show. It depends on which spin-orbit values are chosen. Secondly, the shape of the bands in the 100 direction is very sensitive to the parameters chosen (this applies at least in the k·p calculation method [4-28]).

A slight change in the shape will shift the critical point further out toward X along Δ where the splitting is reduced. (It goes to zero at X.)

Other structure is identified as shown in the table. Only one bit of structure, shoulder G, is not identified. However, a number of the transitions which one might expect to see at $\Gamma_{25'} \rightarrow \Gamma_{15}$ are not seen in electroreflectivity. Thus, in conclusion the bands of Herman et al. seem about as successful as the k·p bands in accounting for the experimental data.

Because of the marked differences in the k·p and first principles bands resulting from the discrepancy in the $\Gamma_{25'} \rightarrow \Gamma_{15}$ energy, there are few similarities in the two models in structural identification aside from the E_1 peaks and certain contributions to the E_2 peak.

One possible way of discriminating between the two models would be to see if the temperature coefficient of peak B is the same as those at A and C. In the k·p model A, B, and C are all part of the $L_{3'} \rightarrow L_3$ transition and hence should have the same temperature coefficient, whereas B is not a part of this transition in the first principles bands. The temperature coefficients are very hard to measure since the peaks are so small. Insofar as we notice a trend, A and B appear to have the same coefficient and that of C is different. This additional point, which only adds confusion, should not be taken seriously since the measurement was highly inaccurate. It does, however suggest a course for further investigation. The R of α-Sn could

be measured in the range 4°K to 80°K where the peaks A, B, and C are visible.

A better test between the two models would be afforded by measuring the pressure coefficients of these peaks since pressure coefficients generally show a wider range of values than do temperature coefficients.

D. H FIELD MEASUREMENTS, THIN FILM STUDIES, AND $\Delta R/R$ WORK IN GERMANIUM

In this section we discuss our other experiments in considerably less detail.

1. Magneto-Reflectivity Measurements in Germanium

One of the original motivations for the construction of the ratio reflectometer arose from the need to determine small changes in reflectivity induced by perturbations in the crystal environment. The expected structure in magneto-reflectivity measurements was of interest since magneto-absorption measurements had been so productive in yielding accurate band gaps and effective masses.

a. A Brief Review of Prior Work. A paper by Burstein et al. [4-47] and another by Elliott et al. [4-78] are particularly instructive in understanding magneto-absorption. They discuss how α, the absorption constant, is modified by a magnetic field due to the creation of Landau levels in the electron density of states. These levels are condensations of energy states (i.e., a merging of a group of states with a range of energy values into one state) and

result in oscillations in α above the energy gap. An analysis in terms of simple nondegenerate bands is extended to account for valence band degeneracies. Selection rules are listed for a variety of conditions. Useful experimental reviews are those of Lax and Zwerdling [4-79] and Lax [4-80], while an extensive review of the theoretical aspects of magnetic fields in solids is found in a tutorial paper by Dresselhaus and Dresselhaus [4-81].

Wright and Lax [4-82] carried out the first magneto-reflectivity study in their work on indium antimonide in 1961. Subsequent efforts in semiconductors were not productive in noting structure due to higher energy interband transitions [4-83],† although considerable information has been gained from interband magneto-reflectance studies of metals and of graphite [4-81], and from magneto-reflectance studies of the electron plasma in semiconductors [4-82]. When experimenters added AC modulation techniques, magneto-reflection began to yield useful information: a paper by Aggarwal et al. [4-86] comments on the magneto piezo-optical reflection spectra of the fundamental direct transition in germanium, and one by Groves et al. [4-59] describes the reflectivity of germanium in crossed electric and magnetic fields.

b. The Λ Measurement in Germanium. The possibility of studying the E_1 and $E_1 + \Delta_1$ peaks in magneto-reflection was discussed by Lax [4-87]

†On the other hand magneto-reflectance studies of low energy interband transitions have yielded structure, as exemplified in the direct gap, infrared measurements in $Cd_{0.17}Hg_{0.83}Te$ [4-84], Cd_3As_2 [4-85], and HgTe [4-73].

who estimated the effective masses at the L point using k·p theory.† We decided to look for the effect of an H field on these peaks, although there was considerable question whether anything could be seen. McLean and Paige [4-49] had studied the temperature dependence of broadening due to phonon scattering. They noted two basic classes of scattering. One class was characterized by those states, such as a conduction band minimum, where there were no lower states nearby to which the electrons (or holes) could scatter. In this circumstance only phonon absorption scattering occurred, and this could be reduced by lowering temperature. In the second class, states such as those along Λ could scatter both up and down in energy. Consequently, on cooling, phonon emission scattering could still occur.

The broadening to be anticipated from this effect (around .02 eV) could well obscure the ripply structure which one could expect to be added to the reflection peak. Groves et al. [4-73], however, noted H field effects in mercury telluride in transitions from deeper lying valence bands where one could expect phonon emission to be a problem. The effects were still evident at fields lower than those at which one might expect scattering to obliterate the structure.

Encouraged by their success, we studied the Λ transitions using fields as high as 31 kilogauss. To improve the data, the

†This was at a time when the E_1 peaks were thought to arise from transitions at L, rather than along Λ.

multichannel analyser was used (Sec. II-B-16). No structure was seen to within .02% in the E_1 peak. We looked for both structure modification in the form of ripples and for the peak shifts predicted by theory. We saw neither. At a later time we looked again at the whole spectral range concentrating on the E_1, $E_1 + \Delta_1$, and E_2 peaks. The multichannel analyser was not used and sensitivity was .05-.1%. Nothing was noted. These measurements were done at room temperature. Lower temperature measurements might be productive, although the improvement will be limited due to phonon emission scattering. We have not made a cryostat tail small enough to fit the magnet gap (0.685 in.).

There was one change noted in the experiment. When the magnetic field was applied, the magnitude of peaks would change slightly (around .1-.5%). This effect arose not in the sample but in the photomultiplier. By shifting the relative positions of the I_0 and I_R images on the photocathode, the sign of the shift could be changed and the size increased or decreased. Increasing the phototube magnetic shielding also reduced the effect.

c. Magnetic Field Effects at Saddle Points. A magnetic field modifies the density of states at a maximum or minimum in a conduction or valence band by creating discrete energy levels known as Landau levels in the plane in $\vec{k}$ space perpendicular to the magnetic field [4-77]. It is these levels which dramatically modify the absorption spectra. The situation is more complex at a saddle point, where the orientation of the magnetic field relative to the saddle

point symmetry axes will determine whether there will be discrete levels, and hence whether the field will create reflectivity structure as is discussed below.

Lifshitz and Kaganov [4-88] first discussed electron orbits near a saddle point in $\vec{k}$ space, employing a semiclassical point of view. Recently, Baldereschi and Bassani [4-89] have examined conduction and valence band saddle points from a quantum mechanical viewpoint. They find that if nondegenerate energy bands are expanded about the saddle point,

$$E(k) = E_0 + \alpha_x \hbar^2 k_x^2 + \alpha_y \hbar^2 k_y^2 + \alpha_z \hbar^2 k_z^2 \quad , \tag{4.12}$$

where the signs of α_x and α_y are different from that of α_z, then there will be discrete levels only if

$$\alpha = \alpha_x \alpha_y H_z^2 + \alpha_z \alpha_x H_y^2 + \alpha_y \alpha_z H_x^2 > 0 \quad . \tag{4.13}$$

These levels will have the energy

$$E - E_0 = (n + \tfrac{1}{2}) \frac{\beta 2e\hbar}{|\beta| c} \alpha^{\frac{1}{2}} + \frac{\alpha_x \alpha_y \alpha_z}{\alpha} (k_H H)^2 \tag{4.14}$$

where spin has been neglected and where

$$\beta = \alpha_y H_x^2 + \alpha_x H_y^2 \quad . \tag{4.15}$$

If $\alpha < 0$, the energies of the electron states in $\vec{k}$ space are continuous. The condition that $\alpha > 0$ is equivalent to requiring that the electron orbits in $\vec{k}$ space be closed.

The E_1 peaks in germanium arise from transitions at an M_1 singularity in the joint density of states. This singularity is a saddle point. If the joint density of states' saddle point is in

turn composed of saddle points in both the conduction and valence bands, we can employ the condition $\alpha > 0$ to determine under what H field directions we might expect to see the effect of discrete levels.† Equivalently, once the H field direction is given, we can determine the limitations on α_x, α_y, and α_z.

In our experimental work we applied the H field in two directions in separate experiments: 111 and 110. Table 4-7 shows the restrictions on the relative values of α_z and $\alpha_x = \alpha_y$ for discrete levels to occur. It was derived using the condition $\alpha = 0$. In interpreting the table, we note that $\alpha_z = 1/m_\ell$ and $\alpha_x = 1/m_t$ and that $m_\ell/m_t = \alpha_x/\alpha_z = 18.6$ at the L point in the conduction band of germanium [4-86].

TABLE 4-7. THE ASYMMETRY REQUIRED IN THE VALENCE AND CONDUCTION BANDS ALONG Λ FOR DISCRETE LEVELS TO EXIST IN THE PRESENCE OF A MAGNETIC FIELD, ASSUMING BOTH BANDS ARE SADDLE POINTS.

H Field Direction	Angle Between H and Λ Directions	Number of Λ Directions Making this Angle with H	Asymmetry
111	0.00°	2	No requirement
	70.55°	6	$\alpha_x > -8.0\ \alpha_z$
110	35.27°	4	$\alpha_x > -0.5\ \alpha_z$
	90.00°	4	$\alpha_z = 0.0$

The table shows that there are always discrete levels for two of the eight Λ directions when H is in a 111 direction and that there

†Conversely, if the conduction (or valence) band is a maximum or minimum, there will be no restriction on the creation of discrete levels.

might be discrete levels for the remaining six Λ directions. When H is in a 110 direction, there are probably discrete levels for four of the eight Λ directions, while the other four have continuous energy states.

Thus, our experiment was contrived to ensure that there were discrete levels under at least some conditions; yet we noted no modification in the reflectivity structure. This was presumably as a result of broadening arising from phonon scattering.

2. Thin Film Effects

Thin films have been a subject of study in optical work for a long time. Their particular relevance as a perturbation on bulk optical properties was noted by Archer [4-33]. In his polarimetric measurements he noted that his sample of germanium had a film of thickness 10 ± 4Å and refractive index of $1.9 \pm .2$. In our own search in the literature for likely values for a germanium oxide refractive index, we came across values ranging from 1.6 to 1.99. GeO_2 in the rutile form has an index of 1.99 [4-90].

Donovan, Ashley and Bennett in their work on germanium corrected their reflectivity data for a 10Å GeO_2 film.

Our own interest in surface films was motivated by the striking results created by thick films of condensed water vapor and CO_2 (Fig. 4-16), and by the observation that severe discoloration took place in germanium samples used in the electrolytic form of the $\Delta R/R$ electroreflectivity experiment. This discoloration was presumably due to the formation of the rutile form of GeO_2 on the germanium surface.

Laubengeyer and Morton [4-90] note that this formation occurs in the hydrolysis of $GeCl_4$, a process occurring when the germanium electrode is submerged in the KCl electrolytic cell. The discoloration was often so severe that the film must have been quite thick.

It thus seemed of interest to extend the work to surface films of much greater thickness than was commented upon in the work cited. The theory is simple. We propose a model shown in Fig. 4-20a. A film of index n_2 and thickness t lies over a bulk reflector of index $n_3 - ik_3$. The film is assumed to be lossless since there are no experimental values for k_2 in GeO_2. The bulk reflector is assumed to be thick enough that no significant light is reflected from its back surface. Light is normally incident on the sample-film combination though air of index $n_1 = 1$. An infinite number of reflections occur at the interfaces between regions 1 and 2 and between 2 and 3. These are summed to give the net reflected signal back through region 1 (the air). This is our measured signal. The calculation is found in Heavens [4-91, p.76] for the more general case of an absorbing film. Setting the k for the film = 0, we have:

$$R = \text{reflected magnitude} = \frac{\rho_{12}^2 + \rho_{12}y + z}{1 + \rho_{12}y + \rho_{12}^2 z} \tag{4.16}$$

$$\rho_{12} = \frac{n_1 - n_2}{n_1 + n_2} \tag{4.17}$$

$$y = 2\,\frac{(n_2^2 - n_3^2 - k_3^2)\cos 2\varphi + 2n_2k_3 \sin 2\varphi}{(n_2 + n_3)^2 + k_3^2} \tag{4.18}$$

$$z = \frac{(n_2 - n_3)^2 + k_3^2}{(n_2 + n_3)^2 + k_3^2} \tag{4.19}$$

$$\varphi = \frac{2\pi n_2 t}{\lambda} \tag{4.20}$$

R was programmed for computer as a function of n_2, n_3, k_3, t and λ. The computation was carried out for germanium for various thicknesses using the GeO_2 value of 1.99 for n_2. The values for n_3 and k_3 were those which Philipp derived, using a Kramers-Kronig calculation, from the reflectivity of Donovan, Ashley, and Bennett [4-92]. The results are shown in Fig. 4-20 for film thicknesses of 0, 10, 40, 100 and 200Å.

We enumerate some of the consequences:

(1) When film thicknesses are slight (the order of 10Å), the only effect is the decrease in reflectivity magnitude: the lower the wavelengths, the greater the decrease.

(2) When effective film thickness, $n_2 t$, becomes comparable with the light wavelength, the interference effects become very pronounced, and interference maxima and minima are imposed on the basic reflectivity. As thickness increases, these maxima and minima move to higher wavelengths (compare 100 and 200Å).

(3) Although thicknesses greater than 200Å are not shown, they result in ever increasing distortion of the basic spectrum so that it soon becomes unrecognizable. In our theory we assumed that $k_2 = 0$. This is generally not so, particularly as one looks into the ultraviolet. The consequence of nonzero k_2 will be to reduce the size of the swing from interference maxima to minima.

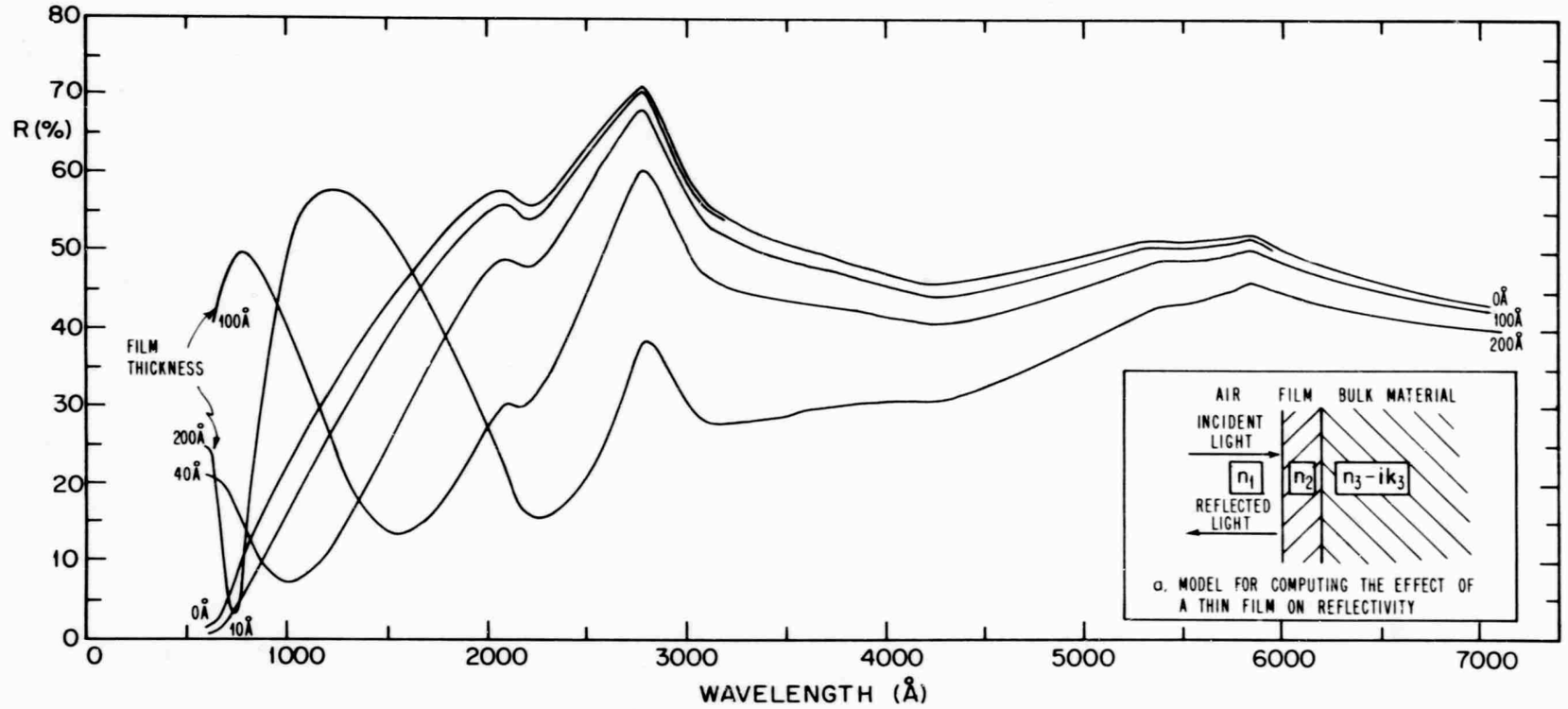

FIG. 4-20 THE EFFECT OF THIN FILMS OF VARIOUS THICKNESSES UPON THE REFLECTIVITY OF GERMANIUM.

(4) The hazard in vacuum ultraviolet measurements at low temperature is obvious. False structure can be created by frozen gas films. Such structure would usually be nonrepetitive since the film thickness would be variable. The danger from normal oxide films in vacuum ultraviolet reflectivity should be slight. The films are thin enough (the order of 10Å) that they will not distort the reflectivity structure other than to modify magnitudes. However, n_3 and k_3 values derived from the reflectivity will be in error, often by large amounts.†

(5) If the oxide films created in electrolytic $\Delta R/R$ studies become great enough that they create false structure in R, then this structure will modify $\Delta R/R$, creating in turn new hollows or peaks. For, in contrast, ΔR will be determined by the bulk material alone (providing that the GeO_2, an insulator, has no transitions in the spectral range of the experiment). We have measured the reflectivity of a germanium sample with high electrolytic discoloration, and it shows an almost unrecognizable structure. An attempt to fit this structure, by varying the film thickness in our thin film computer program, was not successful, probably because of errors introduced by the n_2 = constant, k_2 = 0 assumption.

(6) There is no reason why oil evolving from a diffusion pump or a fore pump employed in a low temperature system could not

---

†The size of these errors is demonstrated in the recent experimental work of Marton and Toots [4-93]. A thirty minute exposure of germanium samples to a pressure of 5×10^{-7} torr resulted in increases in n ranging from zero to 50% over the energy range of 7.7 to 25.2 eV.

be collected on a sample. When a pump is malfunctioning, oil film buildup can be rapid [4-94], reaching thicknesses comparable with the wavelength of light within hours. However, we feel that oil films did not affect our reflectivity measurements. We measured the absorption of fore pump and diffusion pump oils and noted a marked increase below 4200Å and 3200Å respectively, but did not observe any matching structure in our reflectivity.

A more convincing proof of the absence of an oil film under the usual conditions of our experiments was provided by the experience of R. Ludeke of this laboratory [4-95]. Some of his samples were pumped without benefit of a cold trap for periods of many months. He has seen neither absorption nor interference effects from an oil film.

3. $\Delta R/R$ Measurements in Germanium

When $\Delta R/R$ techniques first appeared, their capability for picking out new structure and displaying it accurately with narrow line widths led us to consider these techniques. The electrolytic AC field method proved quickly adaptable to our system. We will not list the system changes which were necessitated, except to note that our experimental readout was in the form $\Delta R/R$ as a result of using a feedback control network keeping I_R constant. A modified Leeds and Northrup recorder provided the servo system, controlling the value of the photomultiplier anode resistor. (Note the similarity to I_0 control in Sec. II-B-20.)

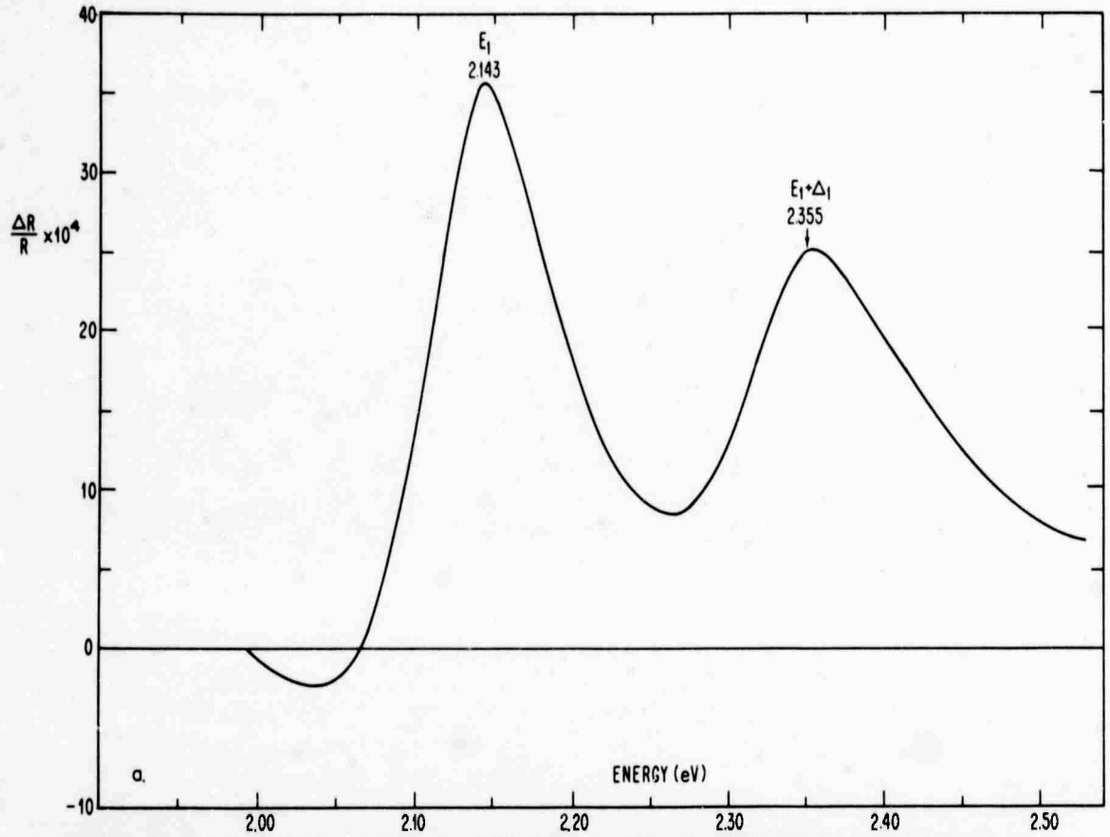

FIG. 4-21a ELECTRO-REFLECTIVITY SPECTRUM OF THE GERMANIUM Λ PEAKS. DC VOLTAGE, 1.55 VOLTS. A C VOLTAGE, 1.0 VOLTS rms.

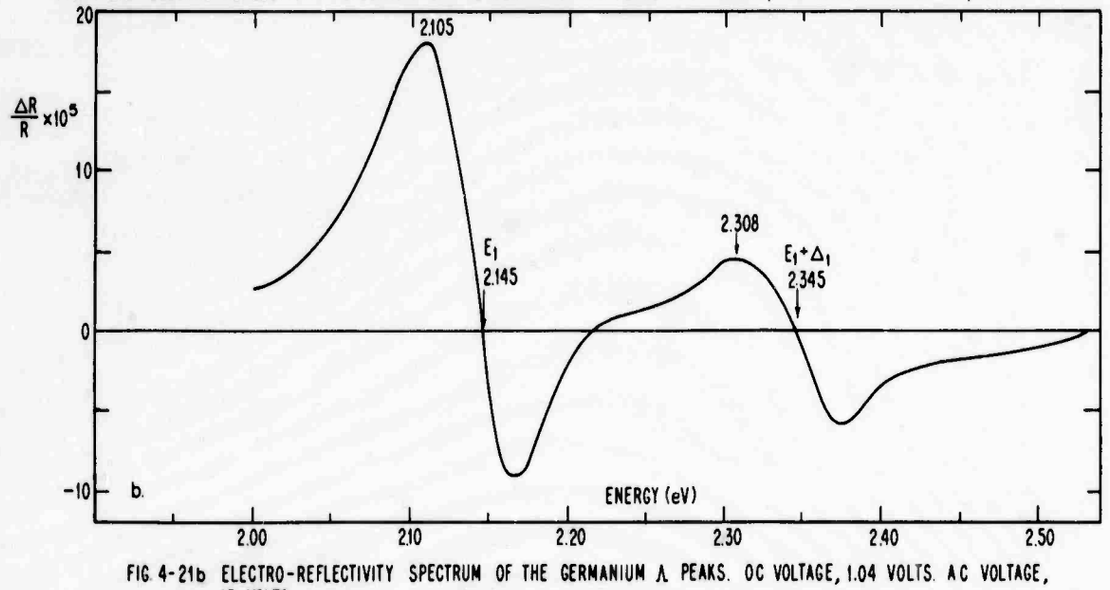

FIG. 4-21b ELECTRO-REFLECTIVITY SPECTRUM OF THE GERMANIUM Λ PEAKS. OC VOLTAGE, 1.04 VOLTS. AC VOLTAGE, .15 VOLTS rms.

Rather than looking quickly over a wide spectral range, we decided to look at the germanium spectrum near the Λ peaks in a little detail. We noted that peaks would shift as one looked at different portions of the sample surface. The .002 eV shifts were of insignificant size and were presumably caused by the varying value of the electric field on the sample surface.

We also noted the change in shape of the experimental signal, shown in Fig. 4-21, as we decreased the value of the AC field. The signal shape at low AC field looks like the derivative of that at higher field. Similar effects are often seen as one sweeps a spin resonance absorption with large or small values of an AC H field.†

The consequences of this shape change have considerable relevance in determining the energy value of the associated transition in $\vec{k}$ space. Some authors feel that these transitions are within .01 and at most .02 eV of the peak in $\Delta R/R$ [4-28]. Note in our drawing that the peak shifts from 2.143 eV at high AC field to 2.105 eV at low field, a difference of .038 eV. When we postulate that the second curve is the derivative of the first, we see that the peak of the first is the same as the zero crossing of the second. In fact the zero crossing has almost the same value, 2.145 eV. Thus one cannot automatically assume that the peak position is the energy of the associated transition.

---

†Hamakawa, Handler, and Germano [4-68] have noticed similar changes in the $\Delta R/R$ signal of germanium at these energies. They attribute the modification with increasing field to electric field broadening. Probably both broadening and the derivative effect are operating simultaneously.

a. Crossed Electric and Magnetic Fields

(1) A Brief Review of Prior Work and of Theory. The first analysis of the effect of crossed electric and magnetic fields on the optical absorption of semiconductors was carried out by Aronov [4-96] in the effective mass approximation. Looking at nondegenerate parabolic bands, he noted that the absorption would decrease in the case of allowed transitions and increase in the case of disallowed transitions as the electric field was increased. Generally, Δn† selection rules break down, permitting one to determine the individual masses of conduction and valence bands rather than just their combined masses. The energy levels are

$$\epsilon_{nn'} = \epsilon_g + \hbar\omega_{c_1}(n + \tfrac{1}{2}) + \hbar\omega_{c_2}(n' + \tfrac{1}{2}) - \frac{(m_1 + m_2)c^2}{2}\frac{E^2}{H^2} \qquad (4.21)$$

implying that the energy gap should decrease as E is increased at fixed H field. Vrehen and Lax [4-97] studied this effect in germanium, noting decreased absorption at allowed transitions and some new absorption features, compared to the zero E field condition.

Zak and Zawadski [4-98] showed that Aronov's approach was valid only for $E \ll H$ (Gaussian units), and Zawadski and Lax [4-99] then considered the problem for arbitrary E and H values, giving energy eigenvalues under a variety of conditions. Ref. [4-99] gives a number of other relevant papers. In parallel Rajagopal [4-100] evaluated $\tilde{\epsilon}$ for crossed electric and magnetic fields of arbitrary relative size. His lengthy paper is one of the most detailed on the subject.

---

†$\Delta n = n - n'$, where n is the index for the Landau levels in the conduction band and n' is the index for those in the valence band.

(2) Our Studies. Some of our most promising results were found in the measurements made in crossed E and H fields. Measurements at the Λ peaks showed changes which were unequivocally the result of the magnetic field. This is in sharp contrast with the H field reflectivity measurements where nothing was seen.

When an H field of 30 kilogauss was applied, the magnitude of the $\Delta R/R$ Λ peaks decreased by 20%. This decrease was not a result of spurious effects in either the source or photomultiplier as was shown by a simple experiment. The magnet was moved 1 inch forward of its regular position at the sample and later 1 inch in back. The change in magnetic field at the sample was large (down to around 10 kilogauss), while that at the source or photomultiplier was slight. If the observed decrease in $\Delta R/R$ were false, it should remain the same in this experiment. In fact it became only 10%, showing that the effect of the H field on the sample was real.

Another effect which was suggested by the data, but not firmly established, was the motion of the two Λ peaks to longer wavelength (lower energy). This is the reverse of what happens in straight H field measurements at the fundamental gap: the gap increases. Equation 4.21 shows that one could expect the narrowing of a gap in crossed E and H fields in the case of an M_0 edge. We have not examined how this would change in the case of the M_1 edge at Λ, nor have we evaluated the relative size of the E and H fields.

The work was terminated awaiting increased light levels, subsequently attained by the addition of wider jawed monochromator slits.

The study of the Λ peaks in crossed fields should be a very promising avenue for additional research. In carrying out this investigation, the combination of AC and DC electric field values should be chosen to give the narrowest line widths. Narrower line widths can also be attained by applying the field to a cooled vapor-deposited sandwich [4-55] rather than with the electrolytic technique. Studies should also be made at the second harmonic since theory [4-97] shows the change in α depends on E^2.

CHAPTER V

COMPATIBILITY RELATIONSHIPS AND THE DEPENDENCE ON LIGHT POLARIZATION OF SELECTION RULES: THEIR APPLICATION TO UNDERSTANDING OPTICAL STRUCTURE AND IN COMPUTING ϵ_2

In Chapter I we noted that the quality of the fit between the experimental and theoretical values of ϵ_2 is a good indication of the quality of the theoretical model. In this chapter we describe a more accurate theoretical method of calculating ϵ_2 than has been used to date.

Because of its symmetry the Brillouin zone for the diamond structure is made up of forty-eight congruent pieces [4-12, Fig. 7b]. First Brust [4-12], and then others [4-10, 4-29], computed ϵ_2 in one of these pieces and then multiplied the result by forty-eight. This procedure is always correct for computing ϵ_2 when it depends solely on the joint density of states -- i.e., when the matrix elements are constant -- but will be in error when the matrix elements depend on $\vec{k}$ and light polarization as they usually do. The matrix elements depend on selection rules which themselves generally depend on the direction of polarization of the light. This direction often varies in relation to symmetry directions from one part of the Brillouin zone to another, and hence will vary from any one of the forty-eight pieces to another. We must sum the effects of these selection rules over the entire zone, i.e., over the star of any given symmetry. Only then will the optical properties be independent of polarization direction as predicted by theory [5-01], and only then will our computed ϵ_2 value be correct.

We carry out this study by considering the optical selection rules for the double (spin-orbit split) group using group theory. The Γ selection rules are derived, and their modification under an electric field is detailed using compatibility relationships, giving information employed in Secs. IV-B-4-b and IV-C-7. The L selection rules are then derived, and the polarization dependence noted and applied to an estimate of the relative size of the effect of the four $L_{3'} \rightarrow L_3$ transitions on ϵ_2. Since the selection rules differ at the various L points, all eight points are included in our calculation.

An inconsistency between the predictions of this theoretical study and our R and $\Delta R/R$ data for gray tin, when interpreted within the framework of the k·p bands, is resolved if one postulates that the band orderings at $L_{3'}$ and L_3 (Fig. 4-12) are both reversed.

We outline also some of the problems which would have to be considered in computing the strengths of the L point transitions in electroreflectivity.

A. SELECTION RULES AND COMPATIBILITY RELATIONSHIPS FOR OPTICAL TRANSITIONS IN THE DIAMOND STRUCTURE

Insight into the identification of reflectivity and electroreflectivity structure with energy band transitions can be gained by an understanding of the optical selection rules as was seen in our discussion of germanium and gray tin found in Chapter IV. These rules indicate whether a transition between two electron states is

allowed or not. They arise directly from the symmetry properties of the crystal and hence of the electron Hamiltonian. Since the rules are determined by symmetry, group theoretical techniques are a particularly relevant way of studying them.

The investigation proceeds in two stages. First, one determines the selection rules for optical transitions in the diamond crystal structure. Then one sees how these rules are modified by the application of an electric field by tracing through the compatibility relationships. The relationships ensure that our descriptions of various symmetry points (such as the Γ's, Δ's, etc.) remain consistent as we change the crystal symmetry on application of an electric field.

1. The Use of Group Theory in Determining Selection Rules

In describing our bands we have used both the single group (e.g., $L_{3'}$) and the double group (e.g., L_6^-). The double group arises from the single when we consider the effects of the coupling of electron spin with the electron's orbital motion. Since the fullest understanding of structure is dependent on the use of the bands as modified by this spin-orbit coupling, we shall describe the selection rules appropriate to the double group.

Although many discussions of selection rules are available in the literature [5-02, 5-03, 5-04, 5-05, 5-06], we were unable to find an explicit statement of these rules for the diamond lattice double group. Therefore, we outline here the procedure for determining them

using the data on crystal point groups (an expression of the symmetry properties) readily available.

A discussion of the group theoretical expression of selection rules can be found in Tinkham [5-07, p.81]. Suppose we have some perturbation, such as the electromagnetic field, which affects the crystal electrons, causing a transition between two electronic states. If this perturbation is described by a Hamiltonian, H', we wish to determine the value of the matrix element, $\langle j|H'|i\rangle$, which tells us how strong the effect of H' is in causing a transition from electron state i to state j. Group theory will give us part of this information by indicating whether this matrix element is zero or nonzero and hence whether the transition is disallowed or allowed.

If $\Gamma_{H'}$ is the irreducible representation of H' in the appropriate crystal symmetry (diamond or some subgroup of diamond), and Γ_i is the irreducible representation of the ith electron wave function, then the transition is allowed if the Γ_j representation is found in the "decomposition" of the product $\Gamma_{H'} \times \Gamma_i$. As a practical matter, the product of the two representations is carried out in terms of their characters. Decomposition is then the process of finding which of the irreducible representations have characters which will sum to give this product.

Functionally, this can be expressed as

$$\Gamma_{H'} \times \Gamma_i = \Sigma_\gamma C_{H'i\gamma} \Gamma_\gamma \qquad (5.1)$$

and the transition from i to j is allowed if the coefficient $C_{H'ij} \neq 0$.

First, one must discover the appropriate irreducible representation for $\Gamma_{H'}$. We can express the effect of an electromagnetic field in terms of an electric dipole transition:

$$H' = e\vec{r}\cdot\vec{E} \sim e\vec{p}\cdot\frac{\vec{A}}{c} \quad \text{[5-07, p.83].} \tag{5.2}$$

Due to the $\vec{r}$ factor, or alternatively, due to the $\vec{p}$ factor, $\Gamma_{H'}$ will transform like a vector. Thus one must find which irreducible representations transform like a vector. Equivalently, we could ask which irreducible representations have x, y, and z as "bases". These representations can then be used for $\Gamma_{H'}$.

If the E field of the electromagnetic radiation is polarized, $\vec{r}\cdot\vec{E}$ will select out certain components of $\vec{r}$. Thus if $\vec{E}$ is polarized in the z direction, the only component of $\vec{r}$ which is of interest is z. Consequently, by choosing x, y, and z separately as the bases for $\Gamma_{H'}$, we can determine the effects of light polarization on our transitions.

The representation for $\Gamma_{H'}$ and Γ_i will vary as we look at transitions at various points and lines in the Brillouin zone, since those points and lines will be described by different symmetries. (Note: Γ_i is a generic label referring to irreducible representations at points throughout the Brillouin zone such as L and Δ and not just those at Γ.)

We find the point group description of the different parts of the diamond Brillouin zone in Koster's article in the Solid State Physics series [5-08, p.230 ff.]: e.g., O_h at the Γ point and D_{3d}

at the L point. (Actually, the true symmetries are combinations of those listed, which are point groups, and some additional factors due to the crystal's translation symmetry; but these latter factors do not affect our using the point group irreducible representations in determining the selection rules for direct transitions.)

The possible representations for these point groups are then found in Properties of the Thirty-Two Point Groups by Koster et al. [5-09]. In addition we find there the bases used for the various representations so that we can determine which ones correspond to $\Gamma_{H'}$ for the polarizations x, y, and z. Multiplication tables for the irreducible representations are included. These give us the decomposition of $\Gamma_{H'} \times \Gamma_i$ directly.

a. Γ Point Transitions. As a first example, let us consider the transitions from the Γ valence band states to the Γ conduction band states. (A view of the band pictures found in Figs. 4-8 and 4-11 will show the labels for each.) The Γ point has O_h symmetry. Table 87 in Koster et al. for O_h shows that Γ_4^- has the bases x, y, and z. (Since it has all three, there is no distinction for the various polarizations.) Thus $\Gamma_{H'} = \Gamma_4^-$. The multiplication table for O_h is readily derivable from that for T_d found in Table 82 of Koster et al., since O_h is the product of T_d and the inversion group C_i. The procedure is described in Eq. 4.1 from Koster et al.:

When $\Gamma_\alpha \times \Gamma_\beta = \Sigma_\gamma C_{\alpha\beta\gamma}\Gamma_\gamma$ as in the T table, then (5.3a)

$$\Gamma_\alpha^- \times \Gamma_\beta^- = \Gamma_\alpha^+ \times \Gamma_\beta^+ = \Sigma_\gamma \, C_{\alpha\beta\gamma} \Gamma_\gamma^+ \text{ , and} \tag{5.3b}$$

$$\Gamma_\alpha^- \times \Gamma_\beta^+ = \Gamma_\alpha^+ \times \Gamma_\beta^- = \Sigma_\gamma \, C_{\alpha\beta\gamma} \Gamma_\gamma^- \text{ .} \tag{5.3c}$$

From Table 82:

Γ_i	Γ_1	Γ_2	Γ_3	Γ_4	Γ_5	Γ_6	Γ_7	Γ_8
$\Gamma_4 \times \Gamma_i$	Γ_4	Γ_5	$\Gamma_4+\Gamma_5$	$\Gamma_1+\Gamma_3+\Gamma_4+\Gamma_5$	$\Gamma_2+\Gamma_3+\Gamma_4+\Gamma_5$	$\Gamma_6+\Gamma_8$	$\Gamma_7+\Gamma_8$	$\Gamma_6+\Gamma_7+2\Gamma_8$

Since the representations we are concerned with are $\Gamma_6^\pm$, $\Gamma_7^\pm$, $\Gamma_8^\pm$, we get from Eq. 5.3:

$$\left.\begin{aligned} \Gamma_4^- \times \Gamma_i^+ &= \Sigma_\gamma \, C_{4i\gamma} \Gamma_\gamma^- \qquad (5.4a) \\ \Gamma_4^- \times \Gamma_i^- &= \Sigma_\gamma \, C_{4i\gamma} \Gamma_\gamma^+ \qquad (5.4b) \end{aligned}\right\} \quad i = 6,7,8,$$

or in tabular form:

TABLE 5-1 PRODUCT DECOMPOSITION OF THE O_h GROUP GIVING SOME SELECTION RULES AT Γ IN DIAMOND

Γ_i^+	Γ_6^+	Γ_7^+	Γ_8^+
$\Gamma_4^- \times \Gamma_i^+$	$\Gamma_6^- + \Gamma_8^-$	$\Gamma_7^- + \Gamma_8^-$	$\Gamma_6^- + \Gamma_7^- + 2\Gamma_8^-$
Γ_i^-	Γ_6^-	Γ_7^-	Γ_8^-
$\Gamma_4^- \times \Gamma_i^-$	$\Gamma_6^+ + \Gamma_8^+$	$\Gamma_7^+ + \Gamma_8^+$	$\Gamma_6^+ + \Gamma_7^+ + 2\Gamma_8^+$

These give us the desired information on allowed transitions. For example, transitions from Γ_7^+ are allowed to Γ_7^- and Γ_8^- but disallowed to Γ_6^- and the set Γ_6^+, Γ_7^+, and Γ_8^+. The latter three we expect to be disallowed on the basis of parity, arising from the inversion operation. The plus (minus) sign indicates that the sign of the appropriate electron wave function remains unchanged (is changed) under inversion.

Note that these selection rules are not just those of zinc blende materials with + or - signs added. From Dresselhaus [5-10] we have for zinc blende:

TABLE 5-2 ZINC BLENDE SELECTION RULES AT Γ

Γ_i	Γ_6	Γ_7	Γ_8
$\Gamma_i \times \Gamma_4$	$\Gamma_7 + \Gamma_8$	$\Gamma_6 + \Gamma_8$	$\Gamma_6 + \Gamma_7 + 2\Gamma_8$

2. Compatibility Relationships for Symmetries Modified by the Application of an Electric Field

When we apply an electric field, we reduce the symmetry of the crystal; for example, inversion symmetry is destroyed. The new symmetry depends on the direction of the electric field relative to the crystal axes, and it must be consistent with the old; for instance, a crystal exhibiting four-fold symmetry about some axis could not have that symmetry changed to hexagonal by the application of an electric field. Compatibility relationships describe the required consistency between the old and new symmetries. Specific examples of compatible representations are found in Koster et al. for electric fields applied along certain directions of high symmetry.

a. Γ Point Transitions. Figure 5-1, taken from Koster et al., shows three possible directions of field in the O_h symmetry. As an example we consider the effects of these three directions of electric field on certain forbidden Γ transitions. From Compatibility Table 88 [5-09]:

TABLE 5-3 COMPATIBILITY RELATIONSHIPS FOR O_h SYMMETRY AND AN ELECTRIC FIELD

Electric Field Direction in Fig. 5-1	Symmetry	Initial State	Final State	
No Field	O_h	Γ_7^-	Γ_6^-	Γ_8^-
z	C_{4v}	Γ_7	Γ_6	$\Gamma_6 + \Gamma_7$
v	C_{2v}	Γ_5	Γ_5	$2\Gamma_5$
w	C_{3v}	Γ_4	Γ_4	$\Gamma_4 + \Gamma_5 + \Gamma_6$

For instance, a field in the z direction changes the symmetry to C_{4v}, and the representations Γ_6 and Γ_7 in C_{4v} are both compatible with Γ_8^- in O_h while only Γ_6 is compatible with Γ_6^-. The significance of Γ_8^- being compatible with two representations is that this four-fold (the two-fold state shown in the band pictures is actually four-fold when we consider the two spin directions) degenerate state will break up into two doubly degenerate states under the action of the electric field.

In the C_{4v} symmetry z is the basis of Γ_1, and x and y are the bases of Γ_5.[†] From the multiplication tables for C_{4v}, $\Gamma_1 \times \Gamma_7 = \Gamma_7$, $\Gamma_5 \times \Gamma_7 = \Gamma_6 + \Gamma_7$.

Thus, $\Gamma_4^- \times \Gamma_7^-$, the product to be decomposed in the absence of a field for all polarizations, becomes $\Gamma_1 \times \Gamma_7 = \Gamma_7$ for z polarization,

[†]Actually, S_x and S_y are listed in Table 33 as the bases, but x and y have the same symmetry properties as S_x and S_y under the symmetry elements of the group C_{4v}, which does not include inversion. The only difference between S and r is their change under inversion.

and $\Gamma_5 \times \Gamma_7 = \Gamma_6 + \Gamma_7$ for x, y polarization when we add an electric field in the z direction. Referring back to the extract from Table 88 [5-09] we see that, for z polarization, transitions are allowed to one (Γ_7) of the two states with representations Γ_6 and Γ_7 but not to the other.

Hence, if we use the O_h labels, the transition is allowed between Γ_7^- and one-half the Γ_8^- levels. In addition the $\Gamma_7^- \rightarrow \Gamma_6^-$ transition is not allowed. However, for x, y polarization the $\Gamma_7^- \rightarrow \Gamma_6^-$ transition is allowed, as is the $\Gamma_7^- \rightarrow \Gamma_8^-$ transition, this time to both of the Γ_8^- levels. We summarize these results in Table 5-4:

TABLE 5-4 THE EFFECT OF AN E(Z) FIELD ON CERTAIN Γ POINT SELECTION RULES

Light Polarization Direction in C_{4v} Symmetry	The Product to be Decomposed in Terms of O_h Representations	The Product Reexpressed in C_{4v} Representations and its Decomposition	The Decomposition Reexpressed in O_h Representations Gives the Allowed Transitions
x,y	$\Gamma_4^- \times \Gamma_7^-$	$\Gamma_5 \times \Gamma_7 = \Gamma_6 + \Gamma_7$	$\Gamma_7^- \rightarrow \Gamma_8^-$ (all degenerate levels) $\Gamma_7^- \rightarrow \Gamma_6^-$
z		$\Gamma_1 \times \Gamma_7 = \Gamma_7$	$\Gamma_7^- \rightarrow \Gamma_8^-$ (2 of 4 degenerate levels)

In the usual electroreflectivity experiment light is propagated in the same direction as the applied electric field, so that only the

x, y polarizations occur in the three geometries of Table 5-3. We see in Table 5-4 for one of these geometries that both of the transitions forbidden in the absence of an electric field become fully allowed.

In Table 5-5 we give similar results for the electric field applied in the v direction. Direction v in Fig. 5-1 for the O_h symmetry is the z direction in Fig. 5-2 for the C_{2v} symmetry of E(v).

TABLE 5-5 THE EFFECT OF AN E(V) FIELD ON CERTAIN Γ POINT SELECTION RULES

Light Polarization Direction in C_{2v} Symmetry	The Product to be Decomposed in Terms of O_h Representations	The Product Reexpressed in C_{2v} Representations and its Decomposition	The Decomposition Reexpressed in O_h Representations Gives the Allowed Transitions
x	$\Gamma_4^- \times \Gamma_7^-$	$\Gamma_4 \times \Gamma_5 = \Gamma_5$	$\Gamma_7^- \rightarrow \Gamma_8^-$ (all levels)[1]
y		$\Gamma_2 \times \Gamma_5 = \Gamma_5$	$\Gamma_7^- \rightarrow \Gamma_6^-$
z		$\Gamma_3 \times \Gamma_5 = \Gamma_5$	

[1] Γ_8^- levels are not split in this field.

When we consider the effects of a field in the w direction, we note that the w direction in the O_h symmetry of Fig. 5-1 is the z direction found in Fig. 5-3 for the C_{3v} symmetry of E(w). With this in mind we compute the selection rules for polarized radiation and

summarize the results in Table 5-6. Γ_1 has the basis z, and Γ_3 has the bases x and y.

TABLE 5-6 THE EFFECT OF AN E(W) FIELD ON CERTAIN Γ POINT SELECTION RULES

Light Polarization Direction in C_{3v} Symmetry	The Product to be Decomposed in Terms of O_h Representations	The Product Reexpressed in C_{3v} Representations and its Decomposition	The Decomposition Reexpressed in O_h Representations Gives the Allowed Transitions
x,y	$\Gamma_4^- \times \Gamma_7^-$	$\Gamma_3 \times \Gamma_4 = \Gamma_4 + \Gamma_5 + \Gamma_6$	$\Gamma_7^- \rightarrow \Gamma_8^-$ (all levels) $\Gamma_7^- \rightarrow \Gamma_6^-$
z		$\Gamma_1 \times \Gamma_4 = \Gamma_4$	$\Gamma_7^- \rightarrow \Gamma_6^-$ $\Gamma_7^- \rightarrow \Gamma_8^-$ (2 of 4 levels)[1]

[1] The character of E, indicating degeneracy, is 2 for Γ_4 and 1 for both Γ_5 and Γ_6.

We see from the tables that both of the normally forbidden transitions become fully allowed for the three field directions with x, y polarization. In particular in gray tin many of the measurements were made on sample faces which were hexagonal in shape, suggesting that they were normal to the 111 direction. Thus, the electric field, normal to the face, was also in the 111 direction, and the forbidden transitions are allowed.

Another forbidden transition, $\Gamma_7^+ \rightarrow \Gamma_6^-$, becomes allowed in the same way as $\Gamma_7^- \rightarrow \Gamma_6^-$, since it turns out that the compatible states of Γ_7^+ are the same as those of Γ_7^-.

B. AN ESTIMATE OF ϵ_2 FOR THE FOUR $L_{3'} \rightarrow L_3$ TRANSITIONS

1. The Polarization Dependence of the L Point Selection Rules

Another region of $\vec{k}$ space of particular interest is that at the L point (Fig. 4-1). Its symmetry is that of the group D_{3d}, which is the product of D_3 and the inversion group C_i. The L point shown in the figure is actually one of eight equivalent points in the Brillouin zone, each located in the center of a hexagonal face. They are equivalent in the sense that O_h group symmetry operations performed about $\vec{k} = 0$ will turn any one of these into itself or any of the others. This group of eight forms the "star" of $\vec{k}$ for the L point. However, the eight are not equivalent in the sense that the subgroup of operations, D_{3d}, performed at one of the L points will interchange that L point with only one of the other seven--namely the one diametrically opposite. This interchange is accomplished by reflecting the Brillouin zone in the plane of the L point hexagon and then translating it by a reciprocal lattice vector.† Thus, any two diametrically opposite L points are not equivalent to the other six. This distinction will be important in the discussion that follows when we consider the dependence on light polarization of transitions between states of D_{3d} symmetry.

The symmetry operations are defined in terms of the geometry of Fig. 5-3 from Koster et al. The z axis is very special. It is along

---

†The equivalence of each set of two diametrically opposite L points leads most authors to speak of four instead of eight L points. However, we find it more convenient to carry out our discussion in terms of all eight.

the particular 111 direction we wish to study. When we look at another L point we shift the z axis.

In D_{3d} symmetry Γ_3^- has the bases x, y, and Γ_2^- has the basis z. This gives us the bases for $\Gamma_{H'}$, and multiplication tables for D_3 can be adapted to give us the D_{3d} selection rules. Koster et al. use a general Γ notation for the L point which can be equated to the more usual L notation given by Elliott [5-11] and which we employ in our band pictures. By equating characters we note the equivalences found in Table 5-7:

TABLE 5-7 EQUIVALENCE OF TWO L POINT NOTATIONS

Author	Representation Labels											
	Single Group[3]						Double Group[3]					
Koster et al. [5-09, Table 55]	Γ_1^+	Γ_2^+	Γ_3^+	Γ_1^-	Γ_2^-	Γ_3^-	Γ_4^+	Γ_5^+	Γ_6^+	Γ_4^-	Γ_5^-	Γ_6^-
BSW [5-12, Table XV] for single group.[1] Elliott [5-11, Table V] for double group.[2]	L_1	L_2	L_3	L_1'	L_2'	L_3'	L_6^+	L_4^+	L_5^+	L_6^-	L_4^-	L_5^-

[1] In Koster [5-08, Table XIX] the characters for L_2' and L_1' are interchanged compared to BSW, apparently due to an erroneous change in the class labels. This poses no problem since the double group of both L_2' and L_1' is L_6^-.

[2] In Koster, Table LVIII, the characters for L_4^- and L_5^- are interchanged compared to Elliott, due to the same error cited above. This switch does not create a problem since L_4^- and L_5^- are degenerate by time reversal symmetry.

[3] The double group is derivable from the single group. The relationships are found in Elliott [5-11] for the diamond structure.

Single Group	L_1	L_2	L_3	L_1'	L_2'	L_3'
Double Group	L_6^+	L_6^+	$L_4^+ + L_5^+ + L_6^+$	L_6^-	L_6^-	$L_4^- + L_5^- + L_6^-$

Then the double group selection rules are given by the following decompositions:

$$\Gamma_2^- \times L_4^{\pm} \equiv \Gamma_2^- \times \Gamma_5^{\pm} = \Gamma_6^{\mp} \equiv L_5^{\mp} \quad \dagger \tag{5.5a}$$

$$\Gamma_2^- \times L_5^{\pm} \equiv \Gamma_2^- \times \Gamma_6^{\pm} = \Gamma_5^{\mp} \equiv L_4^{\mp} \tag{5.5b}$$

$$\Gamma_2^- \times L_6^{\pm} \equiv \Gamma_2^- \times \Gamma_4^{\pm} = \Gamma_4^{\mp} \equiv L_6^{\mp} \tag{5.5c}$$

$$\Gamma_3^- \times L_4^{\pm} \equiv \Gamma_3^- \times \Gamma_5^{\pm} = \Gamma_4^{\mp} \equiv L_6^{\mp} \tag{5.5d}$$

$$\Gamma_3^- \times L_5^{\pm} \equiv \Gamma_3^- \times \Gamma_6^{\pm} = \Gamma_4^{\mp} \equiv L_6^{\mp} \tag{5.5e}$$

$$\Gamma_3^- \times L_6^{\pm} \equiv \Gamma_3^- \times \Gamma_4^{\pm} = \Gamma_4^{\mp} + \Gamma_5^{\mp} + \Gamma_6^{\mp} \equiv L_4^{\mp} + L_5^{\mp} + L_6^{\mp} \tag{5.5f}$$

Recalling that the z axis is perpendicular to a hexagonal face, we can summarize those $L_{3'} \rightarrow L_3$ transitions which are allowed in Table 5-8:

TABLE 5-8 THE DEPENDENCE OF THE $L_{3'} \rightarrow L_3$ SELECTION RULES ON LIGHT POLARIZATION

Light Polarization Direction in D_{3d} Symmetry	Allowed Transitions
x,y	$L_4^- + L_5^- \rightarrow L_6^+$ $L_6^- \rightarrow L_4^+ + L_5^+$ $L_6^- \rightarrow L_6^+$
z	$L_4^- + L_5^- \rightarrow L_4^+ + L_5^+$ $L_6^- \rightarrow L_6^+$

We see that the selection rules are different for the two polarizations.

†Each of these formulae is actually two equations condensed together: one equation is given by the upper set of superscripts, and the other by the lower.

2. A Calculation of ϵ_2 For Gray Tin

This information on the allowed transitions as a function of polarization can be used to estimate the relative strengths of the four $L_{3'} \rightarrow L_3$ transitions in gray tin which are of interest in our optical studies (Secs. IV-C-6-e and 7-a). We will compute ϵ_2 employing Eqs. 4.3 and 4.10, which we have combined and give here.

$$\epsilon_2(\omega) = \frac{2e^2h^2}{m^2} \Sigma_{j,j'} \Omega^{-1} \int \frac{|\langle \vec{k}j|\hat{n}\cdot\vec{p}|\vec{k}j'\rangle|^2}{E^2_{jj'}(\vec{k})|\vec{\nabla}_k E_{jj'}(\vec{k})|} dS_k \qquad (5.6)$$

We make two assumptions to simplify the calculation:

(1) The matrix elements are constant over that portion of the surface, S_k, where the joint density of states, $J_{jj'}(\omega)$ (Eq. 4.6), has significant magnitude. Then ϵ_2 can be written as

$$\epsilon_2(\omega) = \frac{2e^2h^2}{m^2} \Omega^{-1} J_{jj'}(\omega) \Sigma_{8\ \text{L points}} \frac{|\langle \vec{k}j|\hat{n}\cdot\vec{p}|\vec{k}j'\rangle|^2}{E^2_{jj'}(\vec{k})} . \qquad (5.7)$$

(2) $J_{jj'}(\omega)$ is the same for the four L point transitions.

Then the relative strengths of the transitions j to j' can be determined from the quantity $S_{jj'}$, which is defined as

$$S_{jj'} \equiv \Sigma_{8\ \text{L points}} \frac{|\langle \vec{k}j|\hat{n}\cdot\vec{p}|\vec{k}j'\rangle|^2}{E^2_{jj'}(\vec{k})} . \qquad (5.8)$$

We use Fig. 5-4 to define the geometry for the eight L points in the Brillouin zone for the diamond lattice. The L points lie along the four [111] directions. Each lies in the center of a hexagon; the hexagons are numbered 1 to 4 and 1' to 4'. A primed hexagon lies at the opposite end of the diagonal from the unprimed hexagon

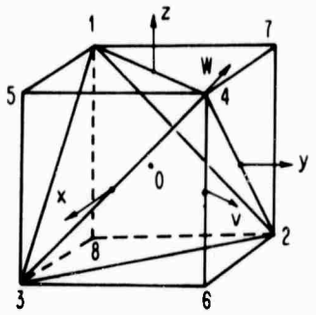

FIG. 5-1 AN ILLUSTRATION FOR THE GROUPS T_d AND O_h. From ref. [5-09, Fig. 4]

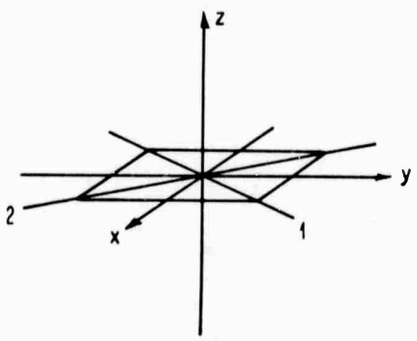

FIG. 5-2 AN ILLUSTRATION FOR THE GROUPS C_2, C_{2v}, AND C_{4v}. From ref. [5-09, Fig. 2]

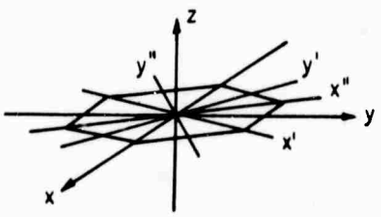

FIG. 5-3 AN ILLUSTRATION FOR THE GROUPS C_{3v}, D_3, AND D_{3d}. From ref. [5-09, Fig. 3]

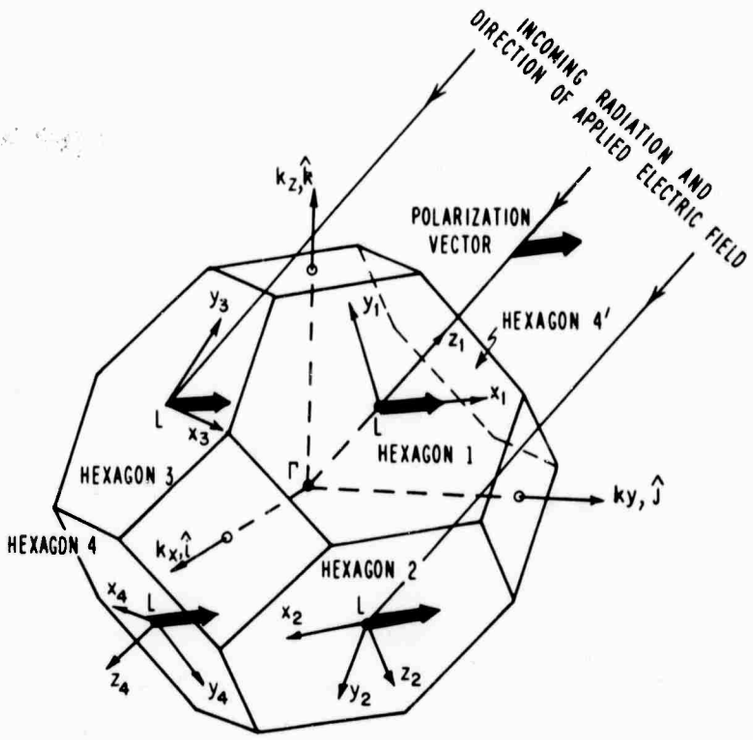

FIG. 5-4 RELATIONSHIP OF THE DIRECTION OF LIGHT PROPAGATION AND APPLIED ELECTRIC FIELD WITH THE VARIOUS L POINTS IN THE DIAMOND BRILLOUIN ZONE.

of the same number. The coordinate systems for the hexagons are related by symmetry operations of the crystal. The directions of the axes for a given hexagon are those found in Fig. 5-3 for D_{3d} symmetry. The unit vectors along the axes of the ith hexagon, $\hat{x}_i$, $\hat{y}_i$, and $\hat{z}_i$, are defined in terms of the unit vectors $\hat{i}$, $\hat{j}$, and $\hat{k}$, which lie along the directions k_x, k_y, and k_z, respectively. The relationship is found in the second, third, and fourth columns of Table 5-9.

We employ this geometry to calculate $\hat{n}\cdot\vec{p}$ found in Eq. 5.8. $\hat{n}$ is a unit vector in the direction of the light polarization. Since the optical properties in a crystal with cubic symmetry are independent of the direction of polarization, we can choose any direction we wish in making the calculation. But once this direction $\hat{n}$ is chosen, it is extremely important that we compute $\left|\langle\vec{k}j|\hat{n}\cdot\vec{p}|\vec{k}j'\rangle\right|^2$ for all eight L points and perform the sum, since the proof of the independence involves a sum over the star of $\vec{k}$ [5-01, p.415]. The star of $\vec{k}$ at the L point is all eight L points. For our calculation we use the polarization shown in Fig. 5-4 lying in the plane of hexagon #1.

$$\hat{n} = \frac{1}{\sqrt{2}}(-\hat{i}+\hat{j}) \tag{5.9}$$

Table 5-9 shows $\hat{n}\cdot\hat{x}_i$, $\hat{n}\cdot\hat{y}_i$, and $\hat{n}\cdot\hat{z}_i$ for the various hexagons. The first two can be used to construct n_{ri}, the component of $\hat{n}$ in the $x_i - y_i$ plane.

$$n_{ri} = \sqrt{(\hat{n}\cdot\hat{x}_i)^2 + (\hat{n}\cdot\hat{y}_i)^2} \tag{5.10}$$

Then $\hat{n}\cdot\vec{p}$ is given by

$$\hat{n}\cdot\vec{p} = n_{ri}p_r + n_{zi}p_z \tag{5.11}$$

where
$$n_{zi} = \hat{n}\cdot\hat{z}_i \ . \tag{5.12}$$

TABLE 5-9 A TABLE SHOWING THE COMPUTATION OF THE CONTRIBUTION OF EACH OF THE EIGHT L POINTS TO THE FACTOR $S_{jj'}$. Computed for Light Polarization in the Direction $\hat{n} = 1/\sqrt{2}\,(-\hat{i} + \hat{j})$.

Hexagon Number i	ith Hexagon Axes in terms of $\hat{i}$, $\hat{j}$, $\hat{k}$			$\hat{n}\cdot\hat{x}_i = n_{xi}$	$\hat{n}\cdot\hat{y}_i = n_{yi}$	$\hat{n}\cdot\hat{z}_i = n_{zi}$	n_{ri}	$\lvert\langle\vec{k}_j\lvert\hat{n}\cdot\vec{p}\rvert\vec{k}_{j'}\rangle\rvert$ (j,j' subscripts dropped)	$\lvert\langle\vec{k}_j\lvert\hat{n}\cdot\vec{p}\rvert\vec{k}_{j'}\rangle\rvert^2$
	$\hat{x}_i$	$\hat{y}_i$	$\hat{k}_j$						
1	$\frac{1}{\sqrt{2}}(-\hat{i}+\hat{j})$	$\frac{1}{\sqrt{6}}(-\hat{i}-\hat{j}+2\hat{k})$	$\frac{1}{\sqrt{3}}(\hat{i}+\hat{j}+\hat{k})$	1	0	0	1	P_r	P_r^2
2	$\frac{1}{\sqrt{2}}(\hat{i}-\hat{j})$	$\frac{1}{\sqrt{6}}(-\hat{i}-\hat{j}-2\hat{k})$	$\frac{1}{\sqrt{3}}(\hat{i}+\hat{j}-\hat{k})$	-1	0	0	1	P_r	P_r^2
3	$\frac{1}{\sqrt{2}}(\hat{i}+\hat{j})$	$\frac{1}{\sqrt{6}}(-\hat{i}+\hat{j}+2\hat{k})$	$\frac{1}{\sqrt{3}}(\hat{i}-\hat{j}+\hat{k})$	0	$1/\sqrt{3}$	$-\frac{\sqrt{2}}{\sqrt{3}}$	$1/\sqrt{3}$	$\frac{1}{\sqrt{3}}P_r - \frac{\sqrt{2}}{\sqrt{3}}P_z$	$\frac{1}{3}P_r^2 + \frac{2}{3}P_z^2 - \frac{2\sqrt{2}}{3}P_r P_z$
4	$\frac{1}{\sqrt{2}}(-\hat{i}-\hat{j})$	$\frac{1}{\sqrt{6}}(-\hat{i}+\hat{j}-2\hat{k})$	$\frac{1}{\sqrt{3}}(\hat{i}-\hat{j}-\hat{k})$	0	$1/\sqrt{3}$	$-\frac{\sqrt{2}}{\sqrt{3}}$	$1/\sqrt{3}$	$\frac{1}{\sqrt{3}}P_r - \frac{\sqrt{2}}{\sqrt{3}}P_z$	$\frac{1}{3}P_r^2 + \frac{2}{3}P_z^2 - \frac{2\sqrt{2}}{3}P_r P_z$
1'	$\frac{1}{\sqrt{2}}(-\hat{i}+\hat{j})$	$\frac{1}{\sqrt{6}}(\hat{i}+\hat{j}-2\hat{k})$	$\frac{1}{\sqrt{3}}(-\hat{i}-\hat{j}-\hat{k})$	1	0	0	1	P_r	P_r^2
2'	$\frac{1}{\sqrt{2}}(\hat{i}-\hat{j})$	$\frac{1}{\sqrt{6}}(\hat{i}+\hat{j}+2\hat{k})$	$\frac{1}{\sqrt{3}}(-\hat{i}-\hat{j}+\hat{k})$	-1	0	0	1	P_r	P_r^2
3'	$\frac{1}{\sqrt{2}}(\hat{i}+\hat{j})$	$\frac{1}{\sqrt{6}}(\hat{i}-\hat{j}-2\hat{k})$	$\frac{1}{\sqrt{3}}(-\hat{i}+\hat{j}-\hat{k})$	0	$-1/\sqrt{3}$	$\frac{\sqrt{2}}{\sqrt{3}}$	$1/\sqrt{3}$	$\frac{1}{\sqrt{3}}P_r + \frac{\sqrt{2}}{\sqrt{3}}P_z$	$\frac{1}{3}P_r^2 + \frac{2}{3}P_z^2 + \frac{2\sqrt{2}}{3}P_r P_z$
4'	$\frac{1}{\sqrt{2}}(-\hat{i}-\hat{j})$	$\frac{1}{\sqrt{6}}(\hat{i}-\hat{j}+2\hat{k})$	$\frac{1}{\sqrt{3}}(-\hat{i}+\hat{j}+\hat{k})$	0	$-1/\sqrt{3}$	$\frac{\sqrt{2}}{\sqrt{3}}$	$1/\sqrt{3}$	$\frac{1}{\sqrt{3}}P_r + \frac{\sqrt{2}}{\sqrt{3}}P_z$	$\frac{1}{3}P_r^2 + \frac{2}{3}P_z^2 + \frac{2\sqrt{2}}{3}P_r P_z$

p_z is the component of $\vec{p}$ outward along each 111 direction, and p_r is the component of $\vec{p}$, measured perpendicular to the symmetry axis, i.e., in a hexagonal plane. The next to last column of the table is $\langle \vec{k}j | \hat{n}\cdot\vec{p} | \vec{k}j' \rangle$, and the last is its square. Since, by symmetry, the $P_{r,jj'}$ at the eight L points are equal, and the $P_{z,jj'}$ are equal, we can sum the elements of the last column to give $S_{jj'}$. We find, taking absolute value signs into account, that

$$S_{jj'} = \frac{1}{E^2_{jj'}} \frac{8}{3} [2P^2_{r,jj'} + P^2_{z,jj'}] \tag{5.13}$$

where $$P_{r,jj'} = \langle \vec{k}j | p_r | \vec{k}j' \rangle \tag{5.14a}$$

and $$P_{z,jj'} = \langle \vec{k}j | p_z | \vec{k}j' \rangle \ . \tag{5.14b}$$

The same value for $S_{jj'}$ is of course found using other polarizations.

$P_{r,jj'}$ and $P_{z,jj'}$ are zero for those transitions which are not listed as being allowed in Table 5-8. A final assumption necessary to the calculation is that the value of

$$P_{r,jj'} = P_r \quad \text{and that} \tag{5.15a}$$

$$P_{z,jj'} = P_z \tag{5.15b}$$

for the various allowed transitions $j \rightarrow j'$ at L. The computed values of $S_{jj'}$ for the four L point transitions are shown in Table 5-10. Since the relative sizes of P_r and P_z are unknown, in one column of the table we compute the four $S_{jj'}$ factors assuming that $P_r = P_z$, and in the last column we use the values for P_r and P_z found in Figs. 15a and 15b of Ref. [4-11] for germanium computed by the k·p method.

TABLE 5-10 A COMPARISON OF THE STRENGTH OF THE FOUR $L_{3'} \rightarrow L_3$ TRANSITIONS

Transition $j \rightarrow j'$	Gray Tin Experimental Structure (k·p bands)	$E_{jj'}$-From Table 4-5 (eV)	$\frac{3}{8} S_{jj'}$		
			Using Table 5-8 and Eqs. 5.13 and 5.15	Assuming $P_r = P_z = 1.06$ (atomic units)	Assuming $P_r=1.06$, $P_z=0.32$ (atomic units)
$L_6^- \rightarrow L_4^+ + L_5^+$	A	4.90	$\frac{2P_r^2}{E_{jj'}^2}$	.0936	.0936
$L_6^- \rightarrow L_6^+$	B	4.63	$\frac{2P_r^2 + P_z^2}{E_{jj'}^2}$	.1572	.1096
$L_4^- + L_5^- \rightarrow L_4^+ + L_5^+$	C	4.41	$\frac{P_z^2}{E_{jj'}^2}$	.0578	.0053
$L_4^- + L_5^- \rightarrow L_6^+$	D	4.14	$\frac{2P_r^2}{E_{jj'}^2}$	.1311	.1311
Ratio of the Strengths A:B:C:D				1:1.68:0.62:1.40	1:1.17:0.06:1.40

In conclusion we note that the strength of the $L_4^- + L_5^- \rightarrow L_4^+ + L_5^+$ transition is predicted to be much weaker than the other three. This is particularly so when the smaller P_z value, given by the k·p method in germanium, is used in the calculation.

3. An Estimate of the $\Delta R/R$ Signal Strength in Electroreflectivity

Estimating the relative strengths of the four $L_{3'} \rightarrow L_3$ transitions in electroreflectivity is much more complex. The contribution of each L point to the $\Delta R/R$ signal is proportional both to a matrix element, whose selection rules are modified by the electric field, and to a factor θ, whose magnitude is determined by the direction of the electric field relative to the L point symmetry axis. We discuss both factors in turn.

Using the same techniques we used in Sec. V-A-2, we can determine the change in the selection rules.

The electric field compatibility tables for D_{3d} [5-09, Table 56] are reproduced here in Table 5-11. The directions for the fields E(z) and E(y) are shown in Fig. 5-3.

TABLE 5-11 COMPATIBILITY RELATIONSHIPS FOR D_{3d} SYMMETRY AND AN ELECTRIC FIELD

Electric Field Direction in Fig. 5-3	Symmetry	Initial States			Final States		
No field	D_{3d}	Γ_4^-	Γ_5^-	Γ_6^-	Γ_4^+	Γ_5^+	Γ_6^+
z	C_{3v}	$\Gamma_4^{\,1}$	$\Gamma_5^{\,1}$	Γ_6	Γ_4	$\Gamma_6^{\,1}$	$\Gamma_5^{\,1}$
y	C_2	$\Gamma_3 + \Gamma_4$	Γ_3	Γ_4	$\Gamma_3 + \Gamma_4$	Γ_3	Γ_4

[1] The table of Koster et al. is in error. It is corrected here.

The new selection rules for the E(z) field are given in Table 5-12.

TABLE 5-12 THE EFFECT OF AN E(Z) FIELD ON CERTAIN L POINT SELECTION RULES

Light Polarization Direction in D_{3d} Symmetry	The Product to be Decomposed in Terms of D_{3d} Representations	The Product Reexpressed in C_{3v} Representations and its Decomposition	The Decomposition Reexpressed in D_{3d} Representations Gives the Allowed Transitions
x,y	$\Gamma_3^- \times (L_4^- + L_5^-) =$ $\Gamma_3^- \times (\Gamma_5^- + \Gamma_6^-)$	$\Gamma_3 \times (\Gamma_5 + \Gamma_6) =$ $\Gamma_4 + \Gamma_4 = 2\Gamma_4$	$(L_4^- + L_5^-) \rightarrow \Gamma_4^+ = L_6^+$
z	$\Gamma_2^- \times (L_4^- + L_5^-) =$ $\Gamma_2^- \times (\Gamma_5^- + \Gamma_6^-)$	$\Gamma_2 \times (\Gamma_5 + \Gamma_6) =$ $\Gamma_6 + \Gamma_5$	$(L_4^- + L_5^-) \rightarrow \Gamma_5^+ + \Gamma_6^+ =$ $(L_4^+ + L_5^+)$
x,y	$\Gamma_3^- \times L_6^- = \Gamma_3^- \times \Gamma_4^-$	$\Gamma_3 \times \Gamma_4 =$ $\Gamma_4 + \Gamma_5 + \Gamma_6$	$L_6^- \rightarrow \Gamma_5^+ + \Gamma_6^+ = L_4^+ + L_5^+$ $L_6^- \rightarrow \Gamma_4^+ = L_6^+$
z	$\Gamma_2^- \times L_6^- = \Gamma_2^- \times \Gamma_4^-$	$\Gamma_2 \times \Gamma_4 = \Gamma_4$	$L_6^- \rightarrow \Gamma_4^+ = L_6^+$

These are exactly the same selection rules that occurred in the absence of a field (Table 5-8).

The geometrical relationships become more complex when we consider the effect of an E(y) field on D_{3d} symmetry. The y direction is given in Fig. 5-3 for D_{3d} and is a two-fold axis of rotation. It replaces z as the prime symmetry direction when the field is applied, and the symmetry becomes C_2. The prime axis for C_2, a two-fold axis, is labeled

z not y, however, in Fig. 5-2 and in Koster et al., the source of our multiplication tables. Thus we must relabel our polarization directions when we go from the D_{3d} to the C_2 symmetry if we are to compute selection rules properly. This relabeling is found in the first two columns of Table 5-13; the rest of the table gives the effect of an E(y) field on the $L_{3'} \rightarrow L_3$ selection rules.

An E(y) field is one lying in the plane of a hexagonal face. We see that all the L transitions are now allowed for all directions of polarization when the field is in this direction.

In most of our gray tin samples the reflecting surface has hexagonal symmetry, implying that it is perpendicular to a [111] direction. Since both the applied E field and direction of light incidence are normal to the surface, the E field is in a [111] direction. This means that two L points (hexagons 1 and 1' in Fig. 5-4) are subject to an E(z) field, have C_{3v} symmetry, and obey the x, y selection rules in Table 5-12. The symmetry of the remaining six will be even lower than the C_2 symmetry they would have with an E(y) field. This lower symmetry must be compatible with C_2, and the new selection rules can be no more restrictive than the rules under C_2 symmetry: in the C_2 symmetry all transitions are allowed.

On the basis of these selection rules we can make a rough prediction of the relative strengths of the four $L_{3'} \rightarrow L_3$ transitions in electroreflectivity. The rules under electric field are either the same or an easing of those in straight optical studies. Thus, we might expect the relative strengths of the four transitions in

TABLE 5-13 THE EFFECT OF AN E(Y) FIELD ON CERTAIN L POINT SELECTION RULES

Light Polarization Direction		The Product to be Decomposed in Terms of D_{3d} Representations	The Product Reexpressed in C_2 Representations and its Decomposition	The Decomposition Reexpressed in D_{3d} Representations Gives the Allowed Transitions
in D_{3d} Symmetry	in C_2 Symmetry			
x z	x y	$\Gamma_3^- \times (L_4^- + L_5^-) = \Gamma_3^- \times (\Gamma_5^- + \Gamma_6^-)$	$\Gamma_2 \times (\Gamma_3 + \Gamma_4) = \Gamma_4 + \Gamma_3$	$L_4^- + L_5^- \rightarrow \Gamma_5^+ + \Gamma_6^+ = L_4^+ + L_5^+$ $L_4^- + L_5^- \rightarrow \Gamma_4^+ = L_6^+$
y	z	$\Gamma_2^- \times (L_4^- + L_5^-) = \Gamma_2^- \times (\Gamma_5^- + \Gamma_6^-)$	$\Gamma_1 \times (\Gamma_3 + \Gamma_4) = \Gamma_3 + \Gamma_4$	$L_4^- + L_5^- \rightarrow \Gamma_5^+ + \Gamma_6^+ = L_4^+ + L_5^+$ $L_4^- + L_5^- \rightarrow \Gamma_4^+ = L_6^+$
x z	x y	$\Gamma_3^- \times L_6^- = \Gamma_3^- \times \Gamma_4^-$	$\Gamma_2 \times (\Gamma_3 + \Gamma_4) = \Gamma_4 + \Gamma_3$	$L_6^- \rightarrow \Gamma_5^+ + \Gamma_6^+ = L_4^+ + L_5^+$ $L_6^- \rightarrow \Gamma_4^+ = L_6^+$
y	z	$\Gamma_2^- \times L_6^- = \Gamma_2^- \times \Gamma_4^-$	$\Gamma_1 \times (\Gamma_3 + \Gamma_4) = \Gamma_3 + \Gamma_4$	$L_6^- \rightarrow \Gamma_5^+ + \Gamma_6^+ = L_4^+ + L_5^+$ $L_6^- \rightarrow \Gamma_4^+ = L_6^+$

electroreflectivity to be roughly comparable with the strengths in reflectivity; that is, that the $L_4^- + L_5^- \rightarrow L_4^+ + L_5^+$ transition be weaker than the other three, its strength increasing from zero as the applied electric field is increased.

A more exact determination of the relative strengths would require a knowledge of three additional factors which we outline here:

(1) A more quantitative determination of the value of matrix elements and how these vary for both forbidden and allowed transitions upon application of an electric field.

(2) Inclusion of the effect of the direction of the electric field relative to the L point symmetry directions. The electroreflectivity signal is

$$\Delta R/R = \alpha \Delta \epsilon_1 + \beta \Delta \epsilon_2 \tag{5.16}$$

where α and β are functions of n and k. Aspnes [4-46] has suggested that the magnitudes of $\Delta\epsilon_1$ and $\Delta\epsilon_2$ for M_0, M_1, M_2, and M_3 edges are determined by $\theta^{\frac{1}{2}}$ where

$$\theta^3 = e^2E^2/2h\mu \tag{5.17}$$

E = the applied electric field

$$1/\mu = 1/E^2\left[\frac{E_x^2}{\mu_x} + \frac{E_y^2}{\mu_y} + \frac{E_z^2}{\mu_z}\right] \tag{5.18}$$

$$\mu_i = |m_i| = \left|\frac{m_{ei}\, m_{hi}}{m_{ei} + m_{hi}}\right| , \quad i = x, y, \text{ and } z. \tag{5.19}$$

We note that μ_i is the absolute value of the combined electron and hole effective masses (equivalently called the joint density of states mass) in the i direction. By convention z is along the

direction of odd sign in M_1 and M_2 edges. This is equivalent to our z direction in Fig. 5-4, and, hence, the μ_z is a longitudinal mass and $\mu_x = \mu_y$ are transverse masses.

Equation 5.18 shows that the direction of the E field relative to the symmetry axes (defined by x, y, and z) will determine μ. μ will vary for different L points and in turn determines first θ in Eq. 5.17 and finally $\Delta R/R$ in Eq. 5.16.

The direction of the applied electric field relative to the axes x_i, y_i, and z_i of a given hexagon is easily determined once we assume that light is incident on a face perpendicular to the 111 direction. In hexagons 1 and 1' the E field is in direction z_1. For the remaining six the component of E along z is E/3, and the component in the x, y plane is $2\sqrt{2}\,E/3$.

(3) Equation 5.19 shows that we need to know effective masses for both the $L_{3'}$ and L_3 bands in order to carry out the calculation. k·p methods [5-13] used to determine the masses show a need for an accurate knowledge of many of the energy separations at L.

There are sufficient unknowns in (1) and (3) to make a quantitative estimate of the relative strengths of the $L_{3'} \rightarrow L_3$ transitions in electroreflectivity inaccurate. Nevertheless, we still expect the relative weakness of the $L_4^- + L_5^- \rightarrow L_4^+ + L_5^+$ transition to persist despite the general relaxation of the selection rules.

4. A Comparison of the Computed Value of ϵ_2 and Our Experimental Results for Gray Tin

The theoretical study summarized in Table 5-10 suggests that the observed reflectivity peaks A and B should be of comparable size and that C should be much weaker. The study also indicates that there should be a fourth peak, comparable in size to A and B, and occurring in reflectivity at the energy of the electroreflectivity peak, D. The actual absence of D in reflectivity is not alarming; energetically, it would occur on the sharply rising slope of the E_2 peak and probably merges with that peak. A more serious inconsistency is the fact that B is predicted to be large and C small, while the reverse actually happens.

This inconsistency disappears if we interchange the order of the two spin-orbit split bands at $L_{3'}$ and also at L_3. Then the energetic order of the transition is modified as shown in Table 5-14.

TABLE 5-14 ENERGETIC ORDER OF OBSERVED STRUCTURE AND OF THE $L_{3'} \rightarrow L_3$ TRANSITIONS IN GRAY TIN, ARRANGED IN ORDER OF DECREASING ENERGY

Observed Structure in R and $\Delta R/R$	Normal Order of $L_{3'}$ and L_3 Levels	Modified Order of $L_{3'}$ and L_3 Levels
A	$L_6^- \rightarrow L_4^+ + L_5^+$	$L_4^- + L_5^- \rightarrow L_6^+$
B	$L_6^- \rightarrow L_6^+$	$L_4^- + L_5^- \rightarrow L_4^+ + L_5^+$
C	$L_4^- + L_5^- \rightarrow L_4^+ + L_5^+$	$L_6^- \rightarrow L_6^+$
D	$L_4^- + L_5^- \rightarrow L_6^+$	$L_6^- \rightarrow L_4^+ + L_5^+$

When this switch is made, it is B which is predicted to be weak in reflectivity. It indeed is in comparison with A and C (Fig. 4-19). In electroreflectivity we expect B to be weak in comparison with A, C, and D, since it is generally disallowed in the absence of a field; in fact, B is not even observed in electroreflectivity (Fig. 4-13).

Thus, when the interchange of spin-orbit split levels is made, the reflectivity and electroreflectivity data are consistent with the theoretical predictions. The remaining question is whether this interchange is proper. We have not studied this question in full detail at the time of writing, although we are continuing our investigation. We mention three factors at this point:

(1) Compatibility relationships along the 111 direction must be satisfied with the interchanged bands.

(2) Pseudopotential, k·p, and first principles band calculations do not give the ordering since all are made using single group representations. Using these bands, one can compute the spin-orbit splittings for various points in $\vec{k}$ space [4-11], but the rationale for choosing the order has not been described and may well be arbitrary. An example of this arbitrariness is found in the recent article by Dresselhaus and Dresselhaus [4-25]; in their Fig. 5 for the double group bands in germanium, the bands along Λ originating at Γ_8^+ have been interchanged compared with the usual order.

Of course there is only one correct ordering. Groves [5-14] has argued that the normal ordering just off $\vec{k} = 0$ is the only correct

one since it alone ensures the proper relative curvature of the Λ_6 and $\Lambda_4 + \Lambda_5$ bands.

(3) One of the early theoretical studies of spin-orbit splittings [5-15] shows the germanium bands along Λ_3 crossing, while later work shows them parallel over most of their extent (Fig. 4-8a); thus, various configurations may be conceived of. We must postulate band crossing in our model; normal ordering (Λ_6 lower than $\Lambda_4 + \Lambda_5$) is necessary just off Γ_8^+ as argued by Groves, and inverted ordering (L_6^- above $L_4^- + L_5^-$) is necessary at L to account for the discrepancy between theory and experiment.

5. Conclusions Concerning the ϵ_2 Calculation

Even if the interchange which we have proposed above should prove to be improper, we have demonstrated a generally valid point of central importance to the accurate theoretical determination of ϵ_2: although ϵ_2 is a scalar, independent of the direction of light polarization in cubic materials, it cannot be computed ignoring light polarization. One polarization direction must be selected (albeit arbitrarily), and ϵ_2 computed using that direction for the entire Brillouin zone, not just for the small portion comprising 1/48th of the zone as is usually done [4-12, 4-10]. This procedure is necessary because of the variation of optical selection rules with polarization direction and because of the differing value of the matrix elements for the various components of $\vec{p}$. While we have applied this concept to only four transitions, located at L, it is relevant for all parts of the zone.

Turning to our calculation, we have shown that one transition, $L_4^- + L_5^- \rightarrow L_4^+ + L_5^+$, should be much weaker than the other three, and have applied this to an interpretation of the observed reflectivity and electroreflectivity structure in gray tin, within the framework of the k·p bands [4-28]. In the first principles bands (Table 4-6) the weak transition is nearly coincident with a strong one, and so could not be separately observed anyway. Thus, this study at the L point does not provide a means for choosing which band model is superior.

Higginbotham, Pollak, and Cardona have more recently reidentified the electroreflectivity structure [4-29]. They identify A as $L_4^- + L_5^- \rightarrow L_4^+ + L_5^+$, C as $L_6^- \rightarrow L_6^+$, and D as $L_4^- + L_5^- \rightarrow L_6^+$, and then compute ϵ_2 from a gray tin k·p band calculation. We have three objections to this reidentification. One is detailed in the note at the end of Sec. IV-A where we cited the great inconsistency of the new spin-orbit splittings with published values. The second is that the $L_4^- + L_5^- \rightarrow L_4^+ + L_5^+$ transition is shown as strong as the $L_6^- \rightarrow L_6^+$ transition in their ϵ_2 calculation, where our work has shown it to be much weaker. The third objection concerns their prediction of a fourth peak in ϵ_2 occurring at 5.35 eV and arising from the $L_6^- \rightarrow L_4^+ + L_5^+$ transition. An ultraviolet study of the reflectivity of gray tin, performed by Scouler [5-16], although not with our precision, shows no optical structure near this energy.†

†The rise in the R curve at energies above the A peak in our data should not be construed as suggesting any structure near 5.35 eV; it is false, arising from a sudden increase in scattered light in a manner described in Figs. 2-6a through e.

Our calculation also has relevance to an inconsistency noted by Brust [4-12]: the theoretical strength of the $L_{3'} \rightarrow L_3$ peak is too high compared to the experimental value in germanium. In his calculation he uses a constant value for his matrix element and probably does not take into account the forbidden transitions.

REFERENCES

NUMBER

CHAPTER I

(of HP-20, ARPA-33)

1-15 W.E. Engeler, H. Fritzsche, M. Garfinkel, J.J. Tiemann, "High Sensitivity Piezoreflectivity", Physical Review Letters 14, 1069 (1965).

CHAPTER IV

4-01 J.C. Phillips, "The Fundamental Optical Spectra of Solids", Solid State Physics, Vol. 18, editors F. Seitz, D. Turnbull (Academic Press, New York, 1966), pp. 55-164.

4-02 F. Herman, R.L. Kortum, C.D. Kuglin, R.A. Short, "New Studies of the Band Structure of Silicon, Germanium, and Grey Tin", Quantum Theory of Atoms, Molecules, and the Solid State: A Tribute to J.C. Slater, editor P. Löwdin (Academic Press, New York, 1966), pp. 381-428.

4-03 R.S. Knox, Theory of Excitons (Academic Press, New York, 1963).

4-04 F. Stern, "Elementary Theory of the Optical Properties of Solids", Solid State Physics, Vol. 15, F. Seitz, D. Turnbull, editors (Academic Press, New York, 1963), pp. 299-408.

4-05 J. Tauc, "Optical Properties of Semiconductors", Proceedings of the International Conference on the Physics of Semiconductors, Exeter, 1962 (The Institute of Physics and the Physical Society, London, 1962), p. 333.

4-06 J. Tauc, "Optical Properties of Semiconductors in the Visible and Ultraviolet Ranges", Progress in Semiconductors, Vol. 9, A.F. Gibson, R.E. Burgess, editors (Temple Press, London, 1965), pp. 87-133.

4-07 J. Tauc, "Optical Properties of Semiconductors", Proceedings of the International School of Physics, "Enrico Fermi", Course XXXIV, The Optical Properties of Solids, J. Tauc, editor (Academic Press, New York, 1966), pp. 63-89.

4-08 R. Zallen, The Effect of Pressure on Optical Properties of Semiconductors, Technical Report HP-12 (Gordon McKay Laboratory, Harvard University, 1964).

4-09 P.M. Grant, The Optical Properties of Thin Germanium Films, Technical Report HP-14 (Gordon McKay Laboratory, Harvard University, 1965).

4-10 E.O. Kane, "Band Structure of Silicon from an Adjusted Heine-Abarenkov Calculation", Physical Review 146, 558 (1966).

4-11 M. Cardona, F. Pollak, "Energy Band Structure of Germanium and Silicon: The k·p Method", Physical Review 142, 530 (1966).

4-12 D. Brust, "Electronic Spectra of Crystalline Germanium and Silicon", Physical Review 134, A1337 (1964).

4-13 F. Seitz, Modern Theory of Solids (McGraw-Hill Book Co., New York, 1940).

4-14 D.T.F. Marple, H. Ehrenreich, "Dielectric Constant Behavior near Band Edges in CdTe and Ge", Physical Review Letters 8, 87 (1962).

4-15 D. Brust, "Band-Theoretic Model for the Photoelectric Effect in Silicon", Physical Review 139, A489 (1965).

4-16 U. Gerhardt, "Polarization Dependence of the Piezoreflectance in Si and Ge", Physical Review Letters 15, 401 (1965).

4-17 R.J. Elliott, "Intensity of Optical Absorption by Excitons", Physical Review 108, 1384 (1957).

4-18 P.W. Anderson, Concepts in Solids (W. A. Benjamin, Inc., New York, 1963).

4-19 G.G. MacFarlane, T.P. McLean, J.E. Quarrington, V. Roberts, "Direct Optical Transitions and Further Exciton Effects in Germanium", Proceedings Physical Society, London 71, 863 (1958).

4-20 B. Velický, J. Sak, "Excitonic Effects in the Interband Absorption of Semiconductors", Physica Status Solidi 16, 147 (1966).

4-21 C.B. Duke, B. Segall, "Nonexistence of Hyperbolic Excitons", Physical Review Letters 17, 19 (1966).

4-22 Y. Toyozawa, M. Inoue, T. Inui, M. Okazaki, E. Hanamura, "Coexistence of Local and Band Structures in the Absorption Spectra of Solids", Proceedings of the International Conference on the Physics of Semiconductors, Kyoto, 1966 (Journal of the Physical Society of Japan, Vol. 21, Supplement, 1966), p. 133.

4-23 J.J. Hopfield, D.G. Thomas, "Theoretical and Experimental Effects of Spatial Dispersion on Optical Properties of Crystals", Physical Review 132, 563 (1963).

4-24 M.L. Cohen, T.K. Bergstresser, "Band Structures and Pseudopotential Form Factors for Fourteen Semiconductors of the Diamond and Zinc-Blende Structures", Physical Review 141, 789 (1966).

4-25 G. Dresselhaus, M.S. Dresselhaus, "Fourier Expansion for the Electronic Energy Bands in Silicon and Germanium", Physical Review 160, 649 (1967).

4-26 F.H. Pollak, C.W. Higginbotham, M. Cardona, "Band Structure of GaAs, GaP, InP, and InSb: the k·p Method", Proceedings of the International Conference on the Physics of Semiconductors, Kyoto, 1966 (Journal of the Physical Society of Japan, Vol. 21, Supplement, 1966), p. 20.

4-27 F. Herman, R.L. Kortum, C.D. Kuglin, R.A. Short, "New Studies of the Band Structure of the Diamond-Type Crystals", Proceedings of the International Conference on the Physics of Semiconductors, Kyoto, 1966 (Journal of the Physical Society of Japan, Vol. 21, Supplement, 1966), p. 133.

4-28 M. Cardona, P. McElroy, F.H. Pollak, K.L. Shaklee, "Electroreflectance and Band Structure of Gray Tin", Solid State Communications 4, 319 (1966).

4-29 C.W. Higginbotham, F.H. Pollak, M. Cardona, "Optical Constants of Germanium and Gray Tin. The k·p Method", Solid State Communications 5, 513 (1967).

4-30 M. Cardona, K.L. Shaklee, F.H. Pollak, "Electroreflectance at a Semiconductor-Electrolyte Interface", Physical Review 154, 696 (1967).

4-31 H.R. Philipp, E.A. Taft, "Optical Constants of Germanium in the Region 1 to 10 eV", Physical Review 113, 1002 (1959).

4-32 H.R. Philipp, H. Ehrenreich, "Optical Properties of Semiconductors", Physical Review 129, 1550 (1963).

4-33 R.J. Archer, "Optical Constants of Germanium: 3600Å to 7000Å", Physical Review 110, 354 (1958).

4-34 J. Tauc, E. Antončík, "Optical Observation of Spin-Orbit Interaction in Germanium", Physical Review Letters 5, 253 (1960).

4-35 J. Tauc, A. Abrahám, "Optical Investigation of the Band Structure of Ge-Si Alloys", Journal of the Physics and Chemistry of Solids 20, 190 (1961).

4-36 M. Cardona, H.S. Sommers, "Effect of Temperature and Doping on the Reflectivity of Germanium in the Fundamental Absorption Region", Physical Review 122, 1382 (1961).

4-37 T.M. Donovan, E.J. Ashley, and H.E. Bennett, "Effect of Surface Damage on the Reflection of Germanium in the 2650-10,000Å Region", Journal of the Optical Society of America 53, 1403 (1963).

4-38 R.F. Potter, "Optical Constants of Germanium in Spectral Region from 0.5 eV to 3.0 eV", Physical Review 150, 562 (1966).

4-39 M. Cardona, G. Harbeke, "Absorption Spectrum of Germanium and Zinc-Blende Type Materials at Energies Higher than the Fundamental Absorption Edge", Journal of Applied Physics 34, 813 (1963).

4-40 G. Harbeke, "Intrinsic Absorption in Germanium", Z. Naturforsch. 19a, 548 (1964).

4-41 B.O. Seraphin, R.B. Hess, "Franz-Keldysh Effect Above the Fundamental Edge in Germanium", Physical Review Letters 14, 138 (1965).

4-42 M.L. Cohen, J.C. Phillips, "Spectral Analysis of Photoemissive Yields in Silicon, Germanium, GaAs, GaSb, InAs, and InSb", Physical Review 139, A 912 (1965). This cites the work of G.W. Gobeli and F.G. Allen on photoemissive yields.

4-43 S.H. Groves, private communication, 1966.

4-44 M. Cardona, "Optical Properties of Semiconductors at Energies above the Fundamental Absorption Edge", Proceedings of the International Conference on the Physics of Semiconductors, Paris, 1964 (Dunod, Paris, 1964), p. 181.

4-45 F. Lukes, E. Schmidt, "Reflectivity of Pure and Heavily Doped Silicon in the Energy Range 0.1-6 eV", Proceedings of the International Conference on the Physics of Semiconductors, Paris, 1964 (Dunod, Paris, 1964), p. 197.

4-46 D.E. Aspnes, "Electric Field Effect on the Dielectric Constant of Solids", Physical Review 153, 972 (1967).

4-47 A.K. Ghosh, "Electroreflectance Spectra and Band Structure of Germanium", (Itek, Lexington Research Laboratories, 1967).

4-48 Y. Hamakawa, F.A. Germano, P. Handler, "Interband Electro-optical Properties of Germanium, I Electroabsorption", to be published.

4-49 T.P. McLean, E.G.S. Paige, "Optical Absorption Edge Broadening in Germanium", Proceedings of the International Conference on the Physics of Semiconductors, Exeter, 1962 (The Institute of Physics and The Physical Society, London, 1962), p. 450.

T.P. McLean, E.G.S. Paige, "Optical Absorption Edge Broadening in Germanium", Journal of the Physics and Chemistry of Solids 23, 822 (1962).

4-50 A.K. Ghosh, "Electroreflectance Spectra of Ge", Solid State Communications 4, 565 (1966).

4-51 K.L. Shaklee, F.H. Pollak, M. Cardona, "Electroreflectance at a Semiconductor-Electrolyte Interface", Physical Review Letters 15, 883 (1965).

4-52 H. Ehrenreich, H.R. Philipp, J.C. Phillips, "Interband Transitions in Groups 4, 3-5, 2-6 Semiconductors", Physical Review Letters 8, 59 (1962).

4-53 D.E. Aspnes, P. Handler, D.F. Blossey, "Interband Dielectric Properties of Solids in an Electric Field", to be published.

4-54 R. Ludeke, W. Paul, "Piezo-absorption of Germanium Thin Films above the Fundamental Energy Gap", to be published.

4-55 R. Ludeke, W. Paul, "Growth and Optical Properties of Epitaxial Thin Films of some II-VI Compounds", International Conference on II-VI Semiconducting Compounds,1967 (W. Benjamin, Inc., New York, 1967).

4-56 B.O. Seraphin, R.B. Hess, N. Bottka, "Field Effect of the Reflectivity of Germanium", Journal of Applied Physics 36, 2242 (1965).

4-57 M.V. Hobden, "Direct Optical Transitions from the Split-off Valence Band to the Conduction Band in Germanium", Journal of the Physics and Chemistry of Solids 23, 821 (1962).

4-58 B.O. Seraphin, "The Effect of an Electric Field on the Reflectivity of Germanium", Proceedings of the International Conference on the Physics of Semiconductors, Paris, 1964 (Dunod, Paris, 1964), p. 165.

4-59 S.H. Groves, C.R. Pidgeon, J. Feinleib, "Infrared Magneto-electroreflectance in Ge, GaSb, and InSb", Physical Review Letters 17, 643 (1966).

4-60 S. Groves, W. Paul, "Band Structure of Gray Tin", Proceedings of the International Conference on the Physics of Semiconductors, Paris, 1964 (Dunod, Paris, 1964), p. 41.

S. Groves, W. Paul, "Band Structure of Gray Tin", Physical Review Letters 11, 194 (1963).

4-61 S. Groves, Transport Properties and Band Structure of Gray Tin, Technical Report HP-10 (Gordon McKay Laboratory, Harvard University, 1963).

4-62 G.A. Busch, R. Kern, "Semiconducting Properties of Gray Tin", Solid State Physics, Vol. 11, F. Seitz, D. Turnbull, editors (Academic Press, New York, 1960), pp. 1-40.

4-63 J.H. Becker, Thesis, Cornell University, 1957 cited in Busch and Kern article, Solid State Physics, Vol. 11 (Academic Press, New York, 1960).

4-64 R.E. Lindquist, A.W. Ewald, "Optical Constants of Single Crystal Gray Tin in the Infrared", Physical Review 135, A191 (1964).

4-65 M. Cardona, D.L. Greenaway, "Reflectivity of Gray Tin Single Crystals in the Fundamental Absorption Region", Physical Review 125, 1291 (1962).

4-66 A.W. Ewald, O.N. Tufte, "Gray Tin Single Crystals", Journal of Applied Physics 29, 1007 (1958).

4-67 E.G. Wilson, S.A. Rice, "Reflection Spectra of Liquid Hg, In, and Bi from 2-20 eV", Physical Review 145, 55 (1966).

4-68 Y. Hamakawa, P. Handler, F.A. Germano, "Interband Electro-optical Properties of Germanium, II Electroreflectance", to be published.

4-69 B. Velický, "The Use of the Kramers-Kronig Relations in Determining Optical Constants", Czechoslovakian Journal of Physics B 11, 787 (1961).

4-70 M. Cardona, D.L. Greenaway, "Reflectivity and Band Structure of ZnTe, CdTe, HgTe", Physical Review 131, 98 (1963).

4-71 M. Cardona, "Fundamental Reflectivity Spectrum of Semiconductors with Zinc Blende Structure", Journal of Applied Physics 32, Supplement, 2151 (1961).

4-72 W.J. Scouler, G.B. Wright, "Reflectivity of HgSe and HgTe from 4 to 12 eV at 12 and 300°K", Physical Review 133, A736 (1964).

4-73 For a recent review see S.H. Groves, R.N. Brown, C.R. Pidgeon, "Interband Magnetoreflection and Band Structure of HgTe", Physical Review 161, 779 (1967).

4-74 P. Aigrain, Selected Constants Relative to Semiconductors (Pergamon, New York, 1961).

4-75 F. Lukes, E. Schmidt, "The Fine Structure and the Temperature Dependence of the Reflectivity and Optical Constants of Ge, Si, and III-V Compounds", Proceedings of the International Conference on the Physics of Semiconductors, Exeter, 1962, A.C. Strickland, editor (The Institute of Physics and The Physical Society, London, 1962), p. 389.

ACKNODLEGMENTS

I offer thanks to Professor William Paul for his assistance at various stages of this work. It was he who originally suggested reflectivity studies to me. He has carefully read this manuscript, and I both appreciate and have used his comments.

Dr. Steven Groves grew the gray tin samples essential to my work. The experiments on gray tin electroreflectivity, cited here, were performed at Brown in collaboration with Professor M. Cardona and his coworkers.

Our technician, Mr. David MacLeod, not only prepared my samples but provided accurate information on a variety of topics.

My wife, Linda, edited every line of this work, looking for internal consistency, while my father assisted in the reduction of some of the data.

5-03 M. Lax, J.J. Hopfield, "Selection Rules Connecting Different Points in the Brillouin Zone", Physical Review 124, 115 (1961).

5-04 J.L. Birman, "Space Group Selection Rules: Diamond and Zinc Blende", Physical Review 127, 1093 (1962).

5-05 R.S. Knox, A. Gold, Symmetry in the Solid State (W. Benjamin, Inc., New York, 1964).

5-06 H. Jones, Theory of Brillouin Zones and Electronic States in Crystals (North Holland Publishing Co., Amsterdam, 1962).

5-07 M. Tinkham, Group Theory and Quantum Mechanics (McGraw-Hill, New York, 1964).

5-08 G.F. Koster, "Space Groups and Their Representations", Solid State Physics, Vol. 5, editors F. Seitz and D. Turnbull (Academic Press, New York, 1957), pp. 173-256.

5-09 G.F. Koster, J.O. Dimmock, R.G. Wheeler, H. Statz, Properties of the 32 Point Groups (MIT Press, Cambridge, Mass., 1963).

5-10 G. Dresselhaus, "Spin-Orbit Coupling Effects in Zinc Blende Structures", Physical Review 100, 580 (1955).

5-11 R. Elliott, "Spin-Orbit Coupling in Band Theory - Character Tables for some 'Double' Space Groups", Physical Review 96, 280 (1954).

5-12 L.P. Bouckaert, R. Smoluchowski, E.P. Wigner, "Theory of Brillouin Zones and Symmetry Properties of Wave Functions in Crystals", Physical Review 50, 58 (1936).

5-13 E.O. Kane, "The k·p Method", Semiconductors and Semimetals, Vol. 1, Physics of III-V Compounds, edited by R.K. Willardson, A.C. Beer (Academic Press, New York, 1966).

5-14 S.H. Groves, private communication, 1967.

5-15 L. Liu, "Effects of Spin-Orbit Coupling in Si and Ge", Physical Review 126, 1317 (1962).

5-16 W.J. Scouler via S.H. Groves, private communication, 1967.

4-76 D.L. Greenaway, M. Cardona, "Reflectivity Measurements on InSb-In_2Te_3 and InAs-In_2Te_3 Alloys and on Pure InSb, InAs, and In_2Te_3", Proceedings of the International Conference on the Physics of Semiconductors, Exeter, 1962, A.C. Strickland, editor (The Institute of Physics and The Physical Society, London, 1962), p. 666.

4-77 E. Burstein, G.S. Picus, R.F. Wallis, F. Blatt, "Zeeman-Type Magneto-Optical Studies of Interband Transitions in Semiconductors", Physical Review 113, 15 (1959).

4-78 R.J. Elliott, T.P. McLean, G.G. MacFarlane, "Theory of the Effect of a Magnetic Field on the Absorption Edge in Semiconductors", Proceedings of the Physical Society, London, 72, 553 (1958).

4-79 B. Lax, S. Zwerdling, "Magneto-Optical Phenomena in Semiconductors", Progress in Semiconductors, Vol. 5 (Heywood and Co., London, 1960), pp. 221-272.

4-80 B. Lax, "Cyclotron Resonance and Magneto-Optical Effects in Semiconductors", Proceedings of the International School of Physics "Enrico Fermi", Course XXII, Semiconductors, R.A. Smith, editor (Academic Press, New York, 1963), pp. 240-340.

4-81 G. Dresselhaus, M.S. Dresselhaus, "Magneto-optical Effects in Solids", Proceedings of the International School of Physics, "Enrico Fermi", Course XXXIV, The Optical Properties of Solids, J. Tauc, editor (Academic Press, New York, 1966), pp. 198-256.

4-82 G.B. Wright, B. Lax, "Magnetoreflection Experiments in Intermetallics", Journal of Applied Physics, Supplement to Vol.32, 2113 (1961).

4-83 R.L. Aggarwal, L. Rubin, B. Lax, "Magneto Piezo-optical Reflection in Germanium", Physical Review Letters 17, 8 (1966).

4-84 A.J. Strauss, T.C. Harman, J.G. Mavroides, D.H. Dickey, M.S. Dresselhaus, "Optical and Electrical Properties of $Cd_xHg_{1-x}Te$ Alloys", Proceedings of the International Conference on the Physics of Semiconductors, Exeter, 1962, A.C. Strickland, editor (Institute of Physics and The Physical Society, London, 1962), p. 703.

4-85 E.D. Haidemanakis, J. G. Mavroides, M.S. Dresselhaus, D.F. Kolesar, "Observation of Interband Transitions in Cd_3As_2", Solid State Communications 4, 65 (1966).

4-86 R.L. Aggarwal, M.D. Zuteck, B. Lax, "Nonparabolicity of the L_1 Conduction Band in Germanium from Magnetotransmission Experiments", Physical Review Letters 19, 236 (1967).

4-87 B. Lax, "[111] Direct Transition Exciton and Magnetoreflection in Germanium", Physical Review Letters 4, 511 (1960).

4-88 I.M. Lifshitz, M.I. Kaganov, "Some Problems of the Electron Theory of Metals. I. Classical and Quantum Mechanics of Electrons in Metals", Soviet Physics-Uspekhi 2, 831 (1959).

4-89 A. Baldereschi, F. Bassani, "Landau Levels and Magneto-Optic Effects at Saddle Points", Physical Review Letters 19, 66 (1967).

4-90 A.W. Laubengeyer, D.S. Morton, "Germanium. The Polymorphism of Germanium Dioxide", Journal of the American Chemical Society 54, 2303 (1932).

4-91 O.S. Heavens, Optical Properties of Thin Solid Films (Dover Publications, New York, 1965).

4-92 H.R. Philipp, in private communication to P. Grant of this laboratory, 1965.

4-93 L. Marton, J. Toots, "Optical Properties of Germanium in the Far Ultraviolet", Physical Review 160, 602 (1967).

4-94 B.B. Kosicki, private communication, 1967.

4-95 R. Ludeke, private communication, 1966.

4-96 A.G. Aronov, "Oscillations of the Optical Absorption Coefficient in Crossed Electric and Magnetic Fields", Soviet Physics - Solid State 5, 402 (1963).

4-97 Q.H.F. Vrehen, B. Lax, "Cross-Field Magnetoabsorption in Semiconductors", Physical Review Letters 12, 471 (1964).

4-98 J. Zak, W. Zawadski, "Effective Mass Approximation for Electrons in Crossed Electric and Magnetic Fields", Physical Review 145, 536 (1966).

4-99 W. Zawadski, B. Lax, "Two-Band Model for Bloch Electrons in Crossed Electric and Magnetic Fields", Physical Review Letters 16, 1001 (1966).

4-100 A.K. Rajagopal, "Dielectric Constant of Bloch Electrons in Crossed Electric and Magnetic Fields", Il Nuovo Cimento, Series 10, Vol. 46B, 46 (1966).

CHAPTER V

5-01 S.L. Adler, "Quantum Theory of the Dielectric Constant in Real Solids", Physical Review 126, 413 (1962).

5-02 P.H. Meijer, Group Theory and Solid State Physics I (Gordon and Breach, New York, 1964).

Unclassified
Security Classification

DOCUMENT CONTROL DATA - R & D

(Security classification of title, body of abstract and indexing annotation must be entered when the overall report is classified)

1. ORIGINATING ACTIVITY (Corporate author)
Division of Engineering and Applied Physics
Harvard University
Cambridge, Massachusetts

2a. REPORT SECURITY CLASSIFICATION
Unclassified

2b. GROUP

3. REPORT TITLE
THE APPLICATION OF THE RATIO REFLECTOMETER TO ENERGY BAND STUDIES IN GERMANIUM AND GRAY TIN

4. DESCRIPTIVE NOTES (Type of report and, inclusive dates)
Interim technical report

5. AUTHOR(S) (First name, middle initial, last name)
Paul T. McElroy

6. REPORT DATE
May 1968

7a. TOTAL NO. OF PAGES
146

7b. NO. OF REFS
116

8a. CONTRACT OR GRANT NO.
N00014-67-A-0298-0012 and ARPA SD-88

b. PROJECT NO.

c.

d.

9a. ORIGINATOR'S REPORT NUMBER(S)
Technical Report No. HP-21
Technical Report No. ARPA-34

9b. OTHER REPORT NO(S) (Any other numbers that may be assigned this report)

10. DISTRIBUTION STATEMENT
Reproduction in whole or in part is permitted by the U. S. Government. Distribution of this document is unlimited.

11. SUPPLEMENTARY NOTES

12. SPONSORING MILITARY ACTIVITY
Office of Naval Research

13. ABSTRACT

In our work we have conducted four principal efforts: (1) the construction of a ratio reflectometer; (2) the description and analysis of a polarization dependent false structure in the reflectivity; (3) the application of the reflectometer to the accurate measurement of reflectivity structures in germanium and gray tin, which are then interpreted in terms of energy band models; and (4) the development of an improved method for theoretically computing ϵ_2 through the study of the dependence of the diamond double group selection rules on light polarization direction.

In this technical report we discuss (3) and (4) while (1) and (2) are considered in Technical Report HP-20 (ARPA-33) entitled "The Construction and Analysis of a Ratio Reflectometer."

(3) Our studies of the reflectivity of gray tin and germanium served a number of purposes: to demonstrate the capability of our system to pick out fine details; to see if reflectivity studies could display structure which is either missing or confused in the differential techniques such as AC electroreflectivity; to provide data for a Kramers-Kronig analysis giving n and k for Ge at low temperature and for gray tin.

In our analysis of structure, we have employed both the Cardona and Herman band models.

We noted the following in germanium: The peak at 3.2 eV splits into a doublet at low temperature and is best interpreted as arising from a $\Delta_5 \rightarrow \Delta_1$ transition. The Σ - X peak at 4.46 eV shows a shoulder at the high energy side and we discuss the lack of a corresponding peak in electroreflectivity. We see some evidence in reflectivity of the $L_{3'} \rightarrow L_1$ transition, noted by Potter in polarization measurements. We also see the direct gap transition from the split-off valence band.

We studied gray tin over the range 95 - 5.2 eV, with sufficient absolute amplitude accuracy to justify a Kramers-Kronig analysis. Studies were made at both 260°K and 80°K.

Between the Λ and Σ - X (3.75 eV) peaks are three small features. Two, at 2.60 and 3.3 eV, are seen in electroreflectivity. The 3.3 reflectivity structure confirms the doubtful electroreflectivity feature. A third reflectivity feature, a shoulder at 2.85 eV, is not seen in electroreflectivity. We discuss varying possibilities for the identification of these features.

We account for the small size of the E_2 peak by an appeal both to Kane's idea that it is made up of transitions throughout a large part of the Brillouin zone and to the considerable band distortion created by the zero fundamental energy gap.

Above the E_2 peak, we have noted three structural features. Two of these coincide with two of the three electroreflectivity peaks in the same energy region. Combining these to give a total of four, we find the structure corresponds to the $L_{3'} \rightarrow L_3$ quadruplet in the Cardona k·p bands.

In our studies of the electroreflectivity of germanium we note major changes in shape and large energy shifts when the AC electric field magnitude is changed. In an E ⊥ H experiment in germanium we note significant decreases in the $\Delta R/R$ signal of Λ as H is increased, which our study of the reflectivity at the Λ peaks under H field showed no effect within .02% of the reflectivity.

We feel that thin oxide films can affect electroreflectivity studies employing the electrolytic technique and that films of CO_2 and water can affect low temperature reflectivity studies. Using a simple model and computer program, we display some of these effects for varying thicknesses of film.

(4) The diamond double group optical selection rules for polarized light and their modification under electric field were essential to our interpretation of the reflectivity and electroreflectivity structure. These rules are applied in two cases -- the $\Gamma_{25'} \rightarrow \Gamma_2$ and the $L_{3'} \rightarrow L_3$ transitions. We then consider an improved method for computing ϵ_2 theoretically by noting the difference of the selection rules at the eight L points. The comparison of theory and the experimental results in gray tin suggests that the double group labels at $L_{3'}$ and those at L_3 should be reversed from their commonly published order.

DD FORM 1 NOV 65 1473 (PAGE 1)
S/N 0101-807-6811

Unclassified
Security Classification

A-31408

14 KEY WORDS	LINK A		LINK B		LINK C	
	ROLE	WT	ROLE	WT	ROLE	WT
Germanium Reflectivity Structure						
Gray Tin Reflectivity Structure						
Fine Structure						
Electroreflectivity						
E x H Effects						
Magnetoreflectivity						
Diamond Double Group						
Polarized Light Selection Rules						
Improved ϵ_2 Calculation						
Modified Band Labels						